2011

Holocene changes in mean sea-surface temperatures from Central Pacific fossil microatolls

Harrison John Schofield
University of Wollongong

Holocene changes in mean sea-surface temperatures from Central Pacific fossil microatolls

Abstract
The equatorial Pacific east-west sea surface temperature (SST) gradient (SST gradient) is a dynamic component of the El Niño Southern Oscillation (ENSO) and is a key determinant of global climate patterns. The SST gradient, which is averaged over decades to millennia, is a major component of the Pacific mean state, and changes in its strength are related to ENSO variability. Understanding the interaction between Pacific SST gradient and ENSO is important because changes in mean SSTs are projected to alter the Pacific mean SST gradient, but it is not clear what impact this will have on ENSO. By investigating the historical relationship between these two parameters, a better understanding of the interaction between the SST gradient and ENSO can be gained. Studies of climate of the past 10 thousand years (kyr) have documented changes in ENSO, yet little is known about the major components of the Pacific mean state, including the mean SST gradient.

In this thesis, 112 *Porites sp.* fossil corals collected from Kiritimati Island (157°25'W, 1°50'N) were available to reconstruct central equatorial Pacific Ocean (CP) SSTs. Thorough screening of every coral sample for diagenetic alteration by XRD and thin section techniques eliminated 64 coral samples, leaving 52 different corals from which SSTs could be accurately reconstructed. Radiocarbon and uranium-thorium dating of 45 of these corals revealed their ages, and the ages of the individual corals were distributed unevenly between 6 kyr BP and the present day. The average SST for each coral was estimated based on the corals' Sr/Ca ratio, which was measured using Inductively Coupled Plasma Atomic Emission Spectrometery. All of these reconstructed SST obtained from the corals, form a time series of central equatorial Pacific SSTs for the mid- to late Holocene. This time series is then compared with other Holocene Pacific SST reconstructions and ENSO records to better understand the Pacific SST gradient and ENSO interaction.

Weighted mean coral Sr/Ca SSTs for every 500-year interval from 6 to 1 kyr before present (BP) indicated that mean SSTs in the CP show centennial to millennial scale change in SSTs, with the largest deviations from modern SSTs occurring at 4.5-4 kyr BP where SSTs mean were ~2.9 °C ± 1.1°C cooler than today. Results also indicated SSTs were ~1.4°C ± 0.6°C cooler from 5.5-4.3 kyr BP, which combined with data from the western equatorial Pacific Ocean (WP) and eastern equatorial Pacific Ocean (EP) and modelling results provides evidence to suggest that a Pacific La Niña-like or La Niña Modoki-like mean state was active during the mid-Holocene.

For the full mid- to late Holocene period, mean SSTs in the CP and the WP appear to have undergone similar centennial to millennial scale variations, whereas EP SSTs show a consistent warming trend. Although CP mean SSTs indicate that mean zonal SSTs have been more variable throughout the mid and late-Holocene than previously thought, mean SST gradients (EP to CP and CP to WP) correlated well with previously documented Holocene SST gradient shifts.

Finally, changes in two mean SST gradients (CP minus EP and EP minus WP) were compared with ENSO evolution from 6 kyr to 1 kyr BP. Results revealed that since the mid-Holocene, both CP – EP and EP – WP gradients have weakened, and El Niño events have increased in frequency. Additionally, the proposed strengthening of the Pacific cold tongue during the 4.5-4 kyr BP correlated with very low El Niño activity. This result suggests that the centennial to millennial trends in mean SSTs have influenced ENSO behaviour since the mid-Holocene.

Holocene changes in mean sea-surface temperatures from Central Pacific fossil microatolls

Harrison John Schofield

This thesis is presented as part of the requirements for the award of the Degree of

Honours Bachelor of Science

of the

Earth and Environmental Sciences Faculty

University of Wollongong

October 2011

Acknowledgements

First and foremost, I would like to express my gratitude to my supervisor Dr Helen McGregor for her guidance, patience, and for giving me the opportunity to undertake such a significant project. Her supervision during this project was nothing short of exceptional.

I would also like to thank Colin Woodroffe for his part in collecting the corals that were used in this thesis from Kiritimati Island with Helen McGregor. A special thanks to Jose Abrantes and Jess Gaudry for their help that allowed me to successfully screen and prepare the corals used in this project. I am also thankful to Matt Dore, Henri Wong and Brett Roland from ANSTO for running the ICP-AES analysis and for their help with the geochemical preparation of the coral samples. Last but not least, I would like to thank to Sarah Pasquale for proof reading my thesis and for always helping me throughout my honours year.

Abstract

The equatorial Pacific east-west sea surface temperature (SST) gradient (SST gradient) is a dynamic component of the El Niño Southern Oscillation (ENSO) and is a key determinant of global climate patterns. The SST gradient, which is averaged over decades to millennia, is a major component of the Pacific mean state, and changes in its strength are related to ENSO variability. Understanding the interaction between Pacific SST gradient and ENSO is important because changes in mean SSTs are projected to alter the Pacific mean SST gradient, but it is not clear what impact this will have on ENSO. By investigating the historical relationship between these two parameters, a better understanding of the interaction between the SST gradient and ENSO can be gained. Studies of climate of the past 10 thousand years (kyr) have documented changes in ENSO, yet little is known about the major components of the Pacific mean state, including the mean SST gradient.

In this thesis, 112 *Porites sp.* fossil corals collected from Kiritimati Island (157°25'W, 1°50'N) were available to reconstruct central equatorial Pacific Ocean (CP) SSTs. Thorough screening of every coral sample for diagenetic alteration by XRD and thin section techniques eliminated 64 coral samples, leaving 52 different corals from which SSTs could be accurately reconstructed. Radiocarbon and uranium-thorium dating of 45 of these corals revealed their ages, and the ages of the individual corals were distributed unevenly between 6 kyr BP and the present day. The average SST for each coral was estimated based on the corals' Sr/Ca ratio, which was measured using Inductively Coupled Plasma Atomic Emission Spectrometery. All of these reconstructed SST obtained from the corals, form a time series of central equatorial Pacific SSTs for the mid- to late Holocene. This time series is then compared with other Holocene Pacific SST reconstructions and ENSO records to better understand the Pacific SST gradient and ENSO interaction.

Weighted mean coral Sr/Ca SSTs for every 500-year interval from 6 to 1 kyr before present (BP) indicated that mean SSTs in the CP show centennial to millennial scale change in SSTs, with the largest deviations from modern SSTs occurring at 4.5-4 kyr BP where SSTs mean were ~2.9 °C ± 1.1°C cooler than today. Results also indicated SSTs were ~1.4°C ± 0.6°C cooler from 5.5-4.3 kyr BP, which combined with data from the western equatorial Pacific Ocean (WP) and eastern equatorial Pacific Ocean (EP) and

modelling results provides evidence to suggest that a Pacific La Niña-like or La Niña Modoki-like mean state was active during the mid-Holocene.

For the full mid- to late Holocene period, mean SSTs in the CP and the WP appear to have undergone similar centennial to millennial scale variations, whereas EP SSTs show a consistent warming trend. Although CP mean SSTs indicate that mean zonal SSTs have been more variable throughout the mid and late-Holocene than previously thought, mean SST gradients (EP to CP and CP to WP) correlated well with previously documented Holocene SST gradient shifts.

Finally, changes in two mean SST gradients (CP minus EP and EP minus WP) were compared with ENSO evolution from 6 kyr to 1 kyr BP. Results revealed that since the mid-Holocene, both CP – EP and EP – WP gradients have weakened, and El Niño events have increased in frequency. Additionally, the proposed strengthening of the Pacific cold tongue during the 4.5-4 kyr BP correlated with very low El Niño activity. This result suggests that the centennial to millennial trends in mean SSTs have influenced ENSO behaviour since the mid-Holocene.

Contents

List of figures

List of tables

1. Introduction

The SST gradient represents the difference in SST between the EP and the western equatorial Pacific Ocean (WP). The larger the difference in SSTs across the Pacific basin, the stronger the SST gradient is. The SST gradient has a considerable influence on the behaviour and development of the El Niño Southern Oscillation (ENSO), which has two opposite phases—El Niño and La Niña (Guilyardi *et al.* 2009). The SST gradient influences ENSO because it is coupled to sea surface level pressure (SLP), which influences the strength of the easterly trade winds; when the SST gradient is strong, easterly trade winds strengthen, which subsequently cools the EP and warms the WP waters (Cane 2005). These components form a Pacific positive feedback loop, known as Bjerknes feedback, which is at the heart of ENSO physics (Wang 2004). A change in the SST gradient will result in a change Bjerknes feedback and the state of ENSO. For example, a stronger gradient characterises a La Niña event, while a weaker gradient characterises an El Niño event.

The instrumental record indicates that ENSO behaviour has shifted significantly from the late 1970s to present, and it has been hypothesised that this change in magnitude and frequency is related to warmer SSTs (Trenberth & Hoar 1996; Timmermann *et al.* 1999; Karspeck & Cane 2002; Wang & An 2002; Karnauskas *et al.* 2009). It is suggested that an increase in the mean SSTs will warm the equatorial Pacific unevenly (more warming in the EP), reduce the east-west SST gradient and more El Niño events will develop (Held & Soden 2006; Solomon *et al.* 2007; Vecchi & Soden 2007). Conversely, another hypothesis has suggested that SST gradients in a warmer climate will increase due to SSTs that will warm more in WP than the EP (Clement *et al.* 1996; Sun & Liu 1996). This theory is supported by measurements of the SST gradient since 1880 that have shown a strengthening trend in the gradient (Karnauskas *et al.* 2009). Although current climate models indicate that the SST gradient varied significantly in the past (Liu *et al.* 2000; Brown *et al.* 2008) and will in the future (Collins *et al.* 2010), their predictions shed little light on how changes in the mean SST gradient will influence ENSO variability under a warmer climate (Cane 2005; Collins *et al.* 2010).

By looking at how the SST gradient and ENSO have interacted in the past, one can gather a more thorough understanding of how changes in the mean SST gradient may influence ENSO in the future (Cane 2005). During the Holocene, changes in Earth's orbit around the sun (orbital forcing) caused changes in the seasonal distribution of solar radiation (seasonality). Since then, ENSO variability has increased, reaching its greatest intensity in the late-Holocene at ~2-1.5 kyr (Tudhope *et al.* 2001; Moy *et al.* 2002; Woodroffe *et al.* 2003; Gagan *et al.* 2004; McGregor & Gagan 2004; Conroy *et al.* 2008; Makou *et al.* 2010).

How the mean SST configuration and mean SST gradient evolved during the mid to late-Holocene, however, is highly controversial and is still debated (Cane 2005; Abram *et al.* 2009). Due to inconsistent data in the EP and limited SST reconstructions from the central Pacific, it is unclear what SSTs and the SST gradient were at ~6-3 kyr BP (Cane 2005; Abram *et al.* 2009). Studies have suggested a strengthened gradient during the mid-Holocene (Liu *et al.* 2000; Koutavas *et al.* 2002{Liu, 2000 #4; Koutavas *et al.* 2006). However, the strength of the mid-Holocene SST gradient has been questioned because the EP may have had warmer SSTs relative to the WP than previously thought (Sandweiss *et al.* 1996; Donders *et al.* 2008), and modelling studies have suggested no change in the mid-Holocene SST gradient (Brown *et al.* 2008).

Recently reconstructed mean SSTs in the WP have indicated a cooling trend during mid-Holocene that potentially signifies a contraction of the Indo-Pacific Warm Pool (IPWP) (Abram *et al.* 2009). Contraction of the western edge of the IPWP could be explained by one of three possible scenarios (Abram *et al.* 2009): (1) a mean La Niña-like state with a strengthened gradient; (2) a mean El Niño–Modoki-like state that is characterised by warming in the central and cooling in the EP and WP and (3) meridional changes in which zonal SSTs tracked north with the movement of the Inter-tropical convergence zone. The lack of clarity regarding aspects of the Holocene mean state (including mean SSTs, SST gradients and zonal SST configurations) highlights the need of further investigation on the Holocene mean state, especially for CP mean SSTs (Abram *et al.* 2009). Mean SSTs from the CP would make it possible to calculate two mean SST gradients (dual gradients) from the EP to the CP and from the WP to the CP and thus, increase the understanding of mean zonal configurations.

In this thesis, fossil coral microatolls from Kiritimati Island in the central Pacific Ocean are used to reconstruct mean SST from 6-1 kyr. Average cool SSTs at Kiritimati Island represent a mean increase in the SST gradient strengths, whereas warm SSTs indicate weakening of the mean SST gradient across the Pacific basin. This data, therefore, provides sufficient evidence to determine what mean state the tropical Pacific was in during the mid-Holocene and in doing so adds clarity to the controversial issue of mean state evolution during this period. Additionally, the mean SSTs presented in this thesis are used in combination with the mean SST records from the WP and the EP to create sub-millennial dual gradients evolution from 6-1 kyr. This data set is compared to ENSO evolution over the corresponding period to further understand the interactions between the mean SST gradient and ENSO.

2. Literature review

2.1 Tropical Pacific climate

2.1.1 Tropical Pacific SST configuration, components and processes

SSTs in the equatorial Tropical Pacific vary significantly by location as a result of the ocean's response to the processes operating in the region. The distribution of SSTs (zonal SST configuration) is characterised by the IPWP in the west and the EP Pacific cold tongue in the east. The IPWP spans from the Pacific to the Indian Ocean and is defined as the area of water where mean SST is greater than 28°C (Yan *et al.* 1992). The IPWP is the warmest body of open-ocean water, and it plays a major role in the earth's climate through its influence on the global distribution of heat and water vapour (Abram *et al.* 2009). The EP cold tongue is a relatively narrow body of cool water (annual mean of ~25°C) that stretches west from the South American continent. This SST pattern results in an east-west gradient where SSTs differ on average by ~4°C (Karnauskas *et al.* 2009). The SST gradient can get as high as 10°C, even though these two regions of the Pacific basin receive the same amount of solar insolation (Cane 2005). To understand why this SST pattern occurs, tropical Pacific components and the processes that link them need to be discussed.

Major components of the tropical Pacific include the equatorial thermocline, upwelling of cold water in the EP, the east-west SST gradient and the Walker circulation. These components are shown in Figure and are discussed in this paragraph in regards to the equatorial Pacific being in its "normal state". The thermocline is defined as the zone in the upper ocean where temperatures decrease rapidly. The thermocline represents the heat content in the upper ocean and has an east-west downwards slope as there is more warm water in the WP that pushed the thermocline deeper (Collins *et al.* 2010). Upwelling relates to the upward movement of deep cold ocean waters in the EP. Upwelling brings the thermocline closer to the sea surface and is intensified when easterly trade winds are stronger (Collins *et al.* 2010). The difference in SST from the east to west reflects the strength of the Pacific SST gradient, which is coupled with the atmospheric circulation (i.e. weaker gradient - weaker atmospheric circulation) (Karnauskas *et al.* 2009). The atmospheric circulation is known as the Walker circulation, and it describes the

convection loops of air in the tropics. The circulation pattern is characterised by air rising in the WP (higher evaporation in warmer water), air currents moving westward in the troposphere, air sinking in the east (low precipitation and stable climate) and lastly, trade winds moving eastward at sea level (known as the easterly trade winds)(Collins *et al.* 2010).

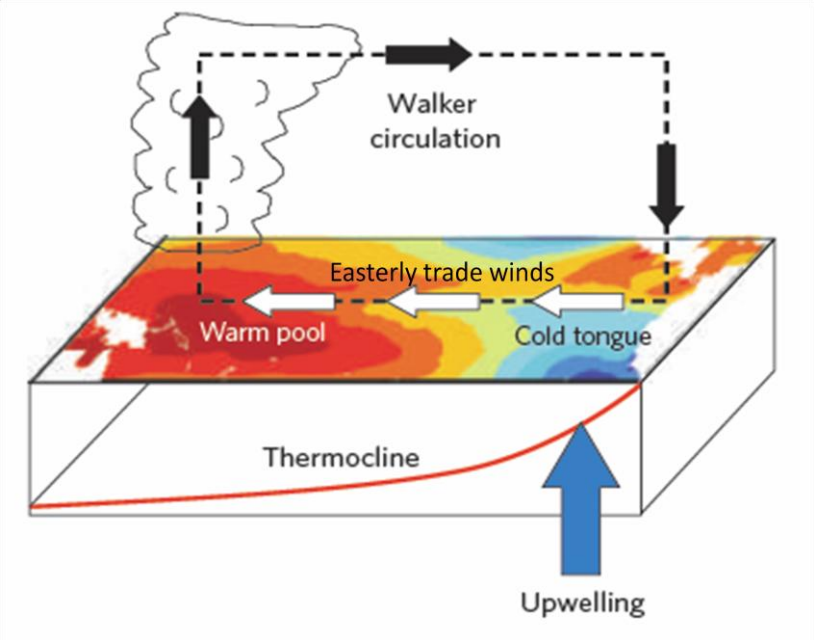

Figure 1. Diagram of zonal SSTs and the Walker circulation in the Tropical Pacific during normal conditions. Figure modified from Collins *et al.* (2010).

It was first thought that the atmosphere and ocean dynamics of equatorial Pacific climate functioned independently of each other (Walker 1923). It was not until the work of Bjerknes (1969) that documented the inter-connected relationship between Pacific Ocean SST an SLP. This work explained that the large differences in SST observed over the equatorial Pacific were due to a positive feedback system, which linked the ocean and atmosphere. The link between ocean and atmosphere means that when a strong SST gradient occurs there will also be a strong SLP gradient across the Pacific basin. The easterly trade winds are a significant process within this feedback system because they link the Walker circulation with the ocean dynamics and drive the positive feedback (McPhaden *et al.* 2006). For example, the easterly trade winds cause upwelling, raise the thermocline, and push cold water up from the south Pacific in the EP and thus, keep SSTs in the EP relatively cool (Cane, 2005). These cool EP SSTs result in a SST difference or gradient and a SLP gradient, which drives the positive feedback. Thus, as the Walker

circulation increases so do the trade winds, which enhance the SST gradient and further strengthen the Walker circulation. An understanding of these mechanisms and the equatorial Pacific positive feedback allowed Bjerknes (1969) to also explain Pacific-wide inter-annual variations in tropical Pacific climate caused by the disruption of this feedback.

2.1.2 Short term variations in Pacific climate

The first scientific work regarding the inter-annual variability of climate addressed the oscillation in SLP from the western and eastern Hemispheres in the 1920s (Walker 1923), and this inter-annual variation was termed the Southern Oscillation. Almost half a century later, a ground breaking study by Bjerknes (1969) linked the Southern Oscillation with anomalous changes in SST of the South American coast. Further studies of these variations lead to the identification of the El Niño–Southern Oscillation (ENSO), which is a basin-wide, naturally occurring set of climate conditions that originates in the equatorial Pacific Ocean. Although ENSO originates in the equatorial Pacific, it impacts global climate, extreme weather events (Guilyardi *et al.* 2009) and thus influences ecosystems and agriculture worldwide (Collins *et al.* 2010). The global impacts ENSO events cause is why ENSO is the most important source of inter-annual, global climate variability (McPhaden *et al.* 2006).

ENSO events occur on average every 4 years (2-7 covers the whole ENSO band) in an irregular fashion as it has no set cycle of frequency or amplitude (Cane 2005). ENSO involves EP SST fluctuating anomalously between cold La Niña and warm El Niño conditions (Guilyardi 2008). The difference in standardized sea level pressure between Darwin and Tahiti is used to measure the Southern Oscillation Index (SOI), which measures ENSO event strength. An ENSO event occurs if SST anomalies Niño 3.4 region (5°N-5°S, 120°-170°W) exceed 0.4°C for 6 months or more after a 5-month running mean is applied (Trenberth 1997). In addition to the traditional two phases of ENSO, observations over 1979 to 2005 have also shown that a tripolar sea level pressure pattern occurs in the tropical Pacific that deviates from conventional El Niño events. The phenomenon was termed El Niño Modoki, and it involves warming in the CP that is flanked by cooler SST anomalies in the east and west tropical Pacific (Ashok *et al.* 2007).

Bjerknes feedback provides an explanation for two ENSO phases. During a La Niña event, there is an increase and intensification of the Bjerknes feedback resulting in a stronger Walker circulation and a larger SST gradient, due to warmer WP waters and cooler EP waters. La Niña events are characterised by an intensification of the normal state of the Pacific (Figure 1) (Guilyardi *et al.* 2009) where anomalously cool surface waters are pushed west from the upwelling zone in the EP, and an enhanced equatorial cold-tongue develops from the EP to the CP. An El Niño event can be thought of as a breakdown or reversal of this feedback that is caused by a positive SST anomaly in the EP. Anomalously warm SSTs in the EP result in weaker trade winds and a disrupted Walker circulation, major convection moving eastward, a flattening of the thermocline and reduced upwelling a(Figure 2) (Collins *et al.* 2010).

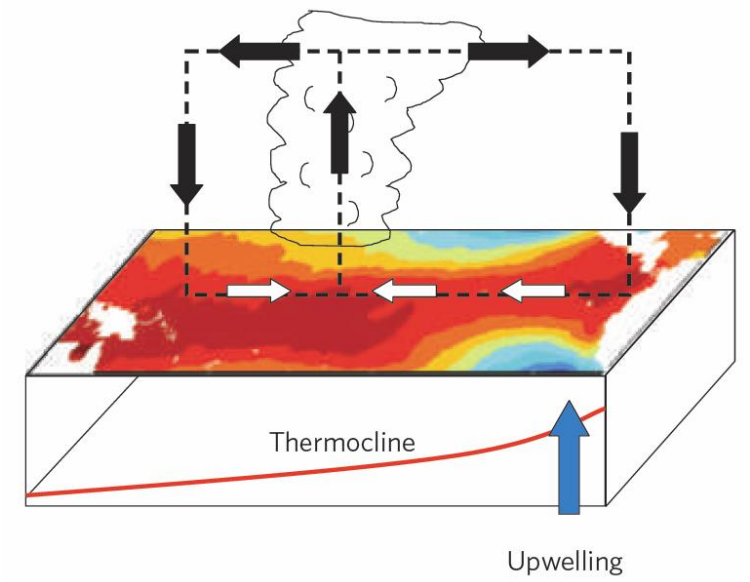

Figure 2. Diagram of SST and disrupted Walker circulation in the tropical Pacific during El Niño conditions. Diagram from Collins *et al.* (2010).

Although Bjerknes (1969) explained the mechanisms of the two preferred states of the topical Pacific, he did not explain the dynamics that are responsible for the oscillations between them or go into detail on how ENSO events develop. A theory of ENSO development starts with anomalous westerly and easterly winds that develop in the far WP that move eastward and finally arrive in the EP, where they develop into an ENSO event (Clarke & Shu 2000). These findings add clarity to the ENSO phenomenon. However, uncertainties regarding the irregular nature of the phenomenon remain, such as why more El Niño events occurred in recent decades (Trenberth 1997; McPhaden *et al.* 2006). The key variable in understanding the oscillation of ENSO states is the thermocline depth,

which is said to be a consequence of wind-driven ocean dynamics (Cane 2005). In ENSO cycles, the wind and SSTs are tightly coupled. The thermocline's response to wind changes, however, is slow and delayed. This delay creates an element that is not in phase with ENSO and subsequently, causes the oscillating-nature of the phenomenon (Cane 2005). Another factor that is crucial to ENSO development and behaviour is the mean state of the Tropical Pacific. The instrumental record reveals ENSO behaviour has shifted significantly from the late 1970s to present, and it has been hypothesised that this change in magnitude and frequency is related to warmer SSTs (Trenberth & Hoar 1996; Karspeck & Cane 2002; Wang & An 2002; Karnauskas *et al.* 2009). This occurrence has increased speculation on how the mean state of the Pacific influences ENSO variability.

2.1.3 Mean state of the tropical Pacific

2.1.3.1 Definition

Components that make up the mean state include time averaged intensity of the Pacific trade winds, mean depth of the thermocline, mean SST temperatures, mean SST gradient (Fedorov & Philander 2001; Cane 2005)..The mean SST gradients are similar to mean zonal configuration, although interpreting mean zonal configuration may require knowledge of mean SSTs from the CP. The length of the averages of these parameters when discussing the mean state varies from decadal scale variations (Guilyardi 2006) to variations over epochs (Koutavas *et al.* 2002).

The terms El Niño-like and La Niña-like are commonly used when discussing past or future changes in the mean state or background state (Koutavas *et al.* 2002; Cane 2005; Abram *et al.* 2009; Karnauskas *et al.* 2009; Makou *et al.* 2010). By using 'El Niño-like' terminology to describe changes in mean state, readers may be misled because the physical mechanisms that are present in a modern event may be considerably different to past and future events (DiNezio *et al.* 2010). For example, future models predict a weakened SLP gradient and a potential strengthened SST gradient, as well as paleo studies suggesting a range of SST gradients and thermocline tilts at the last glacial maximum (Andreasen & Ravelo 1997; Koutavas *et al.* 2002; Otto-Bliesner *et al.* 2009). These mechanisms are atypical of a modern El Niño or La Niña event.

Two major components of the mean state are the mean SST gradient and zonal configurations. The mean SST gradient can be thought of as being in equilibrium with mean state of the topical Pacific since it is created by cool upwelling waters in the EP and by warm surface waters in the WP (Vecchi & Soden 2007). One of the biggest uncertainties with global warming in the tropical Pacific is knowing how the mean state gradient will change and influence the pre-existing natural variations (Collins *et al.* 2010).

2.1.3.2 Implications of changes in the mean state

The mean state of the tropical Pacific is significant because it influences mean wind anomalies, which are fundamental in determining short-term variations in Pacific climate (Cane 2005). A thorough understanding of the mean state is therefore vital for understanding and forecasting future ENSO variability (Vecchi *et al.* 2006; Guilyardi *et al.* 2009). As the mean SST gradient is a major component of the mean state, this significance also applies to the mean SST gradients. Furthermore, it has been argued that the mean SST gradient, not mean SSTs, are fundamental in determining global climate patterns (Cobb *et al.* 2003; Collins *et al.* 2010).

It has been suggested that decadal scale changes in the mean SST and the Walker circulation are interwoven with decadal variations in ENSO (Cane 2005). Additionally, climate models show that even minor changes in the mean state could drive significant centennial scale variations in ENSO (Wittenberg 2009). A general understanding of the interaction between ENSO and the mean state can be explained through the tropical Pacific dynamics that Bjerknes (1969) identified. Because changes in the mean SST gradient occur in conjunction with mean changes in the Walker circulation (Karnauskas *et al.* 2009), an enhanced SST gradient would reflect an increase in the mean trade winds. On ENSO time scales, La Niña events are characterised by an anomalous increase in trade wind strength, and El Niño events rely on a reduction of the easterly winds. Therefore, it can be assumed that an enhanced mean SST gradient correlates with more La Niña events and less El Niño events because the weakening or reversal of winds would be, on average, less likely to occur. But this relationship in reality is no so clear-cut. To better understand how the mean state influences ENSO behaviour, the observed and predicted mean state changes will be discussed.

The instrumental record reveals that ENSO behaviour has shifted significantly from the late 1970s to present, and it has been hypothesised that this change in magnitude and frequency is related to warmer SSTs (Trenberth & Hoar 1996; Timmermann *et al.* 1999; Karspeck & Cane 2002; Wang & An 2002; Karnauskas *et al.* 2009). The timing of the change in ENSO behaviour correlated with a change in mean climate around 1976 and this occurrence gave reason to believe that the mean state changes on decadal time scales and that it directly influences ENSO (Karspeck & Cane 2002; Wang & An 2002). One of the most notable changes in the mean state over the instrumental records is the weakening of decadal mean trade winds (Vecchi *et al.* 2006), which corresponded with an observed increase in El Niño events. This finding provides evidence to suggest that El Niño amplitude has an inverse relationship with mean trade winds (Guilyardi 2006). Because ENSO theory suggests that the SLP and SST gradients are coupled (Bjerknes 1969), it has been assumed that the mean SST gradient strength is also inversely related to El Niño amplitude. As El Niño events are associated with a reduced or absent east-west SST gradient and weaker easterly trade winds, while La Niña events are associated with increased easterly winds and an enhanced SST gradient (McPhaden *et al.* 2006; Collins *et al.* 2010), it makes sense that a mean weakening of the trade winds would correspond with more El Niño events. However, it is ambiguous why measurements based off more than100 years of instrumental data indicate that the mean SST gradient has strengthened (Karnauskas *et al.* 2009) and an increase in El Niño events in recent decades has been observed (Trenberth & Hoar 1997). These inconsistencies highlight the complexity of the mean state's response to global warming and that other mean state components, such as the mean thermocline depth, play a significant role in determining El Niño frequency and amplitude (Fedorov & Philander 2001).

The mean state's response to human-induced warming has been the subject of recent debate because of its potential control over short-term climate variability (Cane 2005; Karnauskas *et al.* 2009). Whether or not the mean state of the Pacific will have an El Nino-like or a La Niña-like response in a warmer climate is unknown (Karnauskas *et al.* 2009). Despite the advances in climate models' capabilities, simulations of how ENSO variability will change in a warmer climate are evenly divided in predictions and offer no certainty regarding the future of the mean state (Cane 2005; Guilyardi *et al.* 2009; Collins *et al.* 2010). Theories based on mass and energy balances of the atmosphere (Held & Soden 2006; Vecchi & Soden 2007) have favoured a weakening of the Walker circulation

and SST gradient, which results in an El Niño-like response. Conversely, another theory has suggested that increasing mean SSTs will be more diluted by strong upwelling in EP and that this will result in a stronger SST gradient and a mean La Niña-like state (Clement *et al.* 1996; Sun & Liu 1996). A recent and thorough assessment of the interactions between ENSO and the mean climate discusses the significant changes that the mean climate of the tropical Pacific will most likely undergo (Collins *et al.* 2010). These changes include weaker trade winds, reduced upwelling, reduced Walker circulation intensity and shallowing of the thermocline. Because the mean state will probably modify one or more of the processes and feedbacks that are so influential in determining ENSO behaviour, it is extremely difficult, if even possible, to predict how ENSO behaviour and frequency will change in a warmer climate (Collins *et al.* 2010). Cane (2005) also found climate models' ability to consistently project future mean state – ENSO interactions to be relatively limited. One way a better understanding of mean state and ENSO can be developed is by testing and improving climate models, which can be achieved by comparing models with reconstructed mean states (Cobb *et al.* 2003; Collins *et al.* 2010). Another way to increase understanding of the relationship between mean state and ENSO is by assessing the mean state at times when it was significantly different from today (Cane 2005).

2.2 Holocene mean state climate

1.1.1 Mean state of the tropical Pacific during the mid to late-Holocene

Currently, the majority of tropical Pacific SST records come from sediment cores in the east and west Pacific. SSTs from these cores are derived from the magnesium/calcium composition of planktonic foraminifera (Stott *et al.* 2002; Koutavas *et al.* 2006) and alkenones (Koutavas & Sachs 2008). Coral Sr/Ca and $\delta^{18}O$ based studies have also reconstructed SSTs from the tropical Pacific (Cobb *et al.* 2003; Woodroffe *et al.* 2003; Abram *et al.* 2009; Glasbergen 2010). However, these records are usually not continuous and only offer "windows" of past SSTs, although numerous bulk coral samples over millennia can indicate variations in mean SST (Abram *et al.* 2009).

All major WP SST records have been collected in the last decade (Stott *et al.* 2002; Stott *et al.* 2004; Stott *et al.* 2007; Abram *et al.* 2009), and the compilation of these records

reveals a common cooling trend over the last 10 kyr in which SSTs were on average ~0.5°C warmer than during pre-industrial times from ~7-10 kyr BP. All the major EP SST records have also been documented in the last decade (Koutavas et al. 2002; Kienast et al. 2006; Koutavas et al. 2006; Lea et al. 2006; Koutavas & Sachs 2008). EP SST records are currently limited due to the inadequate amount of SST data points. Often, reconstructions vary by several degrees, particularly when study sites vary in latitude. For example, studies that have reconstructed SST from ~8°N of the equator (Leduc *et al.* 2007) have recorded SSTs ~6°C higher than other SST records that were obtained closer to the equator (Koutavas *et al.* 2006). This large spatial variation in SST is not observed in the WP SST records (Stott *et al.* 2004). Furthermore, studies that reconstruct SSTs from locations within 1° latitude of each other in the EP have still recorded significant variations of ~4°C over the same time period (Koutavas *et al.* 2002; Koutavas & Sachs 2008). These variations have often led to inconclusive estimates of Holocene mean states (Abram *et al.* 2009). The lack of available EP data can be observed in Figure 3. This figure does not show the large variations in EP SSTs that clearly because two out of the three records have been adjusted by up to 1.7°C to make to mean SST trend more obvious.

SST records from sediment cores in the CP have not been reconstructed as of yet, and only a hand full of $\delta^{18}O$ and Sr/Ca coral records exist (Cobb et al. 2003; Woodroffe et al. 2003; Glasbergen 2010). Records from this region span back ~3.8 kyr BP. From 3.8–2.8 kyr BP it is suggested that conditions were cooler and/or dryer during (Woodroffe *et al.* 2003). Records also indicate that cooler temperatures (Glasbergen 2010) and cooler and/or dryer conditions (Woodroffe *et al.* 2003) occurred ~1.7 kyr BP. At ~1 kyr it has also been suggested that cooler and/or dryer conditions were present in the CP (Cobb *et al.* 2003).

The SST records from the WP and the EP have made it possible to reconstruct mean SST gradient evolution over the Holocene (Koutavas *et al.* 2006; Marchitto *et al.* 2010). Koutavas *et al.* (2006) used SST records from the east and west Pacific to recreate broad changes in the SST gradient from 12 kyr to present (Figure 3). The results show that there has been a large-scale change in the mean SST gradient from the early to mid-Holocene (~10-4 kyr) and the late-Holocene (~4-0 kyr). The early to mid-Holocene is characterised by cooler EP temperatures, warmer WP temperatures, and a stronger SST gradient. The transition between the mid to late-Holocene occurs at ~4-5 kyr, and it was suggested that this period marked the end of the anomalous 'strengthened gradient' period as the climate

transitioned to conditions more similar to the late-Holocene (weaker mean gradient strength) (Koutavas *et al.* 2006).

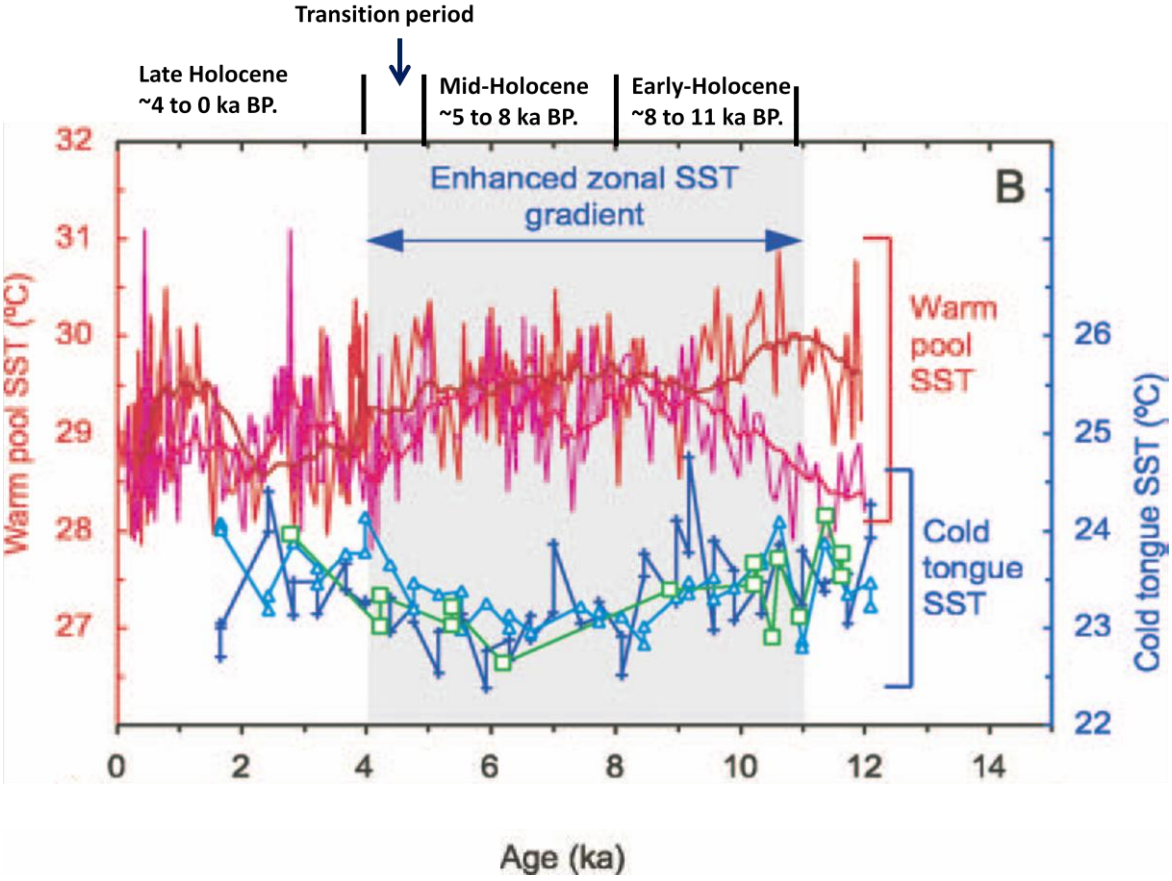

Figure 3: Mg/Ca derived SSTs from the EP and WP revealing changes in the mean gradient strength. WP SSTs (red) is from Stott *et al.* (2004). EP SST records with green open squares (adjusted by +1.7°C) and blue crosses are from Koutavas *et al.* (2006) and blue open triangles (adjusted by +1.2°C) are from Koutavas *et al.* (2002). Figure is modified from Koutavas *et al.* (2006).

The mean SST gradient calculated by Koutavas *et al*. (2006) provides a general indication of gradient strength during the mid and the late-Holocene. More detailed reconstructions of late-Holocene gradients reveal much more variability in the SST gradient (Conroy 2010). The idea that the mean SST gradient was enhanced during the ~9–6 kyr BP is widely agreed upon by various authors. (Koutavas *et al.* 2002; Koutavas *et al.* 2006; Donders *et al.* 2008; Koutavas & Sachs 2008; Marchitto *et al.* 2010). The strength of the mean SST gradient potentially peaked at ~6 kyr when it was 30% warmer (1.5°C) than modern (Koutavas *et al.* 2006). Conversely, it has been suggested that warming in the EP occurred during 8-5 kyr BP, which subsequently resulted in a weakening of the gradient

(Sandweiss *et al.* 1996). Controversy surrounds the timing of the transition to warmer SSTs in the EP and the mean state during the latter parts of the mid-Holocene and during the transition to the late Holocene (Abram *et al.* 2009). It is suggested that at ~5 kyr, warming occured in the EP (Donders *et al.* 2008), which terminated the mid Holocene enhanced SST gradeient. Conversely, other EP SSTs suggest it was still cool in the EP during this period (Koutavas *et al.* 2006).

Modelling studies have offered additional theories of what the mean state was during the mid-Holocene. Studies, such as Brown *et al.* (2008), provide results that deviate from other studies as they indicate unchanged or slightly reduced mid-Holocene equatorial Pacific gradients. These results are not consistent with modelling-based studies (Otto & Bliesner 1999; Liu *et al.* 2000), which have found a cooler EP and an increased zonal gradient. Due to uncertainties in and lack of proxy data from the mid-Holocene (Lea *et al.* 2006), climate models cannot confidently test their highest accuracy against reconstructed mean state components from the mid-Holocene.

Additional SSTs reconstructed from the southern margins of the IPWP have shown that a cooling event occurred at approximately 5.8 – 4.3 kyr BP (Abram *et al.* 2009). This cooling event indicates that a contraction of the southern end of the IPWP may have occurred. Because evidence regarding mean state evolution during this time period is insufficient, the way in which the mean state of the Pacific influenced this contraction is inconclusive (Abram et al 2009). Three hypotheses for the cooling trend at the southern margins of the IPWP were: (1) a mean La Niña-like state; (2) a mean El Niño Modoki-like state and (3) meridional changes in SST. SST from the CP would add valuable information regarding mean zonal SST configurations, which would be useful in addressing these three scenarios.

Additional late-Holocene reconstructions have also indicated more variable strengths of the SST gradient than what was suggested by Koutavas *et al.* (2006). Mean SST gradient reconstructions from the late-Holocene have shown that the strengthening and weakening of the SST gradient occurs on centric timescales (Conroy 2010). Evidence suggests that during the medieval climate anomaly (1000 – 1300 AD), the SST gradient was 1.5 °C stronger than today (Conroy 2010), which comparable to mid-Holocene SST gradient strengths. After this period, it was proposed that the gradient weakened in two steps at 1250-1300 and then at 1650 AD. SST reconstructions from the CP have also been

calculated for the periods that overlap with the data presented in Conroy *et al.* (2010). Results indicate that the SST was strengthened during the Medieval Warm Period (MWP) and weakened during the Little Ice Age (LIA) (Cobb *et al.* 2003). These results are in line with the gradient calculation from Conroy *et al.* (2010), and thus suggest that SST gradients measured from the CP can be achieved accurately. Another mean east-west SST gradient from the CP has been measured at ~1.7 kyr and indicates that there was an increased gradient at this time similar to a modern gradient during a La Niña event (Glasbergen 2010). However, no more mean SST gradient measurements have been calculated from the CP because of limited mean SST data reconstructions from this region.

2.2.1 Mean state and ENSO throughout the Holocene

Holocene ENSO has been reconstructed from lake sediment records (Moy *et al.* 2002; Conroy *et al.* 2008) and from δ18O values preserved in coral (Tudhope *et al.* 2001; Woodroffe *et al.* 2003; McGregor & Gagan 2004). Nearly all paleoclimate ENSO records have been reconstructed over the last decade (Cane 2005), and these have shown the significant variations through which the ENSO phenomenon has been. Lake and ocean sediment records provide a near-continuous record of ENSO, and indicate that it has increased in variability since the mid-Holocene reaching its greatest intensity in the late-Holocene at ~2-1.5 kyr BP (Moy *et al.* 2002; Conroy *et al.* 2008; Makou *et al.* 2010). Coral records have provided a more accurate but less continuous record of ENSO behaviour. These records are consistent with the lake records' findings, which show that ENSO has increased in variability from the mid to late-Holocene (Tudhope *et al.* 2001; Woodroffe *et al.* 2003).

Changes in the behaviour of ENSO throughout the Holocene have corresponded with changes in the SST gradient's mean strength. For example, both climate models (Clement *et al.* 2000) and proxy records (Rodbell *et al.* 1999 {Koutavas, 2002 #31; Tudhope *et al.* 2001; Moy *et al.* 2002; McGregor & Gagan 2004; Conroy *et al.* 2008; Donders *et al.* 2008; Abram *et al.* 2009) have documented the reduction in El Niño activity during the mid-Holocene (amplitude and frequency) that corresponds with an increase in the east-west SST gradient (Koutavas *et al.* 2006). Additionally, both paleo and modelling studies of ENSO during late Holocene indicate that there was increased El Niño activity (Moy *et*

al. 2002; Woodroffe *et al.* 2003; McGregor & Gagan 2004; Conroy *et al.* 2008) at a period when a reduced mean SST gradient was also suggested (Koutavas *et al.* 2006). Furthermore, both model and data-based studies for the last 1 kyr suggest that ENSO varies more with warmer SST than cooler SST in the EP (Cane 2005).

However, other studies have observed an enhanced mean gradient during the late-Holocene (Cobb *et al.* 2003; Glasbergen 2010), which suggests that ENSO is not solely influenced by the mean SST gradient. Additionally, reconstructed ENSO behaviour from corals have shown large scale variability of ENSO that could not be explained by changes in the mean state (Cobb *et al.* 2003). Because ENSO behaviour is not always reflected by the mean state, ENSO variability could be related to the internal dynamic responses of the ENSO system (Cobb *et al.* 2003). Although, ENSO variability and the mean state of the Pacific have been found to be related, the way in which they are related is yet to be fully understood (Zheng *et al.* 2008). The fact that different strengths in the mean gradient have correlated with similar ENSO behaviour indicates that more work regarding these interactions needs to be done to increase the understanding of this relationship; consequently more accurate future predictions can be made. A more thorough understanding of this relationship could be achieved by: (1) clarifying how mean SST gradients changed throughout the mid-Holocene and (2) documenting how the mean SST gradient accompanied major changes in ENSO variance through the Holocene (Cane 2005).

2.3 This project

Previous simulations from the CSIRO MK3L climate model suggest that during 5.5 – 4.3 kyr BP., the CP was anomalously cold relative to the present day SSTs. Yet, no SST data exists from the CP to test the model results. Thus, the first aim of this project is to:

1. Reconstruct CP SSTs for the period 5.5-4.3 kyr BP., using the Sr/Ca ratios of fossil corals collected from Kiritimati (Christmas) Island, CP.

The fossil corals used to achieve aim 1 are a subset of ~120 corals that span the period from ~6-1 kyr. The mid-Holocene, where almost nothing is known about mean SST variability in the CP, falls within this time period. Thus, the second aim of this study is:

2. To reconstruct a near-continuous sub-millennial evolution of mean SST at Christmas Island from 6.4 kyr to present using coral proxy Sr/Ca.

This unique SST dataset from the CP will provide a new perspective on mean gradient evolution from the mid to late-Holocene and will allow two mean gradient to be calculated. Because this dataset will provide a more in-depth understanding of mean state evolution, it will aid in current knowledge of mean state – ENSO interactions. The third aim of this project is to:

3. Compare mean SST evolution from the CP with available SST datasets from the east and west Pacific to create a mean gradient SST evolution from the WP to the CP and the CP to the EP. This newfound perspective on mean state evolution will then be compared with mid to late-Holocene reconstructions.

These aims will be accomplished by using the geochemical signatures preserved in ~120 fossil corals from Kiritimati Island to reconstruct SSTs. Prior to geochemical analysis, each coral will undergo stringent screening methods to ensure that they yield accurate results. The corals that pass the screening procedures will be prepared using recommended techniques (McGregor & Abram 2008; Abram *et al.* 2009). To obtain average SST estimates, bulk samples that vary in length (years of growth), will be collected from each coral sample. The length of the bulk sample will reflect the amount of years the average SST represents. The coral material collected from the coral samples will be analysed for its Sr/Ca ratios at the Australian Nuclear Science and Technology Organisation (ANSTO). The calculated Sr/Ca value and its associated uncertainty will be calibrated to SST. The following section will address current issues regarding the use of Sr/Ca as a SST proxy.

2.4 Reconstructing SST from corals

2.4.1 Past Sr/Ca SST studies

SST is the most documented and most important factor in climate and oceanography studies (Corrège 2006). Since the 1970s, studies have started to identify chemical elements preserved in corals that have an association with past climate variables, most notably SST and sea surface salinity. The two most common and reliable SST tracers from corals are $\delta^{18}O$ and Sr/Ca. It is believed that Sr/Ca is a cleaner tracer than $\delta^{18}O$ due to far less variability of the ratio in seawater over time (Corrège 2006).

Beck *et al.* (1992) was the first study to accurately reconstruct SST from Sr/Ca ratios in corals, which brought widespread attention to this method. This study obtained highly accurate measurements of Sr/Ca through the use of thermal ionization mass spectrometry (TIMS), a device that is still commonly used today (Abram *et al.* 2009). The groundbreaking study by Beck *et al.* (1992) solidified Sr/Ca ratios in corals as a robust SST proxy by showing a correspondence of Sr/Ca reconstructed SST with actual recorded SST at multiple sites. The study applied this reliable method to reconstruct SST from tropical fossil corals dating back approximately 10 kyr.

A summary of all the studies prior to 2006 that link Sr/Ca ratios from corals to SST through calibrations is outlined in Corrège (2006). Although this technique has been used successfully for almost two decades, aspects of it are still not fully understood, particular those that relate to using Sr as a paleothermometer.

2.4.2 Coral skeleton formation

Although coral skeletal formation has been studied for over 120 years, because the processes responsible for the formation of calcium carbonate ($CaCO_3$) aragonite are complex, a thorough understanding as to how skeleton formation occurs has yet to be attained (Cohen & McConnaughey 2003; Corrège 2006). Corals form an exoskeleton through a process called biomineralisation, which occurs beneath a layer of organic matter in cells close to a semi-permeable membrane known as the calicoblastic ectoderm (or

basal ectoderm of polyps) (Figure 4) (Corrège 2006). The coral draws in large amounts of Ca and inorganic C from the surrounding sea water to build a mineral skeleton, which also contains an organic fraction (Allemand *et al.* 2004). At a scale as small as a nanometre, individual aragonite crystals are precipitated and arranged into skeletal elements, such as dissepiments, septa and sclerodermites (Nothdurft & Webb 2007).

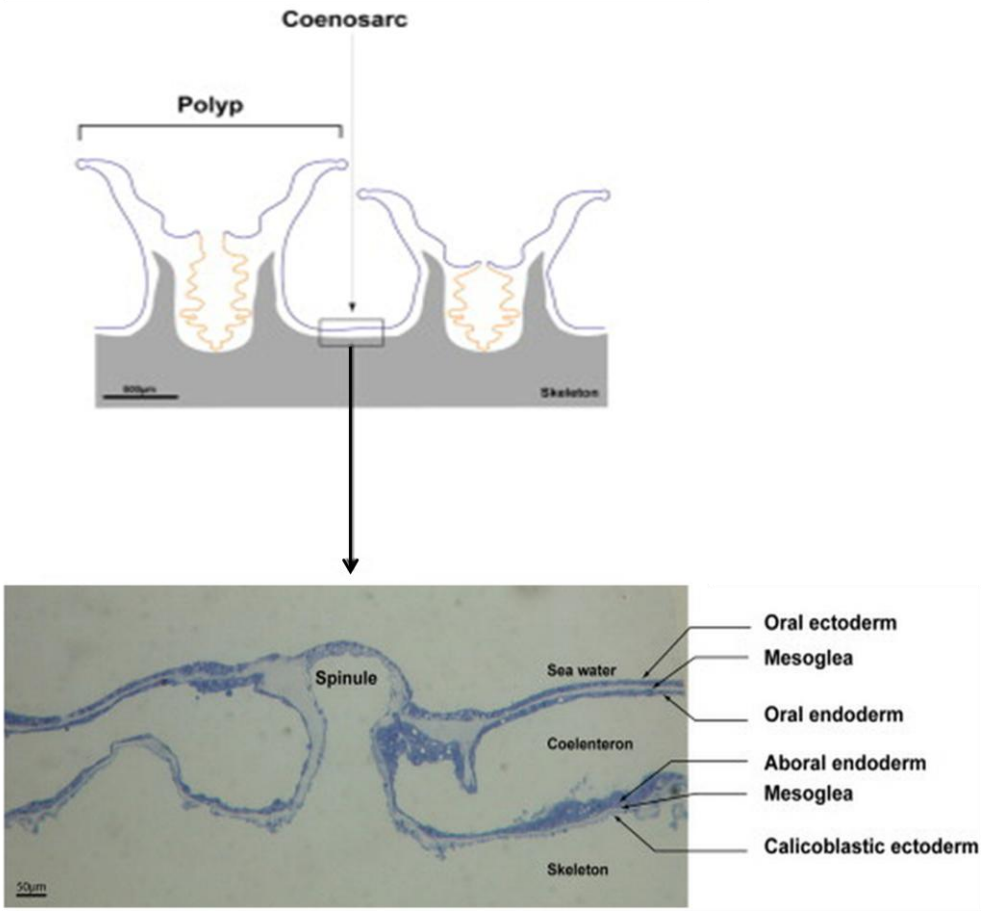

Figure 4. Microscopic anatomy of a coral polyp. **(A)** Shows the coenosarcal tissue that links individual polyps. **(B)** Close up image of coenosarcal tissue showing the anatomy of coral tissue and the calicoblastic ectoderm, the location of biomineralisation. Image modified from Allemand *et al.* (Allemand *et al.* 2004).

A simple view of skeleton formation starts with the centre of calcification (COC), which is described as precipitated granular crystals close to the calicoblastic ectoderm of the polyp. From the COC, crystalline fibres termed 'sclerodmites' radiate out away from the COC (Corrège 2006). There is debate in the literature that regards how organic material is incorporated into the skeleton (Cuif *et al.* 2004) and whether calcification takes place inside cells or outside the ectoderm of the polyp (Corrège 2006). In addition to

determining where calcification takes place, there are also uncertainties regarding the mechanisms that corals use to form their skeleton (Sinclair & Risk 2006). Two major and distinctly different ideas for skeletongenesis have been discussed 'physiochemical calcification' and 'organic matrix calcification'. Physicochemical calcification involves the skeleton freely precipitating from a pocket of sea water modified by enzymatic ion transport, whereas organic matrix calcification starts with and is controlled by an organic matrix secreted by the coral. There is evidence to suggest that both hypotheses of the mechanisms corals use to form their skeleton are correct.

2.4.3 Strontium and corals

Although Sr/Ca-based SST studies over the last two decades (Beck *et al.* 1992; Glasbergen 2010) have repeatedly found that the Sr/Ca in corals has an inverse relationship with SST, the specifics of Sr uptake are not fully understood nor are all of the contributing variables known. Understanding how Sr is incorporated into the coral skeleton is an important factor in determining the robustness of Sr/Ca's role a paleothermometer (Corrège 2006). Two hypothesises for Sr incorporation into the coral are commonly debated in the literature; 1) Sr and Ca are incorporated into the skeleton by similar, active transport pathways (Ferrier-Pagès *et al.* 2002), or 2) Sr is incorporated through passive diffusion pathways, where Ca is transported by different mechanisms, such as the CaATPase pump (Sinclair & Risk 2006). Previous geochemical and model based studies reveal that Ca is incorporated into the skeleton by either diffusional or active Ca^{2+} ATPase pathways. Since Sr most likely substitutes for Ca when it is incorporated into the skeleton (Corrège 2006), it can be said that Sr incorporation is by at least one of the following mechanisms, the diffusional or active Ca^{2+} ATPase pathways (Zeko 2009).

The different Sr incorporation mechanisms can help to explain why corals can exhibit heterogeneity of Sr/Ca values. Because the CaATPase pump is activated by light, active transport dominates during the day. Since this mode of transport favours Ca over Sr, the daytime skeleton is Sr-depleted (Al-Horani *et al.* 2003). When active transport is reduced or is immobile (night time), passive transport dominates. As a result, a skeleton with a higher Sr/Ca ratio is formed (Cohen & McConnaughey 2003).

Sr/Ca concentrations also vary throughout the different structural features of a coral. The selective sampling of corals has shown that the fascicule (fine aragonite crystals that grow from the COC) and COCs can exhibit large Sr/Ca differences, that are not temperature dependent (Allison & Finch 2004). Results indicated that the COC contained a higher Sr/Ca ratio than the fascicule. The findings of reduced Sr/Ca values in the fascicule than the COC are consistent with results found by Cohen & McConnaughey (2003), which indicate that Sr/Ca values decline away from the COC. Although, Allison and Finch (2004) provide evidence for heterogeneity of Sr/Ca in the coral, the study also highlights that the differences in Sr throughout that coral are negligible when sampling resolution is increased, which provides a good explanation for the correlation between Sr/Ca and SST. Additionally, the difference between Sr/Ca values in the COC and fascicule is not a major issue in larger sampling techniques (such as used in this study) because 99% of the skeletal mass is from fascicule or aragonite fibre bundles (Cohen & McConnaughey 2003).

Growth rates are thought to influence the uptake of Sr in corals and subsequently affect the Sr/Ca SST proxy (de Villiers *et al.* 1995). Thus, they can potentially impact the reliability of the Sr/Ca SST reconstructions. Early work regarding the effects of growth rates on Sr/Ca values in corals (de Villiers *et al.* 1995) showed that some coral species that live in the same locality with different growing rates can yield different Sr/Ca SST reconstructions. The idea of growth rates influencing Sr/Ca uptake has been given further attention by Cohen and Hart (2004), who showed that growth rates impact the Sr/Ca ratios in wintertime growing corals, but not the Sr/Ca ratios from summertime growing corals. Additional studies have discussed and noted the influence of growth speed in Sr uptake (Alibert & McCulloch 1997; Reynaud *et al.* 2004; Goodkin *et al.* 2007). In contrast to these previous findings, Sr incorporation into the coral has also been shown to be independent of growth rates. By calculating Sr/Ca values of COC vs. fasiculi at different extension rates, it was shown that the speed at which the coral grew did not affect the Sr incorporation into either part of the coral (Allison & Finch 2004). Numerous studies have documented that growth rates do not affect the Sr/Ca values as long as sampling is done along the maximum growth axis of the corallite fans (Alibert & McCulloch 1997; Gagan *et al.* 1998; Wei *et al.* 2000; Corrège *et al.* 2004). Thus, Sr/Ca ratios can successfully avoid growth rate effects. Furthermore, it has been shown that growth speed only

influences Sr/Ca ratios for corals that grow ≤5mm/year (de Villiers *et al.* 1995) and less than 6mm/year (Felis & Pätzold 2003).

One assumption previously made when reconstructing Sr/Ca ratios in estimating past climate parameters, is that spatial and temporal changes in Sr/Ca are relatively small (Beck *et al.* 1992; Gagan *et al.* 1998). However, modern spatial variations in Sr/Ca have been shown to be as high as 1.4%, which is a level high enough to strongly impact the accuracy of SST reconstructions (de Villiers 1999). Spatial variations in Sr/Ca may be due to the dissolution cycle of celestite skeletons caused by acantharia and calcium carbonate oceanic cycles. To address this issue of spatial variations in Sr/Ca, studies have used site-specific calibrations, in which the Sr/Ca values are calibrated against the local instrumental record to ensure to highest level of accuracy. Various studies have calculated calibrations for Kiritimati Island (Evans *et al.* 1999; Nurhati *et al.* 2009; Glasbergen 2010), although they show considerable differences. (Corrège 2006) has compiled calibrations from all *Porites sp.* based Sr/Ca studies prior to 2006. Of these 37 calibrations, the vast majority fell within ±2°C of 25°C after Sr/Ca value of 9.035 mmol/mol was applied to each calibration. An assessment of these past studies' calibrations allowed an average calibration to be calculated to be Sr/Ca=10.553-0.0607*SST. Error in climate reconstruction from spatial variations in Sr/Ca can be minimised by site-specific calibrations. Variations in Sr/Ca over time, however, could be a bigger issue for authors that assume a consistent Sr/Ca ratio to reconstruct SSTs from fossil corals. It is likely that the Sr/Ca ratio of water has varied by 1-3% during glacial cycles over the last 150 kyr (Stoll *et al.* 1999). Foraminifera and modelling data suggests that Sr/Ca ratios in seawater varied most during glacial maximums and the time periods that followed glacial conditions. Using Sr/Ca to assess past climate over the last 6 kyr is, therefore, a relatively suitable time period in regards to temporal variations of Sr/Ca values, as no major boundary conditions changes have occurred.

2.4.4 Assessing coral preservation

The Sr/Ca values in corals that were incorporated into their mineral lattice at the time of their growth may change significantly over time. If chemical changes occur, fossil corals' ability to accurately reconstruct past climate variables is reduced. A post-depositional change in the geochemistry of a fossil coral is known as diagenesis, and it is now recognised as a major source of error in paleoclimate reconstructions (Müller *et al.* 2001;

McGregor & Gagan 2003; Hendy *et al.* 2007; McGregor & Abram 2008). This section describes the pristine structure of coral skeleton, varieties of diagenesis and commonly used screening methods for diagenesis.

2.4.4.1 Coral skeleton structure

In order to determine the preservation of a fossilised coral, knowing the structure of a pristine coral is necessary. One common feature of corals, the dissepiments, is a thin horizontal sheet on which the polyp sits. As the skeleton precipitates, the polyp pulls itself up the tube in which it is sitting (corallite). It then forms new dissepiments above and leaves the old one behind. An individual polyp occupies the top of the corallite, which is a tube-like skeleton composed of a wall, termed theca, and vertical radiating divisions within the walls that are referred to as the septa. Platform lobes grow off the septa and meet in the middle of the corallite forming the columella (Figure 5) (Cohen & McConnaughey 2003).

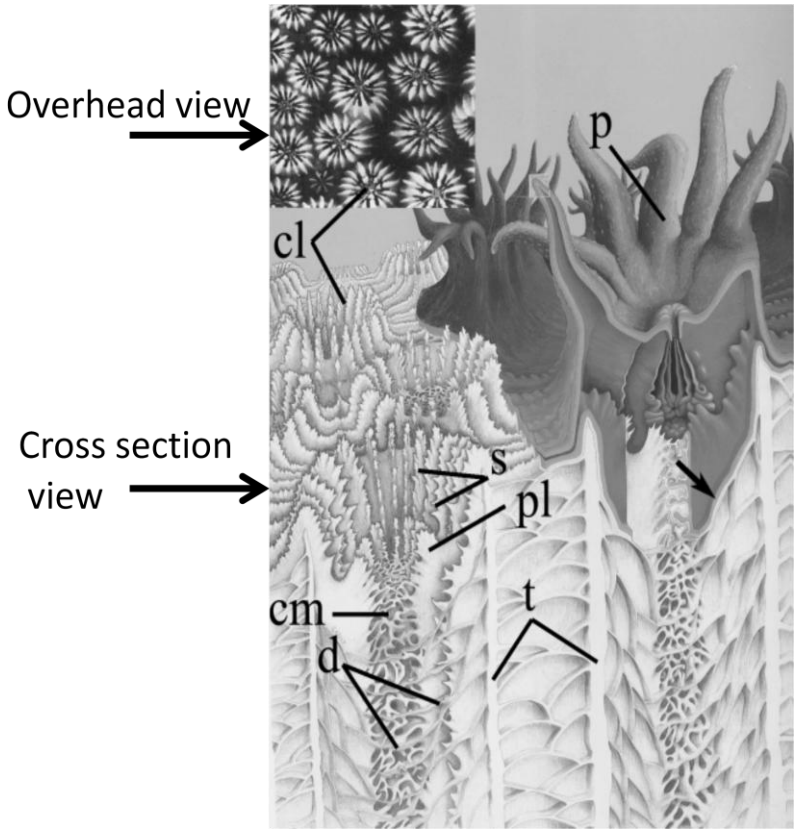

Figure 5. Illistration of coral skeleton, showing the polyp (p), corallite (cl), dissepiments (d), septa (s), theca (t), platform lobes (pl) and the columella (cm). Figure modified from Cohen and McConnaughey (2003).

At a magnification of times 10 to times 20, other skeletal features are useful in determining the preservation of the fossil coral (McGregor & Abram 2008). One feature that it is particularly useful in determining corals' preservation is the COC. The COC was first recognised as a dark blob by Ogilvie (1896), yet today is commonly observed as a dark line in the centre of the trabeculae (McGregor & Abram 2008). The preservation of the COC can help to determine if dissolution has occurred in the fossilised coral (McGregor & Abram 2008). From the COC grow fine aragonite crystals termed fascicule (~0.05-4 μm in diameter) (Figure 6). The fans of fasciculi form fish-scale shaped bundles called sclerodermites. Once multiple sclerodermites are all growing together, they form a vertical spine known as trabeculae. Groups of trabeculae construct the septa, or primary structures of the coral skeleton(Cohen & McConnaughey 2003).

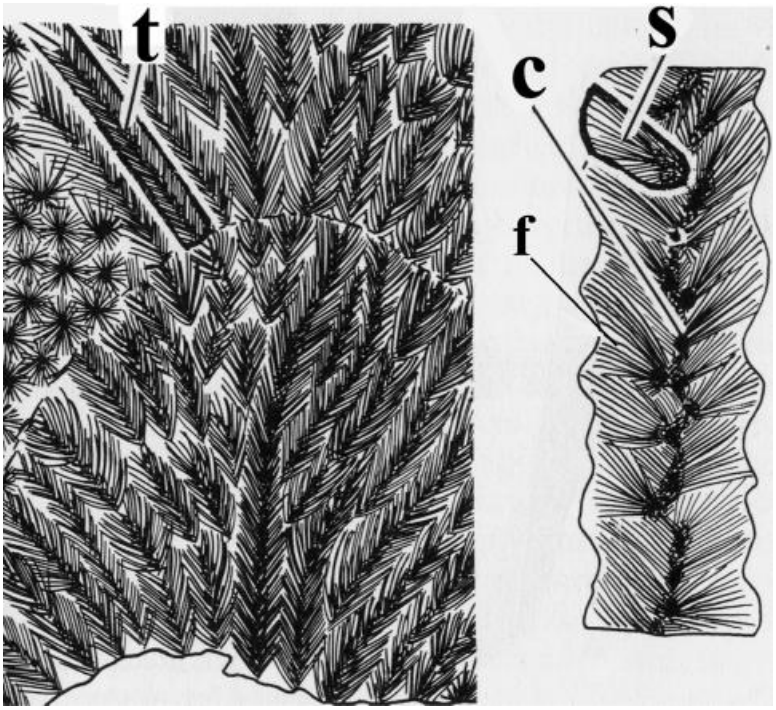

Figure 6. Illustration of fine scale scleractinian coral features, showing fibre bundles or fasciculi (f), sclerodermites (s), COC (c) and trabeculae (t). Image from Cohen and McConnaughey (2003).

2.4.4.2 Sr/Ca in fossil corals

Since diagenesis is a recognised source of error in SST reconstructions (McGregor & Abram 2008), it is necessary to identify different types of diagenesis, discuss how it occurs and influences SST estimates, and finally, explain how diagenesis can be avoided.

As coral geochemistry has become better understood, it has become clear that corals must be screened for diagenesis prior to their inclusion in paleoclimate analysis in order to reduce substantial error (McGregor & Gagan 2003; Hendy *et al.* 2007; McGregor & Abram 2008). In regards to corals, diagenesis has been defined as the precipitation of calcite or secondary aragonite within the skeletal voids or through the replacements of the original aragonite (Bathurst 1975). Another form of diagenesis that has received less attention than calcite and secondary aragonite is dissolution through incongruent leaching. It has been shown that dissolution impacts trace element SST reconstructions, including Sr/Ca analysis (Hendy *et al.* 2007). During diagenesis, isotopes and trace elements are subjected to change, which alters the geochemistry of the skeleton. Therefore, all paleoclimate studies that base their results off the geochemistry of a coral at the time of its formation, including Sr/Ca based reconstructions, must thoroughly screen for diagenesis to avoid erroneous results.

Diagenesis can occur in corals as early as 3 years after the living tissue has left its skeleton (Nothdurft & Webb 2009). Conversely, diagenesis may be absent in a coral for periods longer than 7 kyr (McGregor & Abram 2008). The age of the fossil does not necessarily show a correlation with increased diagenesis, but the zone from where the coral is preserved does increase the likelihood of the type of diagenesis that occurs within the coral (McGregor & Abram 2008). Fossil corals that show growths of secondary aragonite needles are typically associated with marine environments in which the pores of the coral are partly or completely saturated by sea water (Longman 1980). Calcite diagenesis in fossil corals are associated with fossils being preserved in marine and freshwater environments, where there is a mixture of air and water within the pore spaces (vadose zone), and in freshwater zones where the pores are completely saturated (Longman 1980). Dissolution of the coral can occur in any environment and the rate of dissolution is controlled by CO_2 levels (Hendy *et al.* 2007).

The influence that secondary aragonite and coral dissolution has on Sr/Ca SST reconstructions has been estimated to give cooler reconstructed temperatures of -1.7°C and – 1.2°C, respectively (Hendy *et al.* 2007). Secondary aragonite has also been shown to impact Sr/Ca values, where estimates of SST ~4-5°C cooler were recorded in comparison to other diagenetic free parts of a *Porites Lobata* core (Müller *et al.* 2001). Approximately 2% of secondary aragonite has been linked to a reduction of -0.4°C to -0.9°C when reconstructing Sr/Ca SST (Allison *et al.* 2007). Secondary aragonite has recently been

shown to have a much larger impact on Sr/Ca SST based reconstructions than $\delta^{18}O$ SST based reconstructions (Sayani *et al.* 2011). This finding highlights the need to detect and eliminate corals with secondary aragonite, particularly when using Sr/Ca. Calcite levels in corals have been shown to severely impact the accuracy of SST Sr/Ca reconstructions (McGregor & Gagan 2003). Sa/Ca levels drop dramatically when calcite levels of just one percent calcite are present. It was shown that such minimal calcite occurrences can result in warmer temperatures of 1.1-1.5°C being recorded. These results are consistent with the findings from Allison *et al.* (2007), in which 1% calcite contamination increased Sr/Ca SST estimates by 1°C. The error associated with calcite diagenesis is particularly high for Sr/Ca analysis as it is has been shown to be at least five times higher than that of $\delta^{18}O$ (McGregor & Gagan 2003). Evidence from these studies highlights the inaccurate results that diagenesis causes and reinforces the need for vigorous screening to detect and avoid diagenesis in paleoclimate reconstructions.

Screening methods that detect relatively large amounts of diagenetic material (>10%) include coral density profiles, X-radiograph and UV luminescence photographs (Hendy *et al.* 2007). The most common screening method for coral-based paleo studies is X-ray diffraction (XRD). XRD measures the different minerals within a coral. A limitation of XRD is its inability to detect secondary aragonite because it has the same crystal structure as primary aragonite. Also, significant amounts of calcite (<1%) may be undetected due to the detection limits of XRD (Allison *et al.* 2007). Furthermore, XRD cannot detect dissolution of the coral. These limitations can be overcome by using additional screening tools, such as a scanning electron micrograph (SEM) (Allison *et al.* 2007; Hendy *et al.* 2007; Nothdurft & Webb 2009) and a petrographic sections (thin sections) (McGregor and Abram, 2008; Allison et al., 2007). These tools have been successfully used to identify small scale diagenesis (<1%), including dissolution and secondary aragonite. Guidelines to assist scientists in screening for diagenesis through the use of thin sections are presented in McGregor and Abram (2008). Additionally, Hendy *et al.* (2007) describes how to identify a variety of diagenetic features observed through a SEM. Overall, if diagenesis is successfully avoided, robust estimates Sr/Ca can be used to reconstruct past SSTs (Sayani *et al.* 2011).

2.5 Regional setting: Kiritimati Island

Corals from this study come from Kiritimati (Christmas) Island, Republic of Kiribati (157^0 30' W, 2^{0}00' N) (Figure 7). Kiritimati Island has a land area of 321km^2 making it the largest coral atoll in the world (Woodroffe & McLean 1998). This atoll's highest point is 13m, and it is bordered by a narrow coral reef flat (Woodroffe & McLean 1998). Most significantly, the inner island is composed of well-preserved fossil coral carbonates, which are rare and desirable for paleoclimate research. When past sea levels were relatively higher, there was an extensive lagoon in the interior of the island where microatolls grew (Woodroffe *et al.* 2003). Because microatolls live in shallow waters, their vertical growth is restricted by low tide causing them to grow mostly laterally. The corals can reach up to 6m in width and grow for hundreds of years. The large fossil microatolls on the Island contain a wealth of climate information that dates back thousands of years. Smaller records from individual corals are also of importance because they can be used to reconstruct mean SSTs over the last 6 kyr as is done in this project.

The island is positioned well-within the ENSO significant Niño3.4 SST region, which is a region that partially overlaps both Niño3 and Niño4 regions (Figure 7). The NINO indices represent the difference in mean SST from the long-term mean and are used to monitor ENSO events (Bureau of Meteorology a 2011). SST anomalies in the Niño3.4 region have a higher correlation with the SOI index (measures ENSO strength) than does Niño3 index. Average monthly temperatures for El Niño events are warmer at ~30°C and cooler for La Nina events at ~24°C, a range of ~ 6°C depending on which ENSO phase is active (Woodroffe et al. 2003). These SST fluctuations are some of the highest ENSO related fluctuations known (Evans et al. 1998). SSTs change little (<1°C) from the mean (~27°C) during normal annual fluctuations at Kiritimati Island. Kiritimati Island is an optimum location for capturing SST variations caused by ENSO and its location is most advantageous for monitoring ENSO at a range of timescales (Evans *et al.* 1998). Mean SSTs from Kiritimati Island have the potential to link previously constructed SST data sets from the east and west Pacific Ocean. Particularly, mean SSTs between the CP and the EP have the ability to recreate the prominence of the mean equatorial cool tongue over the Holocene.

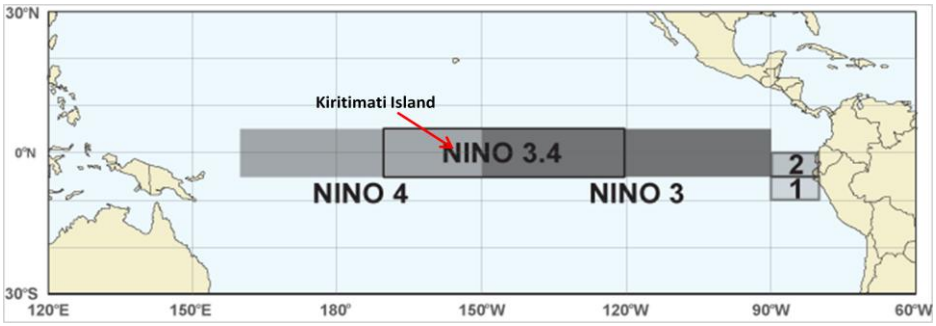

Figure 7. Location of Kiritimati Island and NINO regions in the Pacific Ocean. Image modified from Bureau of Meteorology a (2011)

3. Methods

3.1 Sample collection

Coral samples were collected during the 2007 and 2009 expeditions to Kiritimati (Christmas) Island, Kiribati, which is located at ~157°30'W, 2°00'N (Figure 8A). Samples were taken from fossilised *Porites sp*. microatolls that were preserved at various locations over the low lying atoll. Three types of coral samples were collected: 'hand' (Figure 8B), 'corks' (Figure 8C and D), and large 'slice' samples (Figure 8E). Hand samples were collected using a hammer and chisel and ranged in length from 15-150mm. Cork samples ranged in length from 30-110mm and were collected using a power drill. Slice samples were large lengths of the microatoll (several metres long) and were collected by a concrete saw. Once the samples arrived at the University of Wollongong, a 7 mm piece was cut from the samples using a water-lubricated diamond saw with a 15 cm diameter blade. This piece was used for the geochemical analysis, and the off cuts from the 7mm piece were used for XRD, dating and thin section analyses. A total of 112 coral samples were prepared for both XRD and thin section analysis.

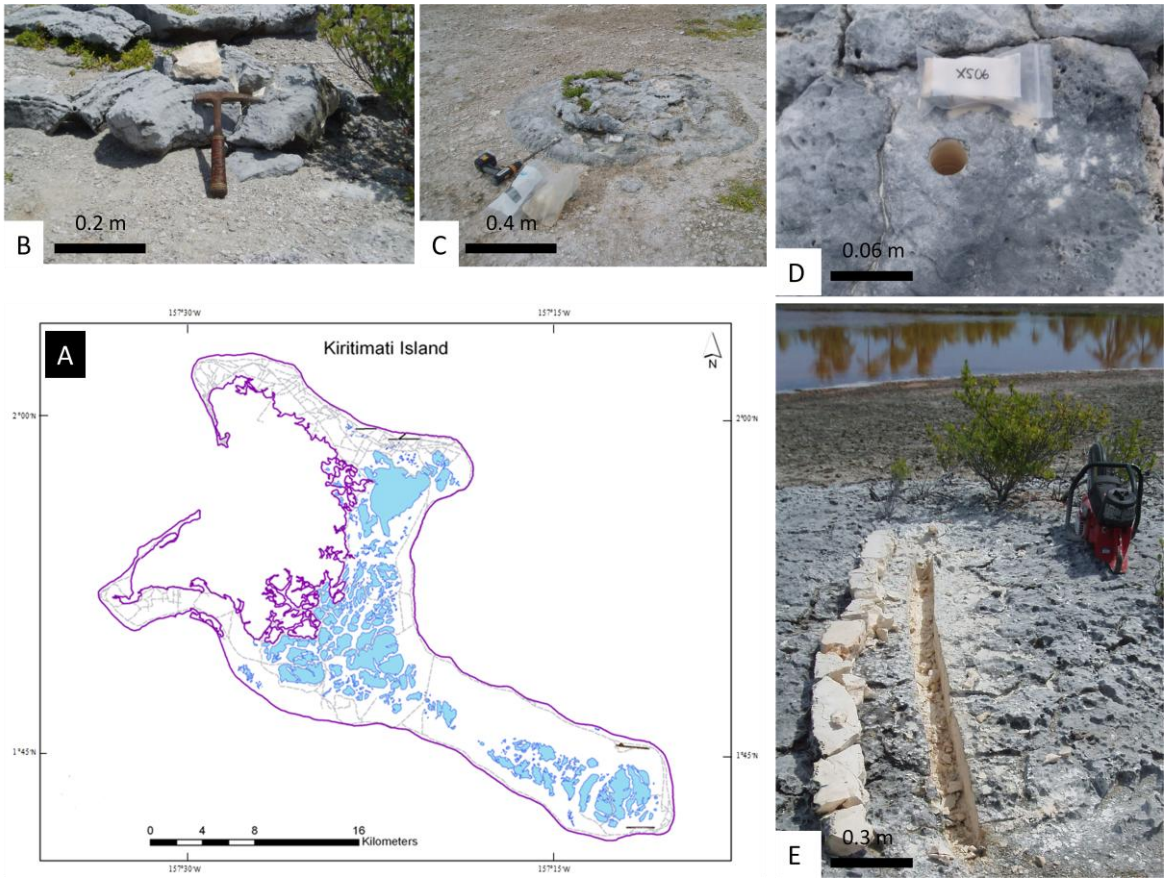

Figure 8. A) Map of Kiritimati Island, Kiribati. **B)** Photograph of the hand sample collection method. **C**) and **D)** show images of the cork collection method. **E)** Photograph of slice sample several metres long. All images were taken from Kiritimati Island in 2009.

3.2 Screening of coral samples

Diagenesis has the potential to be a major source of error in paleoclimate reconstructions (McGregor & Gagan 2003; Allison *et al.* 2007; Hendy *et al.* 2007; McGregor & Abram 2008); see section 2.4.4.2). To avoid diagenesis, all fossil coral samples underwent rigorous screening methods prior to geochemical analysis. Two well-recognised and recommended methods used for screening for diagenesis, XRD and thin section analysis, were carried out for all coral samples (McGregor & Abram 2008; McGregor *et al.* 2011a). Only samples that met the criteria for both XRD and thin section analysis were considered for Sr/Ca analysis.

3.2.1 XRD analysis

Off cuts from every coral sample underwent X-Ray diffraction (XRD) to estimate weight percentages of aragonite and high magnesium calcite. Coral samples were cleaned and crushed in ethanol with a mortar and pestle. Coral material was then measured on a Phillips Goiniometer with a Spellman DF3 Copper X-ray generator run at 1kV and scanned at 2° per minute from a 2θrange of 4-70° spectrum (Glasbergen 2010; McGregor *et al.* 2011a). To measure weight percentages for aragonite and calcite, Traces and SIROQUANT programs were used. The Traces program was used to centre the main aragonite peak at 26.24 degrees theta and to remove the occasional anomalous spike in the XRD results. SIROQUANT V. 2.5 software was used to analyses aragonite and high magnesium calcite percentages. To increase accuracy of the analysis, the background noise was removed in SIROQUANT before values were calculated.

The values for the XRD analysis and the contrast corrected weight values were used to determine the suitability of the coral for further analysis. Corals that recorded aragonite values higher than 99.5% (Aragonite Vs High Mag Calcite) were deemed of a high enough quality for thin section analyses (McGregor pers. comm.).

3.2.2 Thin section analysis

Thin section analysis was used to screen the coral samples for a range of diagenetic features and preservation indicators. Diagenetic features of interest were secondary aragonite, dissolution, other secondary crystals and boring algae. Secondary aragonite is deposited sometime after the coral skeletal aragonite is formed. Primary and secondary aragonite has the same crystal structure and cannot be differentiated by XRD. It is important that samples are free of secondary aragonite as it changes the coral geochemistry, giving cooler SST estimations (Müller *et al.* 2001; Allison *et al.* 2007). Dissolution removes coralline aragonite and is also not detected by XRD (Hendy 2007). Visual techniques, such as thin section analysis, have been proven effective in detecting these and other features that are indicative of the preservation state of the coral (McGregor & Abram 2008).

To prepare samples for thin section analysis, samples were cut along the maximum growth axis and set in an eproxy resin. Samples were then placed on a thin section (60 by 20 mm), and ground down to the thickness of 0.03mm. After reaching the ideal thickness, the thin section was covered by a glass slide and labelled. Thin sections were analysed and photographed using a Leica DM750p polarising microscope with a DFC295 fitted digital

camera and Leica Microsystems Application suite V3 software. The brightness, contrast and colour were adjusted prior to taking the photograph. Photographs were taken at 4, 10, 20 and 40 times magnification in plane and cross-polarized light. Photographs were taken to show the preservation of major features, such as the centre of calcification, septa, dissepiments, trabeculae, fascicule and sclerodermites. Photographs were also taken to show diagenetic features, such as dissolution, boring algae, calcite and secondary aragonite crystals.

Each coral's preservation was ranked excellent, good- excellent, good, good-fair, fair, fair poor or poor. Guidelines for the categories "excellent", "good", "fair" and "poor" were based on recommendations from McGregor and Abram (2008) and are shown Table 1. Example images for each category are shown below in Figure 9 to Figure 12. Only coral samples that had excellent, good-excellent or good preservation and passed the XRD screening methods were considered for further analysis.

Table 1. Guidelines for qualitative thin section analysis of the preservation state of coral samples. In addition to observed secondary crystals and dissolution, other diagenetic features, such as evidence of boring algae, were noted, if observed.

State of Preservation	Amount of observed secondary crystals and dissolution in thin section	Considered for Geochemical analysis
Excellent	None	Yes
Good	Minimal (~1%)	Yes
Fair	Some-common (~5%)	No
Poor	Significant (>10%)	No

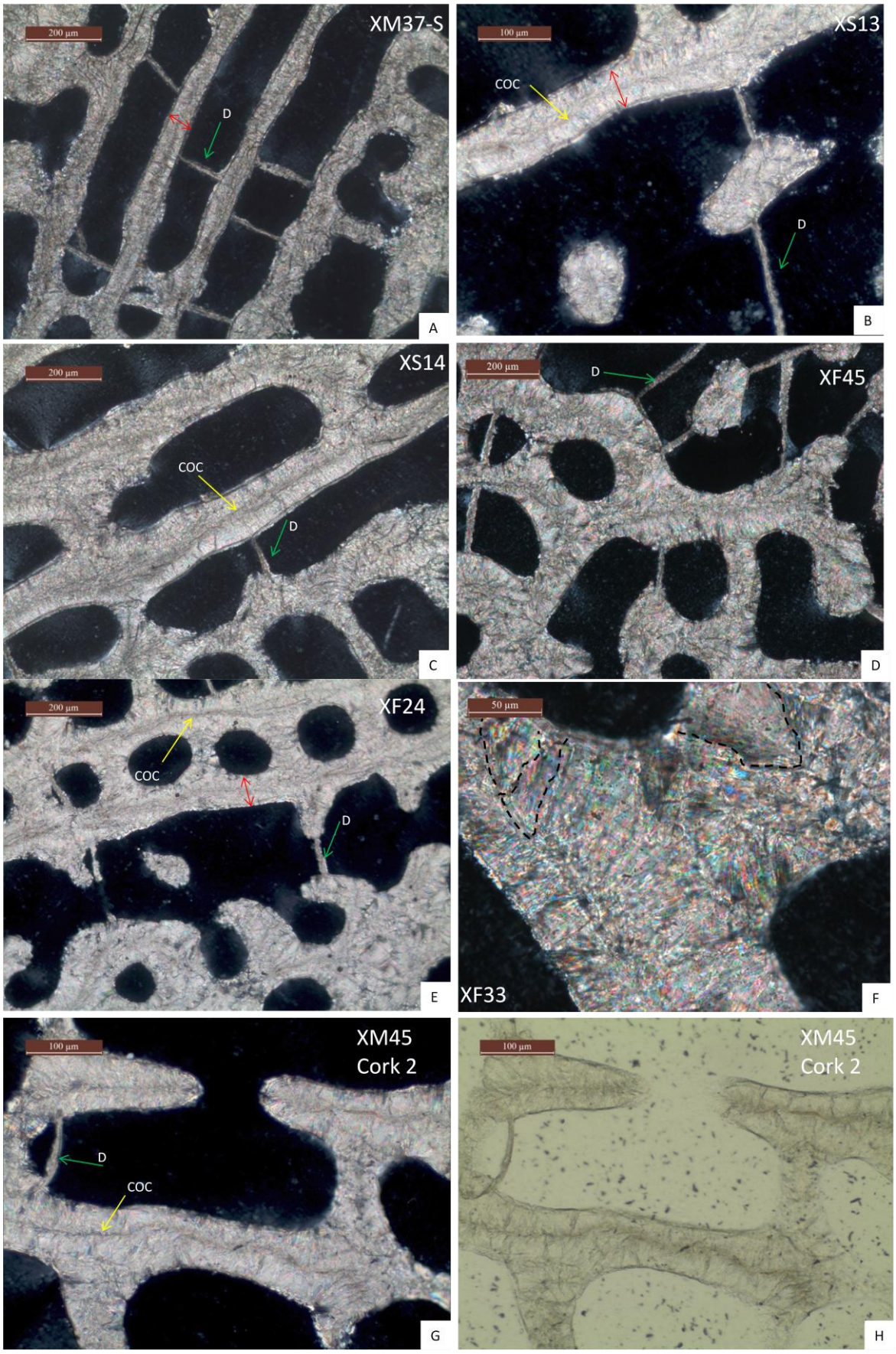
200 µm
XM37-S
D
A
100 µm
XS13
COC
D
B
200 µm
XS14
COC
D
C
200 µm
D
XF45
D
200 µm
XF24
COC
D
E
50 µm
XF33
F
100 µm
XM45
Cork 2
D
COC
G
100 µm
XM45
Cork 2
H

Figure 9. Example thin section images of "excellent" (pristine) fossil coral aragonite. **A)** coral XM37-S **B)** coral XS13 **C)** coral XS14 **D)** coral XF45 **E)** coral XF24 **F)** coral XF33 **G)** coral XM45 Cork 2, all images in cross-polarized light. **H)** coral XM46 cork, is a plane-polarized image of figure 9G. In figures 9A, 9B, 9C, 9D, 9E and 9G green arrow with D reveals exceptionally preserved dissepiments. Preservation of the centre of calcification is highlighted in figures 9B, 9C, 9E and 9G by yellow arrow with COC. Red, double-headed arrows in Figures 9B, 9C and 9E indicate the width of trabeculae, which are perpendicular to the growth of the coral. Figure 9F, shows sclerodermites (dashed black lines), which are made from bunches of fascicule that radiate out from the COC. All images shown in figure 9 have calcite levels below XRD detection limits (0.5%).

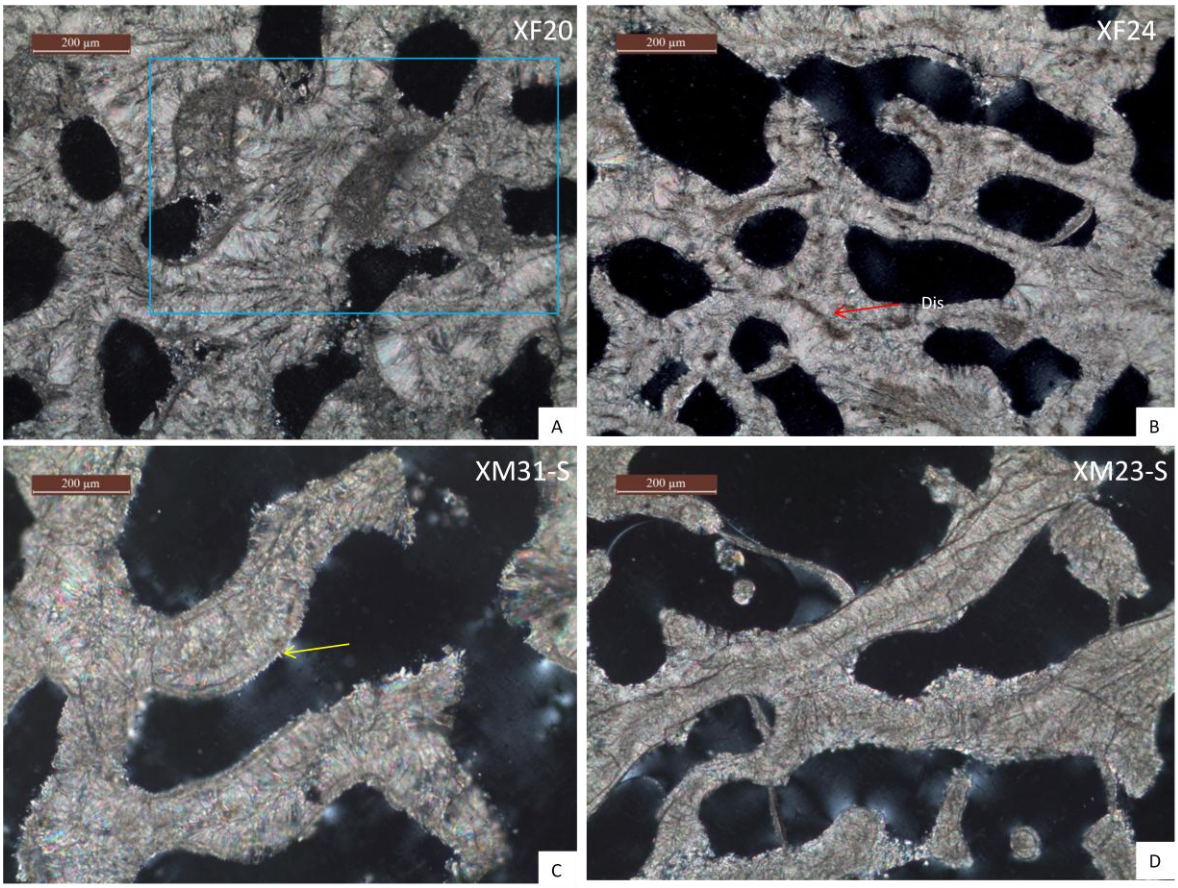

Figure 10. Example thin section images of "good" (minimal diagenesis) fossil coral aragonite. **A)** Coral XF20, blue rectangle represents area with boring algae interference. Boring algae is a post depositional change in the coral and is undetected by XRD. It is not considered to be as significant as other forms of diagenesis, so higher levels of observed boring algae were tolerated. **B)** Red arrow with 'Dis' represents minor dissolution of the COC in coral XF24. **C)** Coral XM31-S, the yellow arrow highlights a very minor crystal fringe that is potentially secondary aragonite. **D)** Coral XM23-S. The features noted in these images were only observed on rare occasions. All images shown in figure 10 are in cross-polarized light and have calcite levels below XRD detection limits (0.5%).

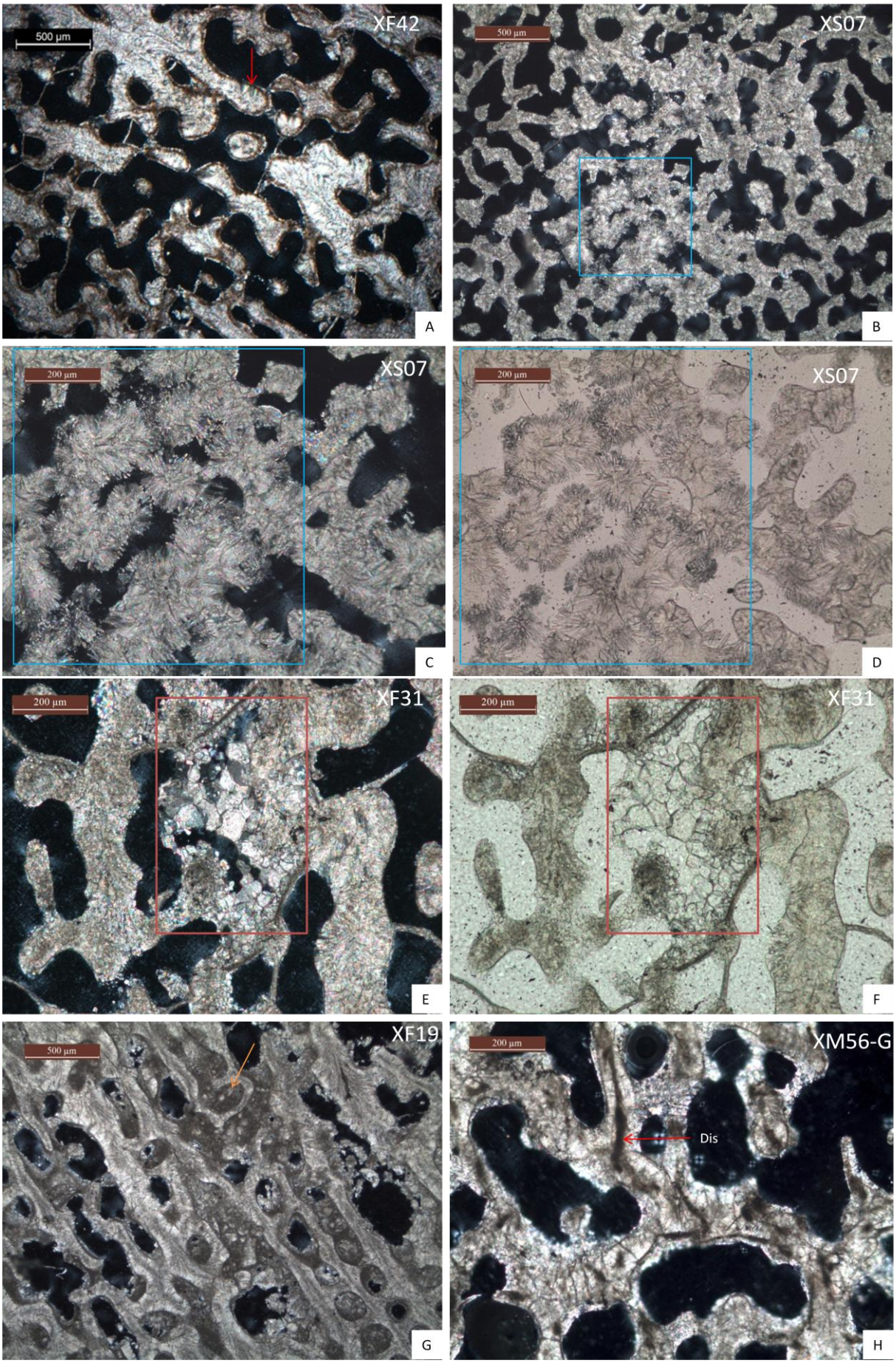
500 µm
XF42
A
500 µm
XS07
B
200 µm
XS07
C
200 µm
XS07
D
200 µm
XF31
E
200 µm
XF31
F
500 µm
XF19
G
200 µm
XM56-G
Dis
H

Figure 11. Example thin section images of "fair" (some-common diagenesis) fossil coral aragonite. **A)** coral XF42 in all in cross-polarized light. Dissolution commonly observed in the form of micritic rims (red arrow). **B)** Coral XS07 at ×4 magnification. Blue rectangle encloses area of secondary crystal growths **C)** Coral XS07 at ×10 magnification shows secondary aragonite needles growing from the aragonite fringe into the voids. Images 11B and 11C are in cross-polarized light. **D)** Coral XS07, plane-polarized image of figure 11C. **E)** Coral XF31, secondary crystals observed within red rectangle. **F)** Coral XF31, plane-polarized image of figure 11E, reveals the shape and size or the secondary crystals. **G)** Coral XF19 in cross-polarized light showing common boring algae (orange arrow) interference. **H)** Coral XM56-G in cross-polarized light shows moderate dissolution of the COC (red arrow with dis). Features that were present in excellent preserved corals are not visible, such as, COC, fasciculi and sharp voids. All corals with a rating of "fair" were excluded from further analysis.

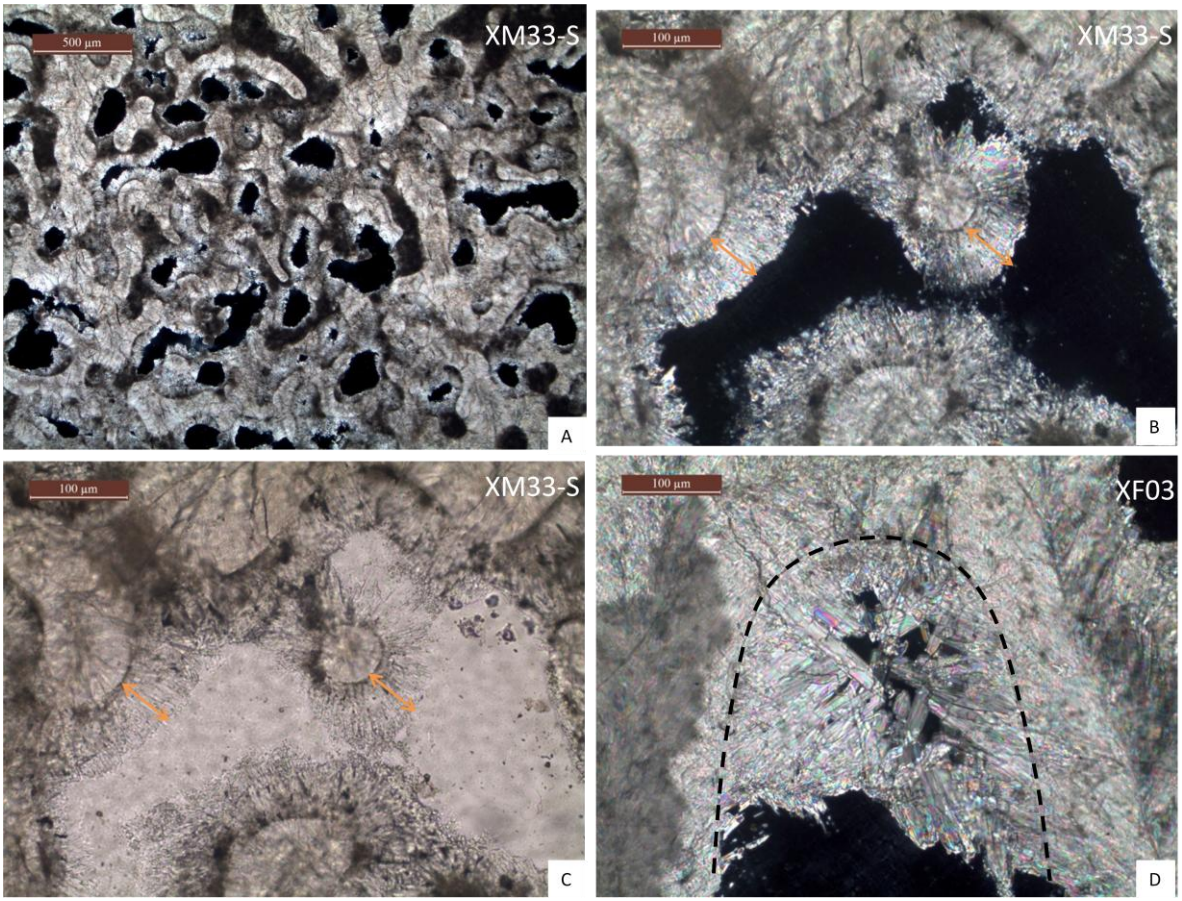

Figure 12. Example thin section images of "poor" (significant diagenesis) fossil coral aragonite**. A)** coral XM33-S at ×4 resolution shows significant widespread diagenesis in the form of crystal growths from fringes. **B)** ×10 magnification of coral XM33-S clearly shows the extent of crystal growths from the fringe (highlighted by orange double sided arrows). Both images are in cross-polarized light. **C)** Coral XM33-S, same image as figure 12B in plane-polarized light. **D)** Cross-polarized light image of coral XF03 showing major void infilling by secondary aragonite. Original void represented by black dashed line. All corals with a rating of "poor" were excluded from further analysis.

3.3 Dating of corals

The corals were dated by either AMS radiocarbon, Laser ablation ICP-MS U-series or solution ICP-MS U-series (see Table 2 for details regarding which coral dating method). Details of the dating methods are described in McGregor et al.(2011a) but in summary: AMS radiocarbon (^{14}C) dating was carried out at Australian Nuclear Science and Technology Organisation (ANSTO). Ages were calibrated using CALIB 5.0 software, the MARINE O4 calibration curve and corrected with a reservoir age (ΔR) of 400 years (McGregor pers. comm.). Laser ablation ICP-MS U-series was measured at the University of Melbourne. Solution ICP-MS U-series dating was carried out at University of Melbourne or the University of Queensland. All coral ages are defined in years before present (BP), where present is 1950 AD.

3.4 Sample preparation methods

Two types of methods used to prepare the coral samples for the Sr/Ca analysis were performed. These different methods are termed the 'crushing' method and 'milling' method. Both methods involved cleaning but only samples that were prepared using the milling method were x-rayed and milled. Samples prepared by the milling method included hand samples, slices and corks, whereas samples prepared by the crushing method only included hand samples and slice samples. Details for the preparation methods are described below. Table 2 provides details of sample type, method and the length of material analysed for each coral, as well as estimated years sampled and growth rates.

3.4.1 X-radiography

Coral samples were x-rayed to determine the annual density bands, the maximum growth axis and growth rate (Figure 13). Because X-ray images can show large-scale diagenetic features through irregular densities in the image (Figure 13A) they help in the screening process (McGregor & Gagan 2003). The 7mm coral slice samples were x-rayed prior to this project by Illawarra Radiology Group. Image brightness and contrast was adjusted to show density bands as clearly as possible. Images were scaled to 1:1 so they could be accurately positioned over the coral to determine the maximum growth axis. Images were

also converted from X-ray negatives to positives, so the darker bands represent denser material. X-ray images for all corals analysed are provided in Appendix 3.

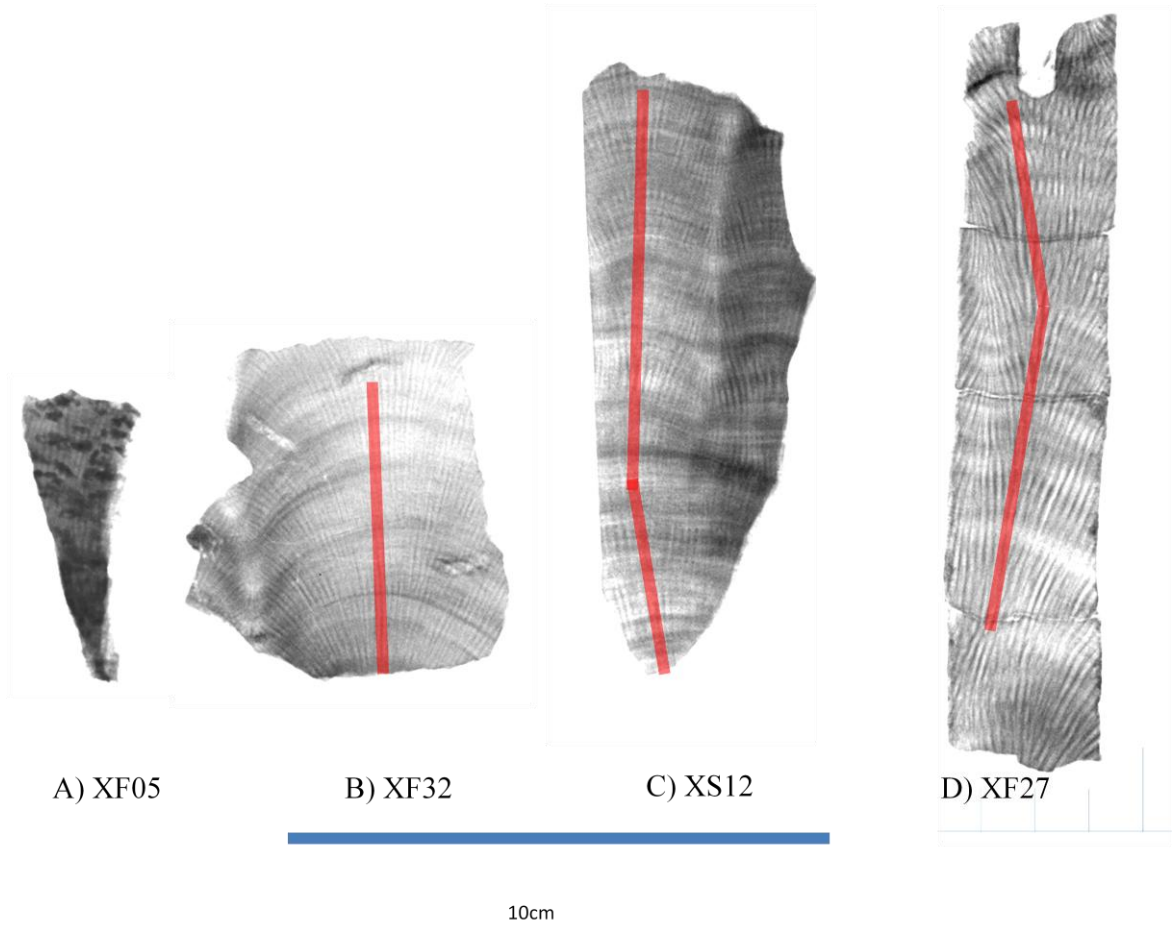

Figure 13. X-ray positives images of Kiritimati Island corals. **A)** X-ray of coral XF05 was not used in the Sr/Ca analysis due to diagenesis. The diagenesis in this coral was large scale as it was picked up by the X-ray through the dark, high density, 2-5mm wide zones. **B)** X-ray of XF32 **C)** X-ray of XF44 **D)** X-ray of XF27. Corals B C and D from this figure were used in the analysis as they passed the screening process. The red lines are along the maximum growth axis and they represent the bulk sampling transects that were used for the Sr/Ca analysis.

3.4.2 Cleaning and milling

Coral samples were thoroughly cleaned in milli Q-H_2O using a Branson 450 ultrasonic probe to remove loose material (potentially boring algae and dissepiments). Once cleaning had begun, corals were only handled with gloves. After the corals were cleaned, they were dried in an oven for 24-48 hours at 40°C and left to cool for half a day before being wrapped in gladwrap.

X-ray images of the samples selected for geochemical analysis were printed on transparency sheets, and mill paths were drawn over images along the maximum growth axis. The transparency paper was then placed over the coral so that the mill path could be accurately marked on the coral. The maximum growth axis was always sampled because it reduces potential error that is associated with different growth rates (de Villiers *et al.* 1995). The mill path is represented by the red lines in Figure 13 and in the Appendix.

The top 1cm of the cork samples was not milled as the material in this zone was commonly stained and most likely contained secondary material (McGregor Pers. Comm.). The coral was positioned on a computer controlled CNC mill, and a path 2mm wide and 0.5mm deep was cut. The length of the cut varied with the length of the sample. In-between different coral samples a compressed air gun was used to thoroughly remove any coral particles from the milling area to eliminate potential for cross contamination of samples.

3.4.3 Crushing preparation method

The majority of 2007 samples used in the analysis were 20mm by 10mm by 6mm blocks derived from hand samples and slices that were previously used for dating. To prepare the samples, ink on the block was removed by a scalpel. The sample was then crushed into small particles by a mortar and pestle, while been submerged in ethanol. The crushed coral was dried in the oven at 40°C for ~1 hour. Crushed samples were estimated to cover one year of coral growth since previous work on Kiritimati island *Porites sp.* corals has estimated growth rates of 15 to 22.5mm/yr (McGregor *et al.* 2011b).

Table 2. Overview of sample preparation details for analysed samples. Samples XF28 and XF45 were sampled twice by milling two similar paths on the same cork in order to assess reproducibility of the same sample.

Coral ID	Sample type	Sampling method	Length of Bulk sample (mm)	~Years sampled	Estimated growth rate (mm/yr)
XF05A	Cork	Milled	28	1.5	18.7
XF10	Hand Sample	Milled	30	2	15
XF13	Cork	Milled	20	1	20
XF15	Cork	Milled	60	4	15
XF16	Hand Sample	Milled	15	2	7.5
XF20	Cork	Milled	67	4	16.8
XF21	Cork	Milled	48	3	16
XF22	Cork	Milled	40	3	13.3

XF24	Cork	Milled	90	6	15
XF25	Cork	Milled	55	4	13.8
XF26	Hand Sample	Milled	33	3	11
XF27	Cork	Milled	110	7	15.7
XF28 - A	Cork	Milled	28	2	14
XF28 - B	Cork	Milled	28	2	14
XF29	Cork	Milled	17	1	17
XF32	Hand Sample	Milled	55	5	11
XF35	Hand Sample	Milled	55	3	18.3
XF43	Hand Sample	Milled	55	4	13.8
XF44	cork	Milled	61	4	15.3
XF45 - A	Cork	Milled	33	4	8.3
XF45 - B	Cork	Milled	29	3	9.7
XF46	Cork	Milled	29	2	14.5
XF47	Cork	Milled	26	1	26
XF48	Cork	Milled	90	5	18
XF49	Cork	Milled	62	4	15.5
XF53	Cork	Milled	80	6	13.3
XM23-S	Hand Sample	Crushed	20	1	20
XM28-S	Hand Sample	Crushed	20	1	20
XM31-S	Hand Sample	Crushed	20	1	20
XM37-S	Hand Sample	Crushed	20	1	20
XM38-S	Hand Sample	Crushed	20	1	20
XM39-S	Hand Sample	Crushed	20	1	20
XM42-cork 1	Cork	Milled	79	7	11.3
XM44	Cork	Milled	90	11	8.2
XM44-S	Hand Sample	Crushed	20	1	20
XM45-cork 1	Cork	Milled	84	6	14
XM45-cork 2	Cork	Milled	140	10	14
XM54-S	Hand Sample	Crushed	20	1	20
XM55-G	Slice	Milled	58	4	14.5
XM56-S	Slice	Crushed	20	1	20
XM59-S	Hand Sample	Crushed	20	1	20
XM62-S	Hand Sample	Crushed	20	1	20
XM63-D	Slice	Milled	73	5	14.6
XM67-2A	Slice	Crushed	20	1	20
XM69-B	Slice	Milled	134	9	14.9
XM70-J	Slice	Milled	122	9	13.6
XS02	Cork	Milled	68	5	13.6
XS03	Cork	Milled	57	5	11.4
XS04	Cork	Milled	34	3	11.3
XS05	Cork	Milled	112	8	14
XS06	Cork	Milled	115	7	16.4
XS09	Cork	Milled	105	9	11.7
XS10	Cork	Milled	47	3	15.7
XS12	Hand Sample	Milled	110	8	13.8
XS13	Cork	Milled	98	4	24.5

3.5 Sr/Ca analysis

3.5.1 Geochemical Preparation

In preparation of the Sr/Ca analysis, 10 mL plastic centrifuge tubes were thoroughly cleaned. The tubes and the lids were fully submerged overnight in a 5% HNO_3 solution. Tubes and lids were rinsed with milli Q water three times and then dried overnight in a ~50°C oven. Approximately 0.550 ± 0.1 mg of coral powder was weighed on an Orian Cahn C-35 microbalance and transferred into the cleaned centrifuge tubes.

For each coral sample, a minimum of three individual samples (repeats) were weighed and prepared for the Sr/Ca analysis. Coral samples had multiple replicates, so reproducibility could be tested and measurement of standard error (SE) or accuracy could be calculated. A 1 % v/v Suprapur HNO_3 (Merck) solution was added to the tubes by a 100µL adjustable Eppendorf pipette to dissolve the coral material. The volume of acid added was adjusted depending on the amount of coral weighted out. To give a final concentration of ~35ppm, 0.1 mL of acid was added for every 0.01 mg of coral material. The tubes were then placed in a 40°C sonicator bath for ~1 hour to ensure that the coral material completely dissolved within the solution.

3.5.1 ICP-AES analysis

Sr/Ca ratios from the coral samples were obtained by an Inductively Coupled Plasma Atomic Emission Spectrometer (ICP-AES) at ANSTO. Mg/Ca ratios were also measured, although, machine settings were optimised for Sr/Ca. The specific instrument used was the Vista-PRO Simultaneous ICP-OES, produced by Varian Inc. Before running the analysis, several blank vials with the same HNO_3 solution added were measured by the ICP-AES to ensure that the vials and the acid were not contaminated.

Two different Sr/Ca analyses were performed at ANSTO (run one and run two) because all coral samples were not prepared in time for run one. All samples were analysed three times in run one (three repeats), however, some of the repeats had to be excluded due to analytical error. Samples analysed in run two were either new coral samples, which were analysed three times (three repeats), or samples that had already been analysed in run one. Over half the samples from run one had one to three additional repeats measured in run

two, as some of the original Sr/Ca values were excluded and because more accurate results could be obtained from more repeat measurements. Because occasional samples in run two were also excluded, the total amount of repeats for each sample ranged from two to six. To ensure the results were consistent between each run, the same ICP-AES settings shown in Table 3 and correcting techniques were used.

Table 3. Instrument settings of ICP-AES

ICP-AES parameter	Setting
Power	1.3 (kW)
Plasma gas flow	16.5 (L/min)
Auxiliary gas flow	1.5 (L/min)
Nebuliser pressure	0.75 (L/min)
Replicate time	5 (s)
Stabilisation time	20 (s)
Sample uptake	40 (s)
Pump rate	10 RPM
Rinse time	20 (s)
Fast pump	On
Replicates	6

A known reference solution or Internal Calibration Verification (ICV) was used to measure internal drift in the machine's measurements during the analysis, and this measurement enabled the corrected Sr/Ca values to account for the in run internal drift. The ICV solution was measured before and after every Sr/Ca measurement. The difference from the recorded ICV values to the expected ICV value was used to correct the raw Sr/Ca values. The precision of the experiment (RSD error) was measured by the average ICV deviation from the expected value. The RSD error is a component of the final uncertainty.

4 Results

4.1 Coral screening and dating

One hundred and twelve coral samples were thoroughly assessed by XRD and thin section analyses to determine if the coral sample was suitable for SST reconstructions. As both these methods need to be used in conjunction with each other to indentify a variety of digenetic features, coral samples were subjected to both screening methods. Only corals that passed both screening methods were included in the geochemical analysis. This section describes the results from the thin section, XRD and dating methods. The screening and dating results for all corals that were analysed are provided in Table 4.

4.1.1 Thin section analysis

One hundred and twelve coral samples available for the project were subjected to the thin section analysis. Corals that revealed greater than 'minimal' (Table 1) amounts of diagenesis were excluded from the Sr/Ca analysis. The thin sections revealed the wide spectrum of preservation states that were described in McGregor and Abram (2008). Of the 112 samples subjected to the thin section analysis, 45 were excluded due to evidence of diagenesis, and 68 were considered of high enough preservation for geochemical analysis. Although the 68 samples passed the thin section screening, they also had to meet the XRD criteria to be included in the final geochemical analysis. Thin section images for all corals are provided in Appendix 2.

4.1.2 XRD

Fifteen coral samples that passed the thin section analysis did not meet the XRD criteria and were excluded from the geochemical analysis leaving 53 suitable coral samples. The majority of XRD weight percentages for calcite and high Mg calcite were below detection limits (<1%). Only seven corals recorded calcite values higher than 1% in run one, with the lowest aragonite value reaching 95.5% (XM33-S). Only corals that recorded aragonite values higher than 99.5% in the XRD analysis were determined to be of a high enough quality for further analysis. Contrast corrected weight values (x^2) were all suitable and did

not influence the exclusion of any corals. Aragonite values for every coral analysed is shown in Table 4 and all XRD results are presented in Appendix 1.

4.1.3 Coral ages

The three dating methods used to date corals used in this study—AMS radiocarbon (AMS), laser ablation ICP-MS U-series (Las U/Th) and solution ICP-MS U-series (Sol U/Th), revealed that the ages of corals analysed ranged from modern to ~5.9 kyr BP. The coral dates were unevenly distributed over the 5.9 kyr. Only two corals' estimated ages were in-between 1950 to 1.4 kyr BP, while 20 corals' estimated ages were within the next 600 years. After 2 kyr BP, the coral dates are well-distributed. The accuracy (positive and negative error) associated with each calculated age varied significantly depending on which dating methods were used. All calculated coral ages, positive and negative error and the dating methods used are shown in Table 4. Seven analysed samples were not dated by the completion of this thesis.

Table 4. Screening and dating results for corals analysed.

Coral ID	Year Collected	Aragonite %	χ2	Thin section rating	Dating method	Calibrated age. kyr BP	(+) error (kyr)	(-) error (kyr)
XF05A	2009	99.5	1.78	Good - Excellent	AMS	0	0	0
XF10	2009	99.5	1.63	Good	AMS	3.2	0.21	0.16
XF13	2009	99.8	0.7	Good	AMS	3.82	0.19	0.17
XF15	2009	99.8	1.68	Good	AMS	1.47	0.15	0.15
XF16	2009	99.9	1.63	Good	AMS	1.49	0.15	0.17
XF20	2009	99.7	1.72	Good	AMS	1.54	0.16	0.16
XF21	2009	99.7	1.65	Good	AMS	1.63	0.15	0.18
XF22	2009	99.8	1.62	Good	AMS	1.88	0.17	0.16
XF24	2009	99.9	1.6	Excellent	AMS	3.7	0.17	0.18
XF25	2009	99.9	1.71	Good	AMS	1.73	0.17	0.15
XF26	2009	99.8	1.62	Good	AMS	1.95	0.15	0.17
XF27	2009	99.8	1.65	Good - Excellent	AMS	1.87	0.16	0.16
XF28	2009	99.5	1.62	Good	AMS	4.43	0.2	0.18
XF29	2009	99.8	1.64	Good - Excellent	AMS	4.39	0.19	0.18
XF32	2009	99.5	1.62	Good	AMS	1.82	0.15	0.16
XF35	2009	99.6	1.59	Good	AMS	1.74	0.17	0.15
XF43	2009	99.7	1.65	Good	AMS	4.14	0.18	0.2
XF44	2009	99.8	1.64	Good - Excellent	AMS	4.7	0.19	0.14
XF45	2009	99.6	1.64	Excellent	AMS	4.68	0.17	0.14
XF46	2009	99.6	1.73	Good - excellent	AMS	3.93	0.18	0.19
XF47	2009	99.6	1.63	Good - excellent	AMS	3.52	0.15	0.16
XF48	2009	99.9	1.68	Excellent	AMS	1.94	0.14	0.17
XF49	2009	99.7	1.71	Good-Excellent	AMS	1.57	0.17	0.15
XF53	2009	99.6	1.68	Good	AMS	2.19	0.16	0.14
XM23-S	2007	99.9	1.73	Good	AMS	1.12	0.15	0.13
XM28-S	2007	99.9	1.62	Good	Laser U series	5.2	0.7	0.7

XM31-S	2007	99.6	1.73	Good	AMS	1.9	0.17	0.16
XM37-S	2007	99.5	1.73	Good - Excellent	Laser U series	2.35	0.49	0.49
XM38-S	2007	99.5	1.73	Good	AMS	3.69	0.17	0.17
XM39-S	2007	99.8	1.72	Good	Laser U series	3.91	0.6	0.6
XM42	2009	99.7	1.75	Good	Sol U series	5.9	0.04	0.04
XM44	2009	99.6	1.65	Good - Excellent	Laser U series	5.38	0.5	0.5
XM44-S	2007	99.6	1.74	Good	Laser U series	5.38	0.5	0.5
Xm45-Cork 1	2009	99.6	1.69	Good	AMS	4.97	0.5	0.24
XM45-Cork 2	2009	99.6	1.61	Excellent	AMS	4.97	0.5	0.24
XM54-S	2007	99.8	1.73	Good	AMS	2.94	0.17	0.18
XM55-G	2007	99.7	1.7	Good - Excellent	AMS	1.83	0.2	0.19
XM56-S	2007	99.7	1.7	Good	AMS	1.64	0.14	0.17
XM59-S	2007	99.6	1.74	Good	AMS	1.6	0.17	0.17
XM62-S	2007	100	1.61	Good	Laser U series	1.48	0.58	0.58
XM63-D	2007	99.8	1.67	Good - Excellent	AMS	1.67	0.19	0.21
XM67-2A	2007	99.9	1.74	Good	AMS	3.87	0.23	0.22
XM69-B	2007	99.5	1.67	Good	AMS	1.89	0.18	0.18
XM70-J	2007	99.9	1.64	Good	Sol U series	1.84	0.03	0.18
XS02	2009	99.7	1.66	Good	Sample not dated			
XS03	2009	99.7	1.61	Good	Sample not dated			
XS04	2009	99.6	1.75	Good	Sample not dated			
XS05	2009	99.6	1.67	Good - Excellent	Sample not dated			
XS06	2009	99.6	1.72	Good - Excellent	Sample not dated			
XS09	2009	99.7	1.63	Good	Sample not dated			
XS10	2009	99.6	1.74	Good	Sample not dated			
XS12	2009	99.6	1.65	Good	AMS	2.627	0.211	0.148
XS13	2009	99.6	1.68	Excellent	AMS	3.038	0.189	0.191

4.2 Geochemistry results

4.2.1 Preliminary Sr/Ca results

Sr/Ca results for each repeat and the calculated standard error for every sample analysed are presented in Figure 14. Calculated standard error ranged significantly from 0.005 to 0.226 with an average of 0.057. Geochemistry results are provided in Appendix four.

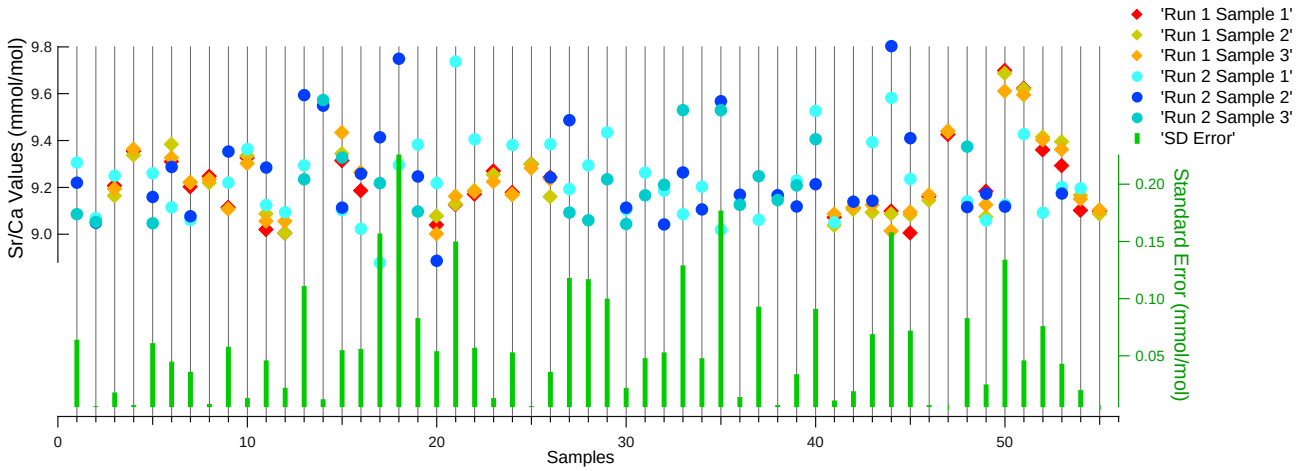

Figure 14. Standard error and Sr/Ca repeat variability. Kiritimati coral Sr/Ca values (coloured circles and diamonds) and standard error (green bars). Diamonds (run 1) and dots (run 2) show the variability of Sr/Ca values measured for each sample. The samples that have a low spread of values are more accurate and thus have a lower calculated standard error.

4.2.2 Mg/Ca results

The Mg/Ca value of the samples repeats were used to perform a final check on the diagenetic screening of the results (Figure 15). High Mg/Ca values suggest calcite contamination (Allison *et al.* 2007). This additional assessment is particularly important because calcite levels that are around 1% are near XRD detection limits and have been shown to significantly impact the coral geochemistry (McGregor & Gagan 2003; Allison *et al.* 2007). When calcite contamination is present in *Porites sp.*, Sr/Ca values decrease, while Mg/Ca values increase significantly. Previous measurements reveal that calcite contamination can affect Mg/Ca values ~4.9 times greater than Sr/Ca values (Allison *et al.* 2007).

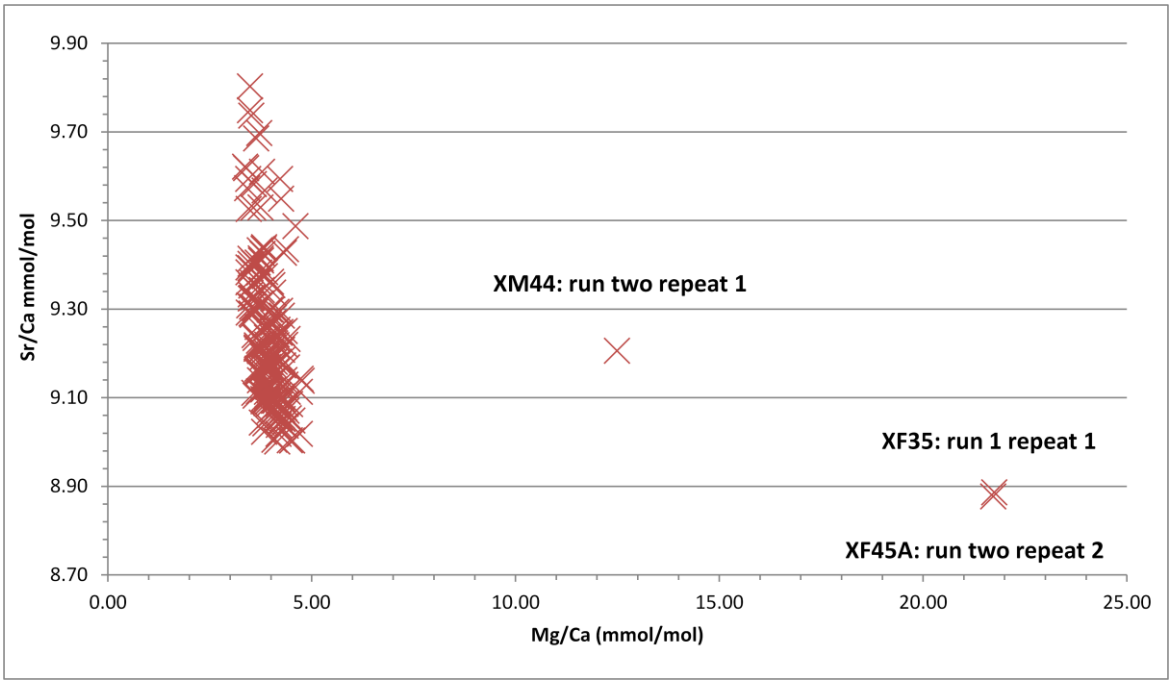

Figure 15. Sr/Ca repeat values plotted against Mg/Ca repeat values. Three repeats, XF35 run one repeat 1, XF45 run two repeat two and XM44cork run two repeat 1 all show anomalously high Mg/Ca values. This finding provides strong evidence to suggest these values are influenced by diagenesis and should be excluded from the analysis.

Three repeat values showed elevated Mg/Ca values and suggest that calcite contamination was present in the samples. However, the XRD values and the thin section rating for these samples were all satisfactory (Table 4). Because calcite cements can occur in various locations in the coral (Hendy *et al.* 2007), it is possible that at small scales some sections may contain calcite, while others may not. Thus, although calcite was not found in the screening methods, it could have still have been present in the coral material analysed. Interestingly, two of the three (XF35 and XF45 A) repeats with high Mg/Ca also have the lowest Sr/Ca, further suggesting there is diagenesis in those replicates. The three replicates identified in Figure 15 as having high Mg/Ca will not be included for further analysis. Hereafter, calculated averages of Sr/Ca and SE for the three samples that had repeats with a high Mg/Ca value will be calculated with their remaining (calcite free) repeat Sr/Ca values.

4.3 Potential methodological error

4.3.1 Sample weight and standard error

The weight of coral material that was dissolved in the vials for every repeat was plotted against sample SE, to visually assess if samples with a higher spread in weight also had a higher standard error (Figure 16). A potential source of error in the results could be attributed to the weight of coral material, particularly because the range of these values, which was 0.447 mg to 0.828 mg, was outside the recommended weight range of 0.55 ± 0.5 mg for Sr/Ca analyses. As the range of weight values does not correlate with calculated SE, it can be assumed that weight of the coral material analysed did not influence the variability of the results.

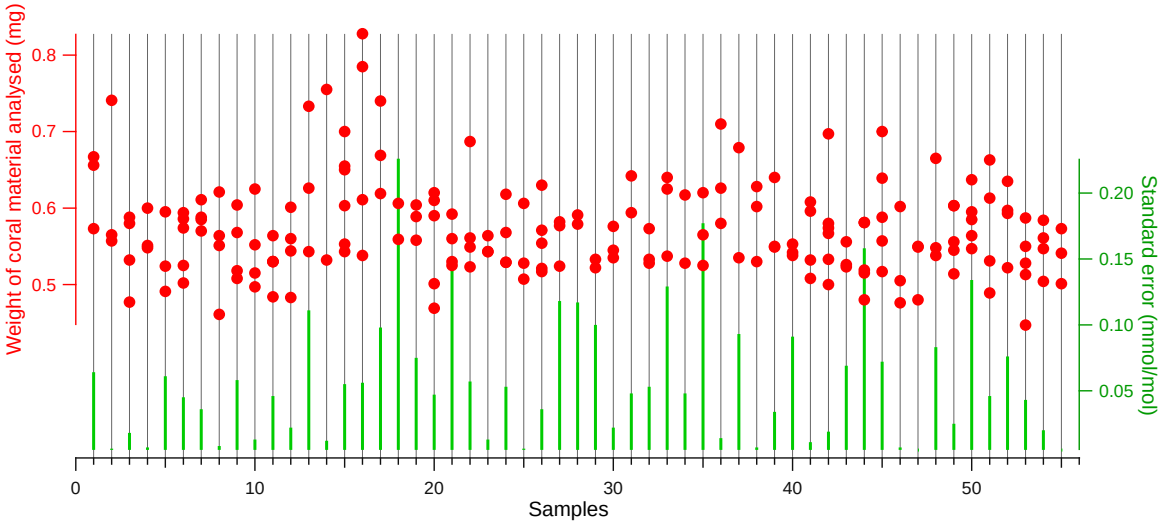

Figure 16. Weight of coral material in each repeat compared with SE. The plot shows that weight does not influence the variability in the results as several samples with a large range of weight values have recorded a low SE (i.e. sample 2, 14, 16).

4.3.2 Average Sr/Ca and standard error

To visualise the range of averaged Sr/Ca values for every coral sample and to see if there is a correlation with average Sr/Ca and SE Figure 17 was plotted. Averaged Sr/Ca values ranged from 9.039 to 9.565 mmol/mol. No correlation between average Sr/Ca and SE is observed.

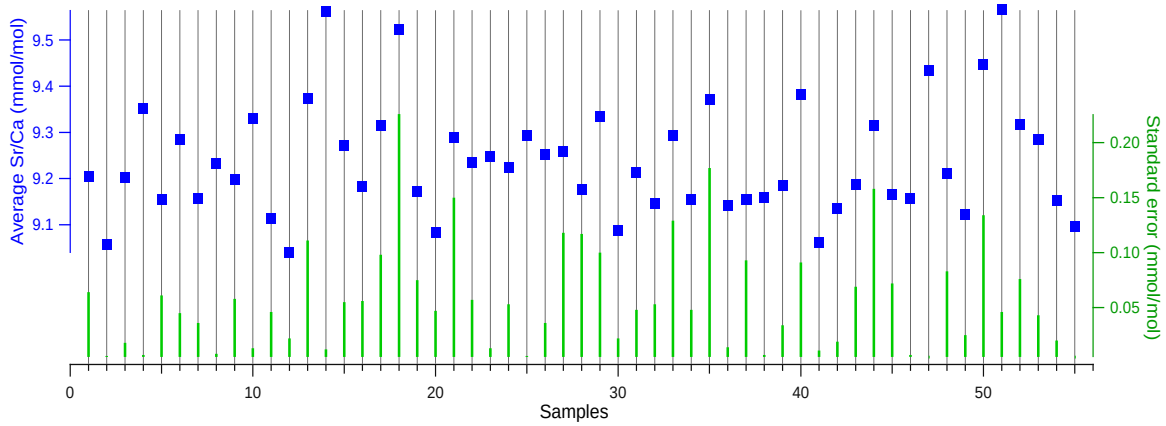

Figure 17. Average Sr/Ca compared with SE. A large range of average Sr/Ca values is shown but no correlation between Sr/Ca and SE is observed.

4.3.3 Comparison of average Sr/Ca results with different preparation methods

Comparing the average Sr/Ca values from the crushing and milling method allows for assessment as to whether or not the results consistently varied between sampling methods (Figure 18). The crushing sample preparation method used (see section 3.4.3) to estimate Sr/Ca values in this study are considerably different from those used in previous studies. Past studies opted to use the milling method because it enables an accurate estimate of the years sampled to be made (Hendy *et al.* 2002; Abram *et al.* 2009). Because the milling method has proven reliability, whereas the crushing has not, it is necessary to determine if the methods yielded significantly different Sr/Ca values. The crushing samples may have yielded erroneous results because the method did not selectively sample along the mill path, and significantly more coral material was homogenised. Furthermore, the years sampled was estimated at one year's growth; however it is possible that the sample could have covered ~one and a half years growth. If one and half years of coral growth were included in bulk sample, the measurement may favour warmer or colder seasonal temperatures. To also account for variations in Sr/Ca over time, the two sampling techniques were both plotted over the 6 kyr BP period. Thus, only corals that were dated could be used in the comparison. It would be ideal to compare the Sr/Ca ratios from each method over a shorter time period (i.e. 1-2 kyr BP), as opposed to the 6000 year period covered in this study, however, due to the lack of values from the crushing method, this comparison is not feasible.

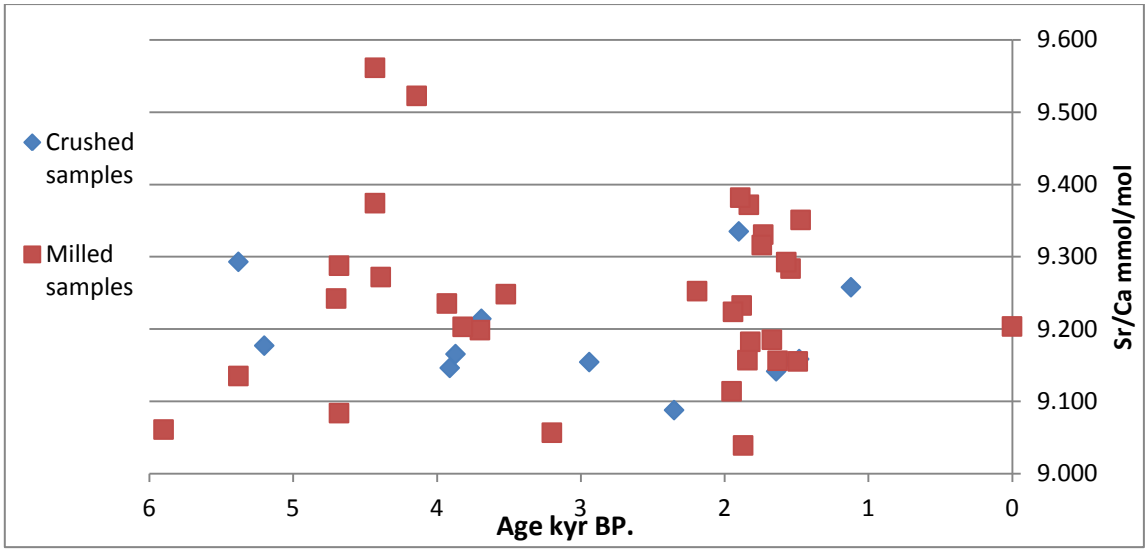

Figure 18. Comparison averaged Sr/Ca values for different preparation methods. Average Sr/Ca values from crushing (blue diamond) and milling (red square) sampling methods are plotted against each other over time, showing that neither of the sample types produced consistently different results.

The comparison indicates that there is no clear difference between the two sampling methods for Sr/Ca values, although the milled samples appear to have a larger spread in values, particularly because of the two samples with values higher than 9.5 (mmol/mol). To calculate if there is a statistical difference between the methods for their Sr/Ca results, a t-test was used, where a P value <0.05 equates to a significant difference. Results for dated and undated samples were included in the t-test analysis. The mean Sr/Ca for each of the two methods—milling and crushed, did not differ significantly according to a t-test, $t(53) = 1.572$, $p<0.05$ at $p=0.059$. On average, the Sr/Ca mean for corals analysed using the crushing method was 9.190, while the Sr/Ca mean for corals analysed using the milling method was 9.251. The methods were not expected to differ significantly given the similarity in the spread of values (Figure 18) and the similarity between mean values for both methods, but the small p-value of 0.059 does indicate that the two methods are somewhat different. This difference could exist because there were only 12 samples that were prepared by the crushing methods and this number may be too small to be statistically significant. Overall, the crushing method, which is being used for the first time, does not reconstruct results that statistically different to tried and tested milling preparation method. Thus, Sr/Ca results from this method can be used to confidently reconstruct Holocene SSTs.

4.3.4 Comparison of average Sr/Ca results with number of years sampled

As the coral material analysed between samples covered a range of years of coral growth (1-11 years), it is necessary to determine if the amount of years of coral growth in each bulk coral sample impacted the results (Figure 19). Average Sr/Ca values were placed in two groups: (1) less than 5 years of coral growth and (2) equal to or greater than 5 years of coral growth. The two categories were plotted against time.

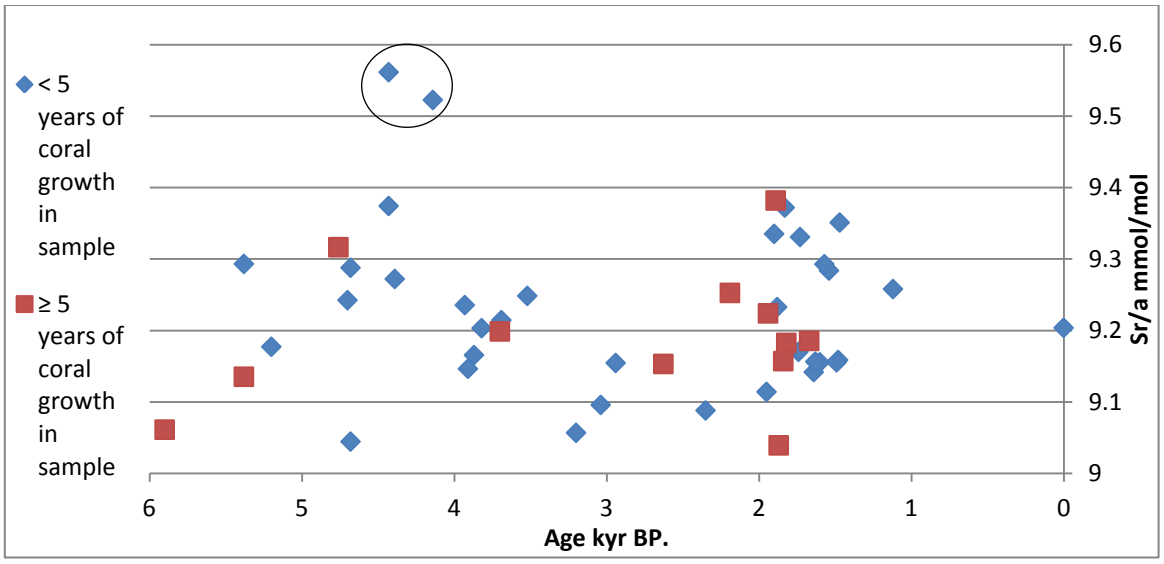

Figure 19. Comparison of coral samples that included < 5 years and ≥ 5 years of coral growth. Coral samples that covered < 5 years of coral growth show more variable results over the 3-6 kyr BP period. Both categories show similar variability over the 1-2 kyr BP period. Identified outliers (inside black circle) are both samples that included < 5 years of coral growth.

The comparison shows that samples with less than 5 years of coral growth have slightly more variable results over the 3-6 kyr BP period. However the 1-3 kyr BP period, which has a similar amount of values for both categories, shows a relatively even distribution.

The increase in variability (on average) for the < 5 years category was somewhat expected because Sr/Ca values from this time period are more likely to be influenced by ENSO events. Averages from longer time periods (5 – 11 years), however, would be less impacted by one ENSO event as the average is made up of numerous year of growth.

It is noteworthy the Sr/Ca values from XF28 B and XF43 (circled in Figure 19) have substantially higher Sr/Ca (>0.1 mmol/mol) values when compared with the next highest Sr/Ca value. XF28 B and XF43 cover 2 and 4 years of coral growth, respectively and were both milled in the preparation for the Sr/Ca analysis. It is possible that the high Sr/Ca value of these samples represents are period that is similar to a prolonged present day La Niña event, in which anomalously cool SST are present at Kiritimati (Sr/Ca inversely related to SST). But because both these averages are only calculated from two repeats their average value is not as robust as other averages. Since values from XF28 A and XF28 B are from the same piece of coral, all the repeat values can be averaged together making one instead of two Sr/Ca averages. Additionally, XM44-S and XM44 and XF45 A and XF45 B are also from the same coral and their values can be averaged to form two instead of four Sr/Ca values (Table 5).

Table 5. Combined Sr/Ca results for corals that had two samples.

Coral ID	Average Sr/Ca (mmol/mol)	SD (mmol/mol)	SE (mmol/mol)
XF28 - A	9.374	0.192	0.111
XF28 - B	9.561	0.017	0.012
XF28 (combined)	9.449	0.171	0.076
XF45 - A	9.084	0.095	0.047
XF45 -B	9.288	0.300	0.150
XF45 (combined)	9.186	0.233	0.082
XM44-S	9.293	0.224	0.129
XM44	9.117	0.015	0.007
XM44 (combined)	9.193	0.160	0.060

The resulting Sr/Ca value for XF28 is 9.449 mmol/mol. This process leaves only XF43 as a potential outlier as its Sr/Ca average is final. Sample XF43 has a significantly higher SE (0.226) than the mean (0.059 mmol/mol), but its influence on the final results will be minimised through a mean weighted average analysis, where more accurate samples have greater pull on the combined average (Galbraith *et al.* 2005).

4.3.5 Geographical influences

Because fossil corals that grow in lagoon type conditions may experience different SSTs to corals that form on open reefs with exposure to the open ocean, geographical influences

on the results have been assessed (Table 6). To assess geographical influences whilst minimising temporal influences, average Sr/Ca values from 1.1—2.4 kyr BP were compared. Corals that grew in this period come from two regions on the Island, the middle and the south. Although there was one more coral that grew outside these regions during this period, it was not used in the comparison as one was insufficient. These regions are represented by the dashed line in Figure 20. In addition to average Sr/Ca a standard deviation was calculated to assess if one region had more variable results.

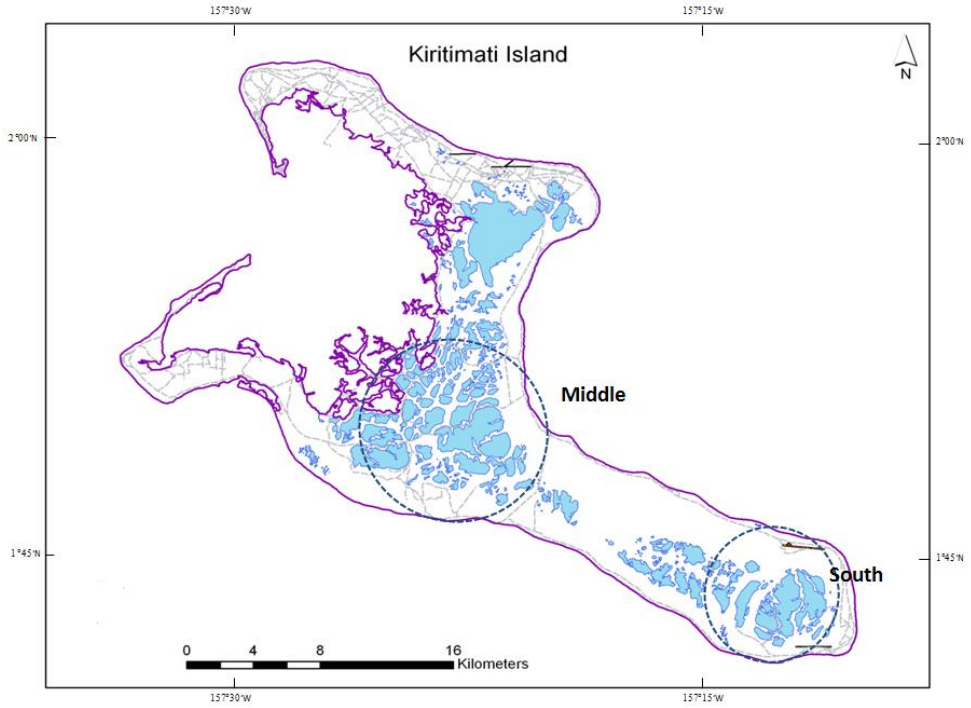

Figure 20. Map of Kiritimati Island showing two regions of the island where fossil corals that were used in the geographical comparison were collected.

Table 6. Geographical influences on Sr/Ca results

Region	Number of values	Standard dev	Average Sr/Ca	Average SST
Middle	13	0.10	9.225	26.2
South	9	0.10	9.204	26.5

The similarity in average Sr/Ca from the two regions implies that there are no geographical influences on the results. Furthermore, the standard deviation for both regions is comparable, which suggests that one region did not have a larger range in Sr/Ca values over the other region.

4.4 Inter-coral Sr/Ca difference

An important component of uncertainty for Sr/Ca SST based reconstructions is the recording difference (or inter-coral difference) of Sr/Ca between different corals. Typically, the Sr/Ca ratios incorporated into different corals at the same SST will show similar but not identical values. Thus, there is an associated uncertainty with each reconstructed Sr/Ca value that needs to be included in the final error calculation. Sr/Ca values used to calculate the inter-coral difference at Kiritimati Island come from two previously reconstructed high resolution data sets that overlap for ~4 years (Nurhati *et al.* 2009; Glasbergen 2010) (Figure 21). The inter-coral difference was calculated by subtracting the averages from each and equalled 0.096 mmol/mol.

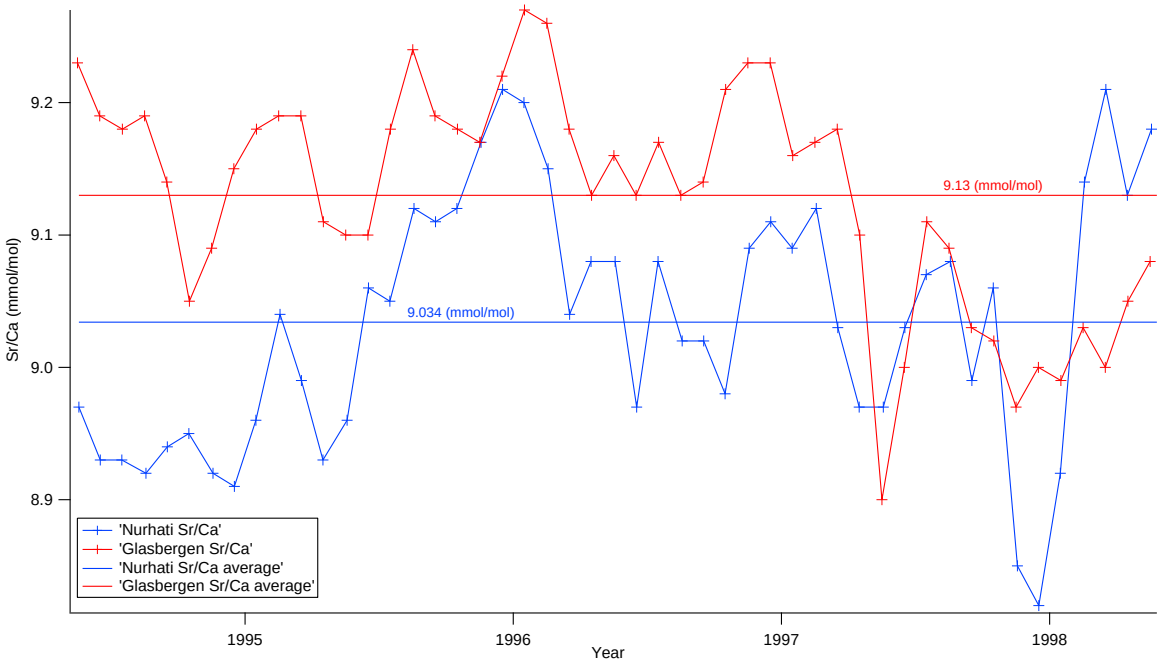

Figure 21 Comparison of monthly resolution Sr/Ca values from two different *Porites*. Red values (Glasbergen 2010) have an average Sr/Ca value of 9.13 mmol/mol. Blue values (Nurhati *et al.* 2009) have an average Sr/Ca value 9.034 mmol/mol. The difference in average Sr/Ca values is 0.096 mmol/mol. This value represents part C of the combined error.

4.5 Final uncertainty and Sr/Ca results

The final Sr/Ca results published in this thesis all included an uncertainty or error range, which is calculated from three components: (1) the analytical precision (RSD error) from the ICP-AES analysis, which was 0.2% for run one and 0.1% for run two; (2) the standard

error or each samples repeat values; (3) inter-coral difference. To calculate total error the following equation is used:

$$Combined\ Error = \sqrt{(a^2+b^2+c^2)}$$

Final Sr/Ca values, which include averaged and excluded repeats, and their combined Sr/Ca error and age estimates, are presented in Figure 22. It total, 45 dated Sr/Ca estimates have been calculated within this thesis. In addition to these estimates, one fossil coral (XM72-C) and one modern coral (XM22) estimates that were previously reconstructed in Glasbergen (2010) were added to the data set, which consists of 47 Sr/Ca estimates (Figure 22).

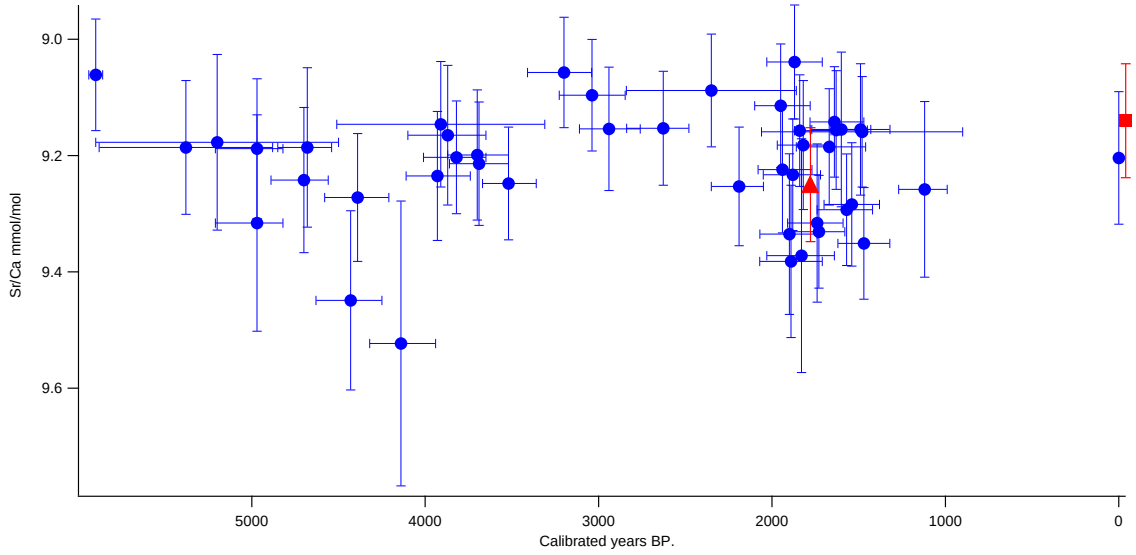

Figure 22. Final bulk Sr/Ca estimates with combined uncertainty and estimated age range since mid-Holocene. Blue data points represent data derived from this study. Red triangle (XM72-C) and red square (XM22) are additional points added from Glasbergen (2010). XM22 represent modern average Sr/Ca values.

5. Discussion

5.1 Calibrating Sr/Ca to SST

As no universal Sr/Ca to SST calibration exists for *Porites sp.*, location-specific Sr/Ca-SST calibrations must be calculated (Corrège 2006). Three calibrations for Kiritimati Island have been produced (Evans *et al.* 1999; Nurhati *et al.* 2009; Glasbergen 2010). The

equation from Evans *et al.* (1999) was calculated for SST anomalies, so it was not appropriate for this project. The Nurhati *et al.* (2009) and Glasbergen (2010) equations calculate SSTs at a Sr/Ca value of 9.1mmol/mol to equal 26.3°C and 27.84°C, respectively (Figure 24). Since the Glasbergen (2010) equation was based on a microatoll, was produced from the same laboratories and utilised the same procedures used in this study, it was selected as the calibration to use in this project. However, results from the Nurhati *et al.*(2009)study was used to calculate the inter-coral variability across the island and was included in the Sr/Ca SST errors (see section 4.4).

Because the resolution for this calibration was monthly, the calibration needed to be recalculated at yearly intervals to be more consistent with the data resolution from this study. The instrumental (IGORR) (Reynolds *et al.* 2002) SST from Kiritimati Island and coral data (XM22) used in the original calibration were averaged each full year from 1995 – 2006 (Figure 23). The linear trend line from Figure 24 (blue trend line and box) calculates a calibration of:

$$SST\ (°C) = (Sr/Ca - 11.125) / - 0.0726\ (r^2 = 0.85)$$

The calculated annual calibration for this study was very similar to the Glasbergen (2010) derived calibration (red dashed box and trend line in Figure 24), which was expected since they were calculated from the same data. The calibration from this study and Glasbergen (2010) did deviate slightly from the Nurhati *et al.*(2009) derived calibration (green dotted box and trend line in Figure 24), which has the highest slope out of the three calibrations.

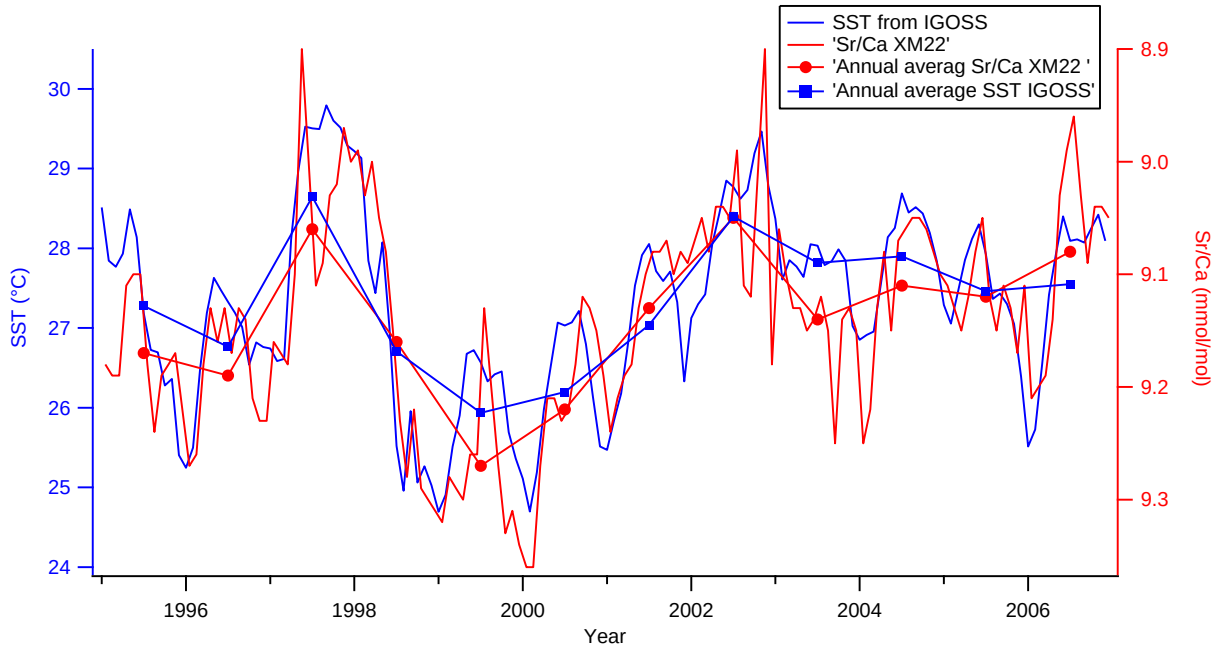

Figure 23. Correlation between reconstructed monthly and annual Sr/Ca values from coral XM22 (red) and 1° by 1° grid IGOSS SST (Reynolds *et al.* 2002) (blue) centred on 157.5°W 1.5°N. Annual averages for each year are represented by the blue square (instrumental) and red circle (coral). The correlation in both resolutions is very high, which suggests that fossil corals can be used back in time to reconstruct mean annual SST variations.

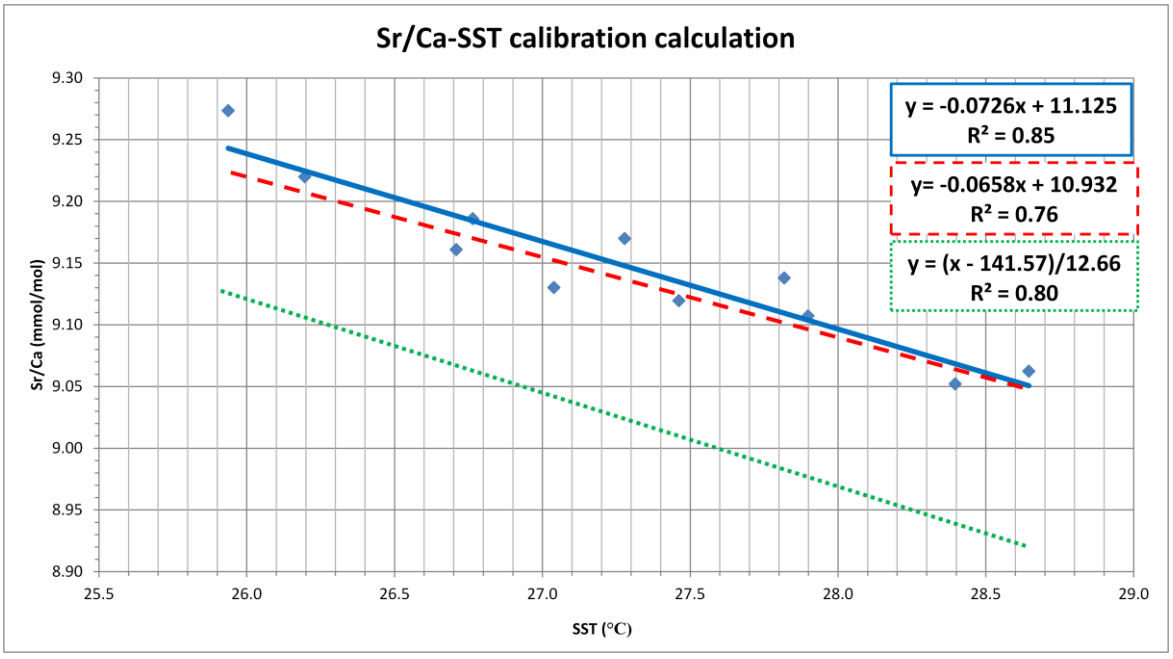

Figure 24. Annual resolution Sr/Ca to SST calibration trend line and equation used in this study (Blue line and blue box), monthly resolution calibration trend line and equation from Glasbergen (2010) (red dashed line and box) and sub-monthly resolution calibration trend line and equation from Nurhati *et al.* (2009) (green dotted line and box). The annual calibration (blue) is based on annual averages from Figure 24. High R^2 value suggests a

strong correlation between Sr/Ca and SST. The blue slope is used to reconstruct Holocene SST from fossilised corals is this study.

5.2 Kiritimati Island geochemistry as climate recorder

High (monthly) resolution Sr/Ca reconstructions from modern corals at Kiritimati Island have been compared to local climatology and Pacific-wide ENSO indices in order to assess their recording capabilities (Zeko 2009; Glasbergen 2010). This assessment provided clear results, showing that coral geochemistry from Kiritimati Island is an excellent proxy for local climatology and Pacific-wide ENSO variability. Low Sr/Ca values (warm SST) correlated with El Niño events as did high Sr/Ca values (cool SST) with La Niña events.

The annual averages for the calibrated SST from coral XM22 fit very well with the instrumental IGOSS SST dataset (Reynolds *et al.* 2002) (Figure 25). Additionally, the 5 year mean for both calibrated SST and instrumental SST are remarkably close at 27.21°C and 27.3°C, respectively. In comparison to monthly SST records from Kiritimati, ENSO events, which are indicated by the SOI and NINO 3.4 SST, are not as easily distinguished in the inter-annual scale SST record, but there is still an obvious correlation between the annual SST and the ENSO indices observed (Figure 25). If the resolution decreases further from annual averages to ~5 year averages (~average years of bulk samples used in this study), individual ENSO events would hardly be observed in the Sr/Ca SST records.

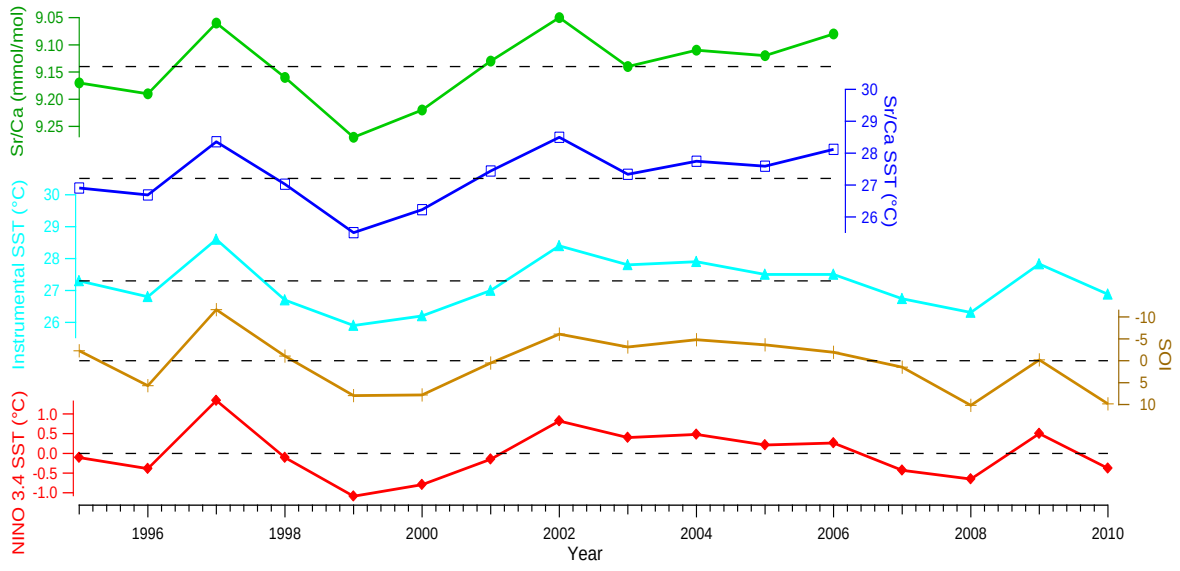

Figure 25. Annual averages of coral Sr/Ca (green) and calibrated SST (dark blue) compared with local instrument SST (light blue) and the SOI (brown) and NINO 3.4 (red) ENSO indices. Annual Sr/Ca values are from coral XM22. SST is calibrated from the same Sr/Ca values using the annual calibration (see section 5.1). Instrumental SST is from 1° by 1° grid IGOSS SST dataset (Reynolds *et al.* 2002) and is centred on 157.5°W 1.5°N. Annual SOI averages are calculated from monthly values (Bureau of Meteorology 2011). Annual NINO3.4 averages are calculated from weekly values (Global Change Master Directory 2011)

5.3 Reconstructing central Pacific mid to late-Holocene SSTs

The previously calculated calibration in section5.1 is used to convert Sr/Ca values from 47 microatolls (shown in Figure 22) to SST. The bulk SST estimates ranged from 22.1°C to 28.7°C (Figure 26), which is slightly lower than the range of monthly mean SSTs from the 2° by 2° ERSST dataset (Xue *et al.* 2003; Smith *et al.* 2008) since 1854 of 24.32 °C to 29.72 °C. The weighted mean program calculates a mean value in which samples with lower error have more influence on the final result (Galbraith *et al.* 2005). This calculation was done for every 500 yr period (or window) where data is available to produce a millennial scale evolution of SST (Figure 26). The program also recalculated SST error, which was generally lower when more data points were used.

The results show a strong millennial-scale trend with distinct fluctuations of mean SST. The trend shows two peaks (6-5.5 kyr BP and 3.5-3 kyr BP) and two troughs (4.5-4 kyr BP and 2-1 kyr BP) with gradual transitions between each. The results have been compared to modern annual averages when strong ENSO events occurred (1997/98 El Niño and the 2010/11 La Niña). Additionally, the mean SST from XM22, which was calculated at 27.3°C, provides a comparison for the fossils SSTs. This value was calculated by applying the bulk calibration to the average Sr/Ca values from 1995-2007 (Figure 23). The majority of the weighted mean 500 year averages fall below the modern average, though many are within error of the present, and none (including error) lie completely above the average SSTs recorded from the 1997/98 El Niño event. However, the mean SSTs during the 4.5-4 kyr BP period fell significantly below the 2010/11 La Niña annual average SSTs, which implies that there was a substantial shift in the mean state towards cooler SSTs in the mid-Holocene. Mean SSTs during this period were ~2.9 °C ± 1.2 °C colder than modern. However, the errors for the corals in this period are large, and further analyses on these samples are required to confirm this result. Similarly, the

period from 6-5.5 kyr BP consists of just one coral, so additional analyses from corals in this time window are required.

This degree of variation of the weighted mean SST estimates could be related to the 500-year "windows" chosen for constructing the weighted mean. For example, if 500-year windows were averaged at different intervals, such as 4.25-4.75 kyr BP and 4.75-5.25 kyr BP, the trends may not be as well-defined. In general, however, using the weighted mean of 500-year windows, the different errors for each SST estimate and the uneven temporal spacing of the corals are well accounted for. The weighted mean used here likely captures the general trend in the coral data and acts as a good first-order estimate of the centennial-millennial scale variations in CP SST. Alternative ways of averaging the data could be explored in the future.

Direct comparison of the microatoll Sr/Ca SST dataset with other records from the CP is not possible because no sediment core results have been published from this region, and only a hand full of coral records exist. The Kiritimati bulk Sr/Ca SST estimate is consistent with a small number of previous findings from the 1.5-2 kyr BP period. Sr/Ca SST results for 1.7 kyr BP from Kiritimati suggest cooler temperatures (Glasbergen 2010), and $\delta^{18}O$ records at approximately the same time suggest cooler and/or drier conditions (Woodroffe *et al.* 2003). The numerous data points in the 2–1.5 kyr BP period provide strong evidence that mean temperatures at this time were 1.1°C ±0.3°C less than the modern average. Three coral $\delta^{18}O$ records from Woodroffe *et al.*(2003) suggest that conditions were also cooler and/or drier during 3.8–2.8 kyr BP. These results are in agreement with the results from 4-3.5 kyr BP period presented in this study. The weighted mean average SST from this period is particularly robust since there are 5 relatively clustered data points. From 3.5-2.5 kyr BP, however, SSTs are above or close to modern SSTs, which was not indicated by the $\delta^{18}O$ records in Woodroffe *et al.*, (2003). Both these windows are limited in accuracy as they were only calculated from two corals. The accuracy of SST reconstructions from $\delta^{18}O$ results is also limited as it reflects changes in precipitation as well as SST. More Sr/Ca and $\delta^{18}O$ data from the 3.5-2.5 kyr BP period would help to clarify this discrepancy.

Climate conditions in the Palmyra Island CP (6°N, 162°W) have been reconstructed from $\delta_{18}O$ at ~1.1 kyr to present and showing that is was cooler and drier ~1 kyr (Cobb *et al.* 2003). The overlapping results from Cobb et al.(2003) and this study are consistent with

each other as the 1.5-1 kyr BP window indicates SSTs were ~1°C cooler than modern temperatures. Although the results form Cobb *et al.* (2003) are from Palmyra Island north of Kiritimati, they help to fill in the 1 kyr to present SST gap from this study.

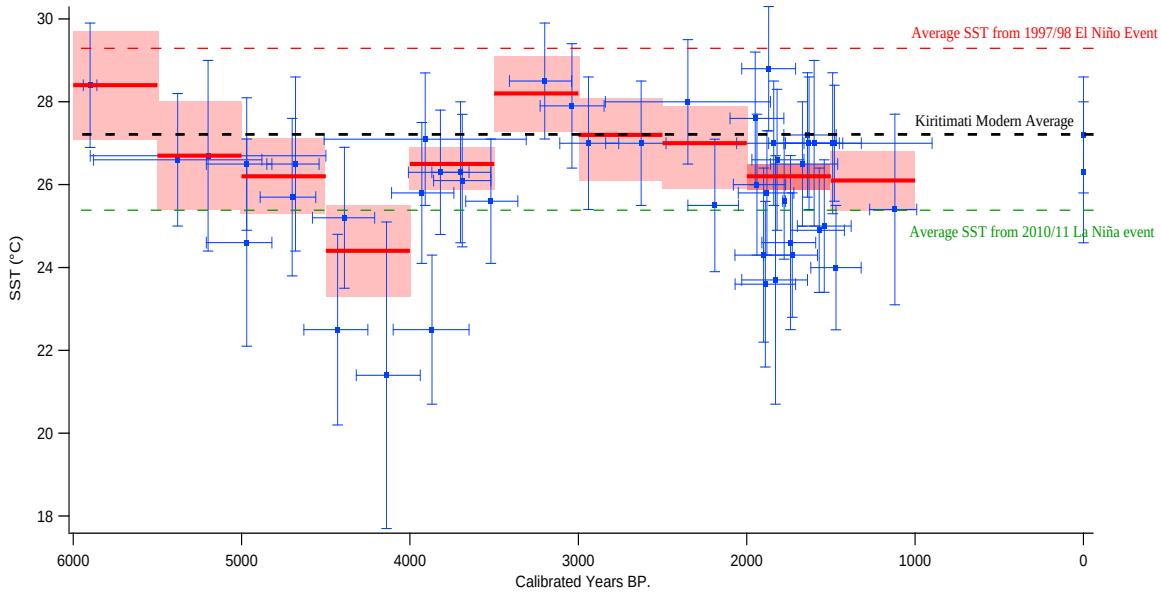

Figure 26. Coral Sr/Ca SST estimates of SST at Kiritimati Island since the mid-Holocene. SST error bars shows age range on age estimates (Table 4) and combined error on mean SST estimates. Red lines indicate weighted mean SST and red shading indicates the uncertainty range (Galbraith *et al.* 2005). Weighted mean estimates were calculated for every 500 yr period with available data. Black dashed line represents modern mean SST at Kiritimati Island (derived from XM22). The green and red dashed lines represent annual averages of 1° by 1° grid IGOSS SST centred on 157.5°W 1.5°N (Reynolds *et al.* 2002) from the 2010-2011 La Niña and the 1997/98 El Niño events, respectively.

5.4 Comparison with Indo-Pacific Warm Pool evolution

The CP SST data set from this study provides a good basis to address unresolved issues regarding Pacific zonal SST configuration during the mid-Holocene. Mean SST data from the IPWP showed pronounced cooling of events that occurred approximately 5.8 – 4.3 kyr BP at the margins of the IPWP (Figure 27), which potentially indicates a contraction of the southern end of the IPWP (Abram *et al.* 2009). Three possible scenarios for the contraction of the IPWP were proposed by Abram *et al.* (2009):

1) A mean La Niña-like state: During such an event, cooling in the WP may be related to a cold-water tongue that stretches across the equatorial Pacific, which would also be cooling SSTs in the CP

2) A mean El Niño Modoki-like state: This event is characterised by warming in the CP and cooling in the EP and WP. As a result, the cooling in the WP would have occurred without the cold-tongue extending across the equatorial Pacific.

3) Meridional changes: This scenario is characterised by zonal SSTs across the equatorial basin following the northerly movement of the Inter-tropical Convergence Zone. During this event, the IPWP and the upwelling in the EP would have shifted north. If upwelling and the easterly trade winds, which drive upwelling, moved north, it could be assumed that SSTs in the CP would warm because the cooler surface water that normally extend to Kiritimati would not occur.

Preliminary investigations of the likelihood of either of these three scenarios acting in the mid-Holocene using coarse resolution climate modelling data from the CSIRO Mk3L climate system model suggested that a mean cooling event occurred in the CP from 5.5-4.3 kyr BP (Figure 27), and that a mean La Niña-like state (scenario 1), or a La Niña Modoki (the opposite configuration of scenario 2) was active during the mid-Holocene. However, the strength of these predictions was limited as they could not be compared with reconstructed mean SST data from the CP. The data from this study provides valuable insight into the zonal configuration of the Pacific Ocean during the IPWP contraction. To aid the understanding of the relationship between CP and IPWP SSTs, the data from this study and from Abram *et al.* (2009) have been plotted together (Figure 28).

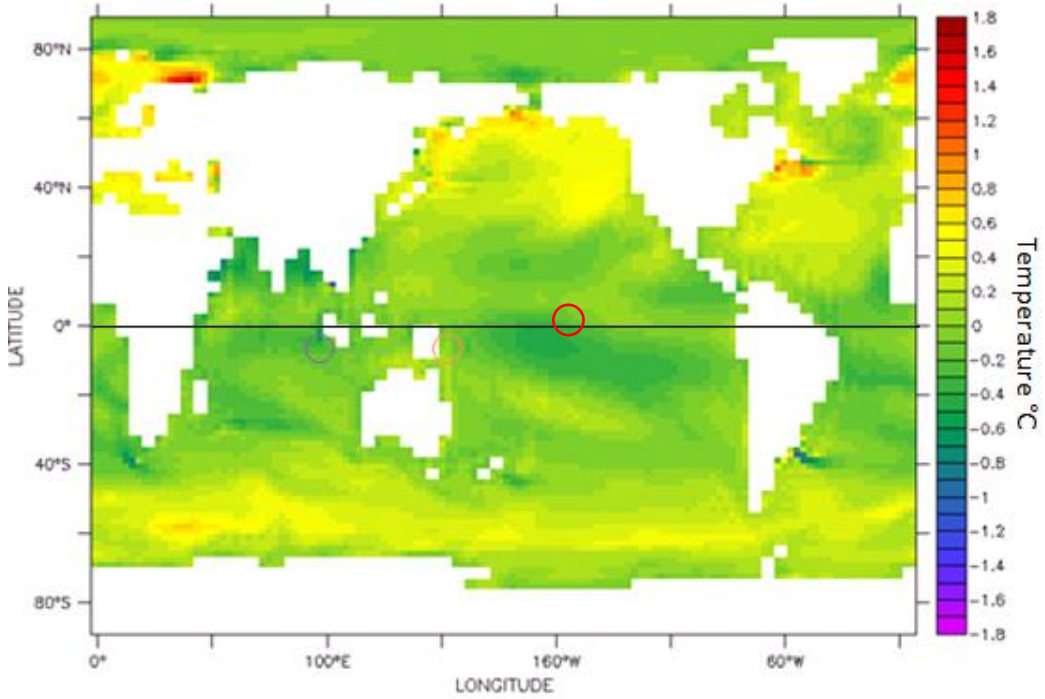

Figure 27. Global SST anomaly map averaged over 5.5 to 4.3 kyr BP. Map derived from the CSIRO Mk3L climate system model. Mean SST anomalies calculated by subtracting the modelled calculated orbital forcing SST by non orbital forcing SST. Study sites from Abram et al (2009), are represented by orange circle Muschu/Koil), and purple circle (Mentawai) and SSTs from this Kiritimati Island is represented by red circle. The black line represents the equator. The figure shows that the modelled results indicate that on average cooler SSTs occurred in the CP over 5.5 to 4.3 kyr BP.

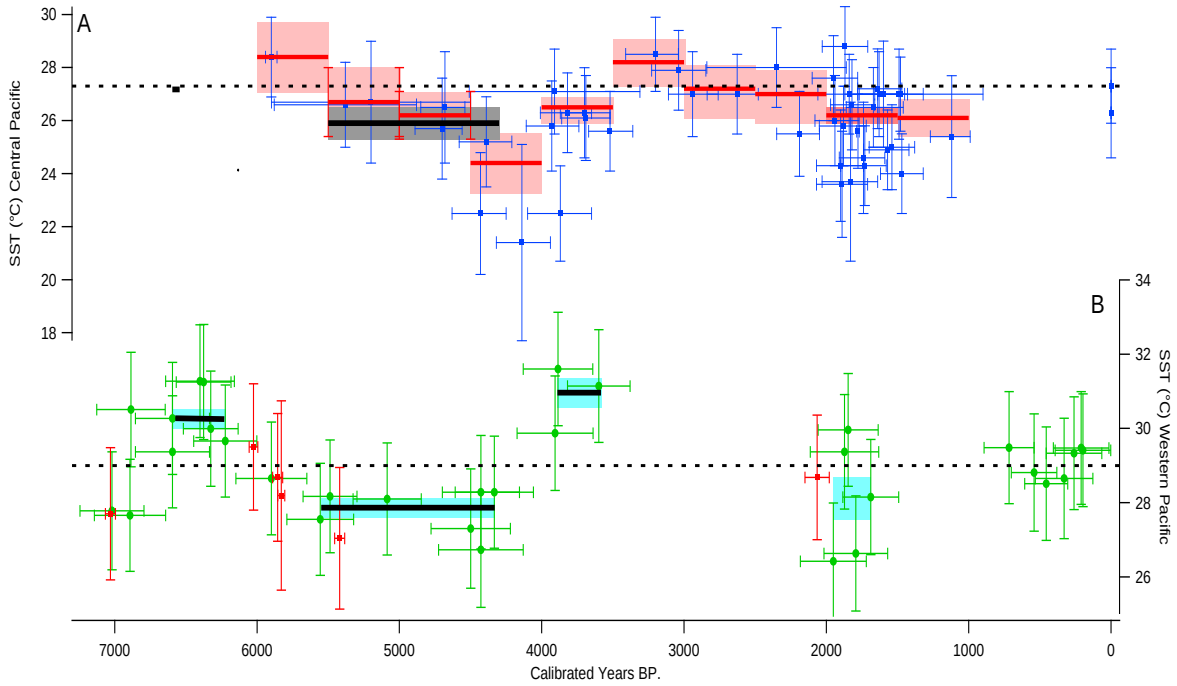

Figure 28. Comparison of Kiritimati Sr/Ca SST data (this study) with IPWP mean SST evolution (Abram et al. 2009) since the mid-Holocene. **A)** Black line shows weighted mean SST from 5.5 to 4.3 kyr BP and grey shading represents error (details as in Figure 26). **B)** Sr/Ca estimates of mean SST at the Mentawai (green) and Muschu/Koil (red) study sites (see Figure 27)(Abram *et al.* 2009). Black lines show weighted mean SST and grey and aqua shading represents error range. For a direct comparison the black weighted mean SST in (A) corresponds with the same time period in B). Both results are below modern (within error range) day mean SSTs. Mean SST from both the CP (blue) and WP (green) show similar trends since the mid-Holocene.

The results from this study confirm that a cooling event in the CP during the mid-Holocene (5.5 – 4.3 kyr BP) occurred. This result is consistent with previous climate modelling data that has suggested anomalously cool SSTs in the CP as a result of orbital influences. By using this results to address the three scenarios outlined in Abram *et al.* (2009), scenario two, a mean El Niño–Modoki-like state, can be ruled out as SSTs in the CP would have warmed during this scenario. The results also indicate that scenario three, meridional changes, is unlikely because stable or slightly warming mean SSTs would have occurred in the CP. Because cooling occurred in the CP during the 5.5 – 4.3 kyr BP, scenario three, a mean La Niña-like state, is the most likely scenario to have occurred. However, cool SSTs in the CP do not confirm that a cold tongue stretched as far as Muschu/Koil (Figure 27). Furthermore, the consistency in results between the modelling data and the mean SSTs from Kiritimati provides evidence to suggests that either mean

cooling was isolated in the CP in a La Niña Modoki-like fashion or that a mean La Niña-like state was active during the mid-Holocene.

Interestingly, decadal and millennial scale changes in SST evolution at Kiritimati are somewhat similar to the same scale SST trends observed in the results from Abram *et al.* (2009). This correlation may imply that mean SST at CP and east and west southern margins of the IPWP responded similarly to changes in radiative forcing, which may be due to slight changes in orbital parameters. The relationship between the CP and WP SSTs can further be explored by comparing the results presented in this study with all WP SSTs.

5.5 Comparison against equatorial Pacific SST records

The changes in Sr/Ca SSTs for the CP can be explored further by comparing results from this study with all the Holocene SST proxy records available from the east and west Pacific. Seven SST records were used from the WP, and 10 records were used from the EP. Table 7 shows each study's core name, coordinates, and the method used for all SST data sets used in Figure 30.

To better compare the background state of the equatorial Pacific during this period, the weighted mean values from the CP coral Sr/Ca SSTs were compared with the averaged SSTs from the corresponding 500 year periods in the east and west Pacific (horizontal black lines in Figure 30). The 500 year averages from the east and west Pacific were calculated by averaging every value from all studies from each period. Plotting the corresponding 500 year blocks provides for a visual comparison of sub millennial SST evolution across the Pacific basin.

Table 7. Locations and methods for studies that were used in the gradient calculation

Location ID	Core name	Region	Core Location	Method	Study and core name
A	MD98-2181,	West Pacific	6.3°N, 125.83°E	Mg/Ca	Stott et al. 2002
A	MD98-2181	West Pacific	6.3°N, 125.83°E	Mg/Ca	Stott et al. 2004
A	MD98-2181	West Pacific	6.3°N, 125.82°E	Mg/Ca	Stott et al. 2007
B	MD98-2176	West Pacific	5°8' S, 133° 26'E	Mg/Ca	Stott et al. 2004
C	MD98-2170	West Pacific	10°35'S,125°23'E	Mg/Ca	Stott et al. 2004
Figure 27	Corals	West Pacific	Muschu/Koil	Sr/Ca	Abram et al. 2009
D	V21-30	East Pacific	1°13' S, 89°41' W	Mg/Ca	Koutavas et al. 2002

D	V21-30	East Pacific	1°13'S, 89°41'W	Mg/Ca	Koutavas et al. 2006
D	V21-30	East Pacific	1°13'S, 89°41'W	Mg/Ca	Koutavas et al. 2006
D	V21-30	East Pacific	1° 13'S, 89°41'W	alkenone	Koutavas & Sachs 2008
E	ME0005A-24JC	East Pacific	0°1.3'N, 86°27'W	alkenone	Kienast et al. 2006
F	TR163-2	East Pacific	0°31'N, 92°24'W	Mg/Ca	Lea et al. 2006
G	V19-28	East Pacific	2°22'S,84°39'W	Mg/Ca	Koutavas et al. 2006
G	V19-28	East Pacific	2°22'S, 84°39'W	alkenone	Koutavas &Sachs 2008
G	V19-30	East Pacific	3° 23'S, 83°31'W	alkenone	Koutavas & Sachs 2008
H	V19-27	East Pacific	0° 28'S, 82°40'W	alkenone	Koutavas & Sachs 2008

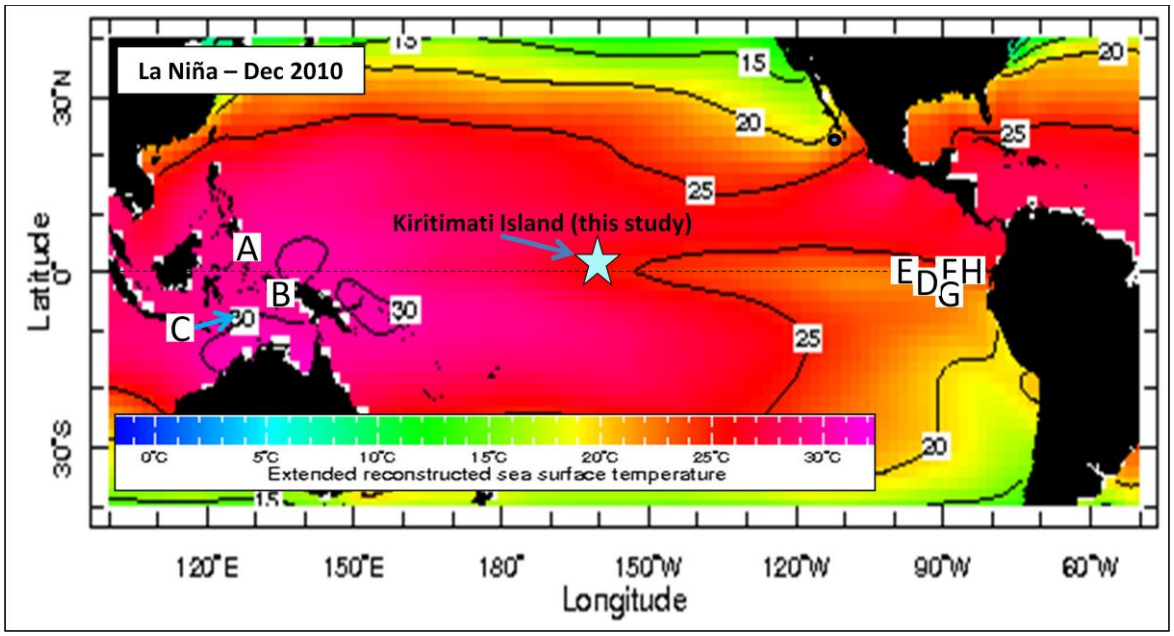

Figure 29. Pacific Ocean SST map showing core locations from the studies used in Figure 30. SSTs in this image are averaged from December 2010 when a strong La Niña event was present. SST data on image is from Xue *et al.* (2003) Smith *et al.* (2008). Letters correspond with the letters in Table 7, where details on all the SST data used in Figure 30 are presented.

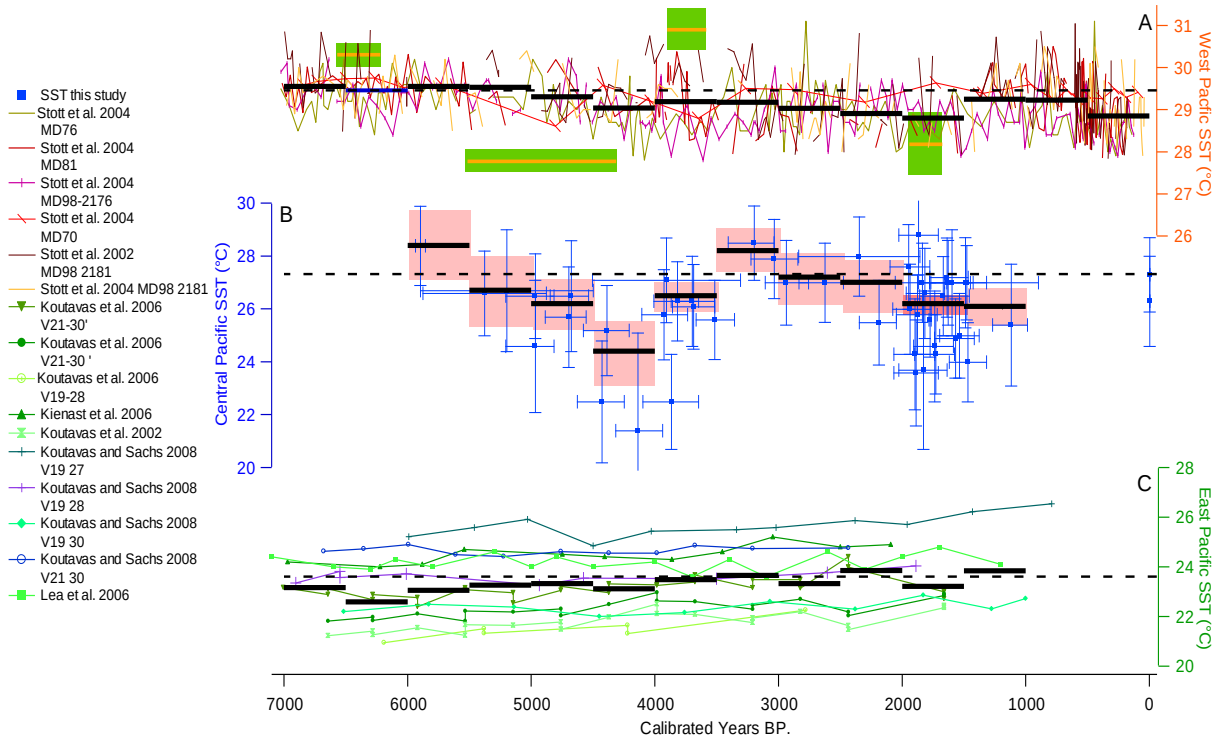

Figure 30. Comparison of CP SSTs with all available SST proxy records from the east and west Pacific since the mid-Holocene. (**A)** Six WP SST records from since 7 kyr (details in Table 7). **(B)** Central Pacific SST records reconstructed in this study (details as in Figure 26). **(C)** 10 EP SST records since 7 kyr (details in Table 7). Thick black lines in the CP represent 500 year weighted mean values. Thick black lines in the east and west Pacific represent 500 year averages of every value from all studies from each period. Weighted mean SST estimates from Abram *et al.* (2009) (same as in Figure 28) were added to the WP SST records and are represented by green rectangle (error range) and the horizontal yellow line (mean SST). These values were not included in the WP 500 year averages. This figure shows centennial-millennial mean SST evolution across the Pacific basin. The WP SSTs evolve similarly but less pronounced to the CP SSTs, whereas the EP SSTs trends are unlike the CP and WP as it shows a warming-natural trend since the mid-Holocene.

The sub millennial SST evolution from the equatorial Pacific shows a warming trend in the east and a cooling trend in the west from 7 to ~2 kyr, which is consistent with previous findings (Koutavas *et al.* 2006; Marchitto *et al.* 2010). However, the SSTs from the CP suggest that this trend is complex and that the zonal SST configuration has varied significantly. The comparison of millennial scale SST variations shows that the CP has varied substantially more than the EP and the WP.

With the error range taken into account, there is a significant cooling event during 4.5-4 kyr BP. Small decreases in mean SST are also observed in the EP and WP during this period. The same situation in which a mean cooling trend is observed in all three regions

occurs at 2-1.5 kyr BP. Because the mean SST estimate from this period for the CP is highly accurate, it serves as a quality standard for comparison that models can use to determine their accuracy.

When comparing the mean SST trends from all three regions, some interesting similarities are observed. The WP records shows a similar but less pronounced correlation with the bulk SST estimates from the CP, and no correlation is observed between in EP and CP. For example, during two extended periods, 4-6 kyr and 1.5-3.5 kyr, mean SSTs in the CP and WP indicate a cooling trend, yet the CP shows a warming-neutral trend at these times. Mean SSTs from the southern margins of the IPWP (Abram *et al.* 2009) show a stronger correlation with the CP SSTs than the other WP SSTs as they have similar sized deviations from the mean SST. These findings may suggest that mean SSTs from the CP and the WP have had similar long-term trends in mean SST evolution. However, mean SSTs trends at the margins of the IPWP are more closely linked to the CP SSTs than SSTs in more central locations of the IPWP. The correlation between the CP and the WP were somewhat unexpected since decadal trends from the instrumental record show that the EP and CP have comparable trends and variability and that no correlation between the CP and WP exists.

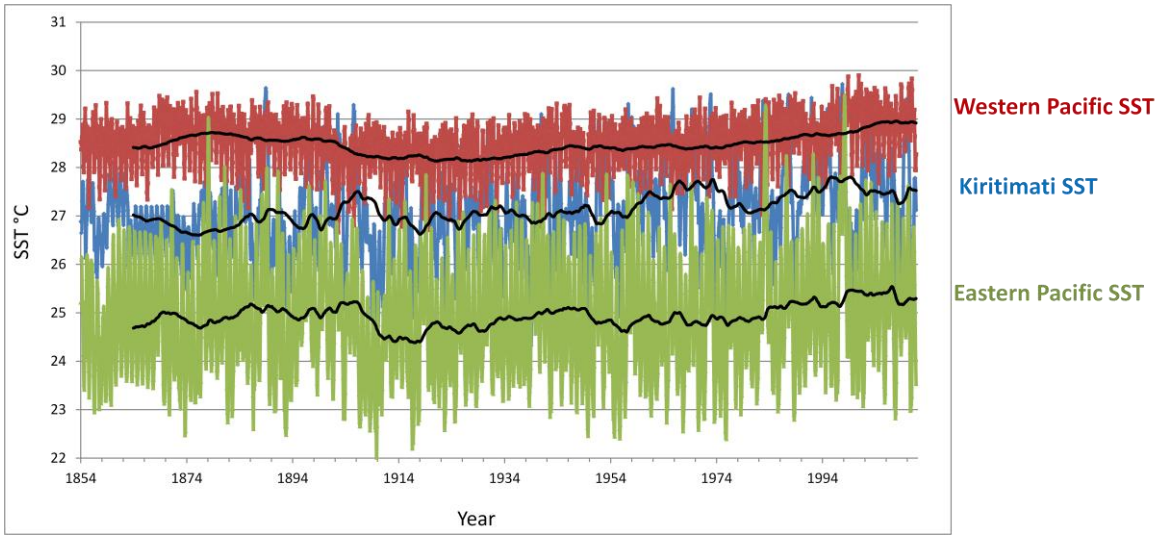

Figure 31. Comparison of instrumental SST at Kiritimati Island (158°W 2°N), WP (124°E to 134°E by 6°S to 6°N) and EP (92°W by 82°W to °4S to 4°N) since 1854. Thick black line represents a 10 year moving average. Data is from monthly mean SSTs from the 2° by 2° ERSST dataset (Xue *et al.* 2003; Smith *et al.* 2008). Mean SSTs in the EP and at Kiritimati show similar trends, which are considerably different and more variable than the WP mean SST since ~1864.

A comparison between the WP mean SSTs and the EP mean SSTs indicates that there was a weakening of the gradient during this period. The result is consistent with Koutavas *et al.*(2006), and it was expected since there is overlapping data from both regions. The comparison presented in this thesis however, is a more robust results because only five SST datasets were used in Koutavas *et al.*(2006), and 15 were used in this study. Thus, data compiled from the WP and EP presented in the study provides further evidence to suggest an overall weakening of the east-west mean SST gradient. To better quantify changes in mean zonal SSTs, three gradient measurements for each 500 year window were calculated.

5.6 Equatorial Pacific SST gradients

5.6.1 Modern gradient

To better understand Holocene SST gradients, the gradient relationships between modern SSTs in the east, central and west equatorial Pacific were explored. Pacific SST gradients have previously been calculated by either subtracting the EP SST from the WP SST (Glasbergen 2010) or by subtracting WP SST from EP SST(Conroy 2010). Either way, values further from zero equate to a stronger gradients. In this thesis three gradients are calculated (Figure 32):

G1) SSTs from the CP minus WP SSTs, more negative values indicate that the CP is cooler than the WP

G2) EP SSTs minus CP SSTs, more negative values indicate that the CP is warmer than the EP

G3) SSTs from the EP minus WP SSTs, more negative values indicate that the EP is cooler than the WP

Replacing the traditionally-used east-west SST gradient (Koutavas *et al.* 2002; Koutavas *et al.* 2006; Conroy *et al.* 2009) with two gradients presents an advantage in reconstructing zonal SST configuration across the basin since SSTs do not increase at a consistent rate across the basin. For example, in a La Niña event (Figure 29), SSTs from the EP to the CP

are relatively consistent because of the increased easterly winds that cause upwelling, which results in a more prominent EP cold-tongue. But, as you move from the CP to the WP, the cold tongue dissipates, and SSTs warm at an increased rate. This change in the dynamic of ocean waters in the CP is only noticeable when two gradients are plotted, i.e. a dual gradient.

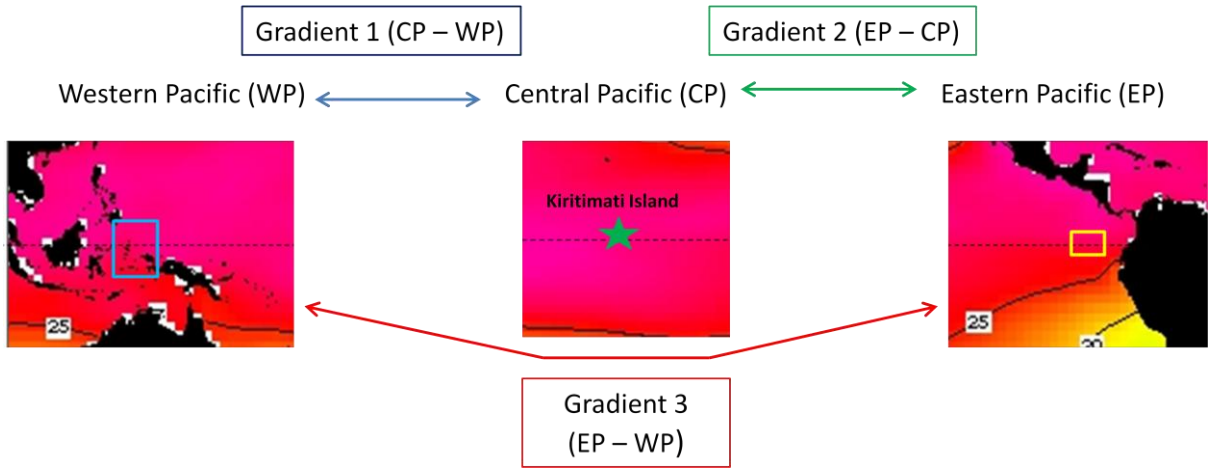

Figure 32. Dual (G1 and G2) and traditional gradient (G3) calculation diagram. Modern SSTs for the gradient calculations in Figure 33B were averaged SSTs from the blue box (124°E to 134°E by 6°S to 6°N) for the WP, the yellow box (92°W by 82°W to °4S to 4°N) for the EP and from the green star (158°W 2°N) for the CP. SST data is from monthly mean SSTs from the 2° by 2° ERSST dataset (Xue *et al.* 2003; Smith *et al.* 2008).

Changes in the modern SST gradients are most pronounced during ENSO events. During El Niño events, the SST gradient is significantly reduced across the Pacific basin, and on occasions, the gradient can reverse causing warmer SSTs in the EP. During La Niña events, the SST gradient is enhanced, and a stronger gradient is recorded. To increase understanding of mid to late-Holocene dual gradient evolution, a range of modern gradients has been plotted from the regions shown in Figure 32A. These modern gradients include two modern averages and annual averages of SST that correspond with strong ENSO phases (Figure 33B). A recent average (1981-2011) and a long-term average (1854-1980) were both plotted to determine if the well-documented, recent increase in ENSO activity was reflected in the gradients (Trenberth & Hoar 1996; Karspeck & Cane 2002; Wang & An 2002; Karnauskas *et al.* 2009).

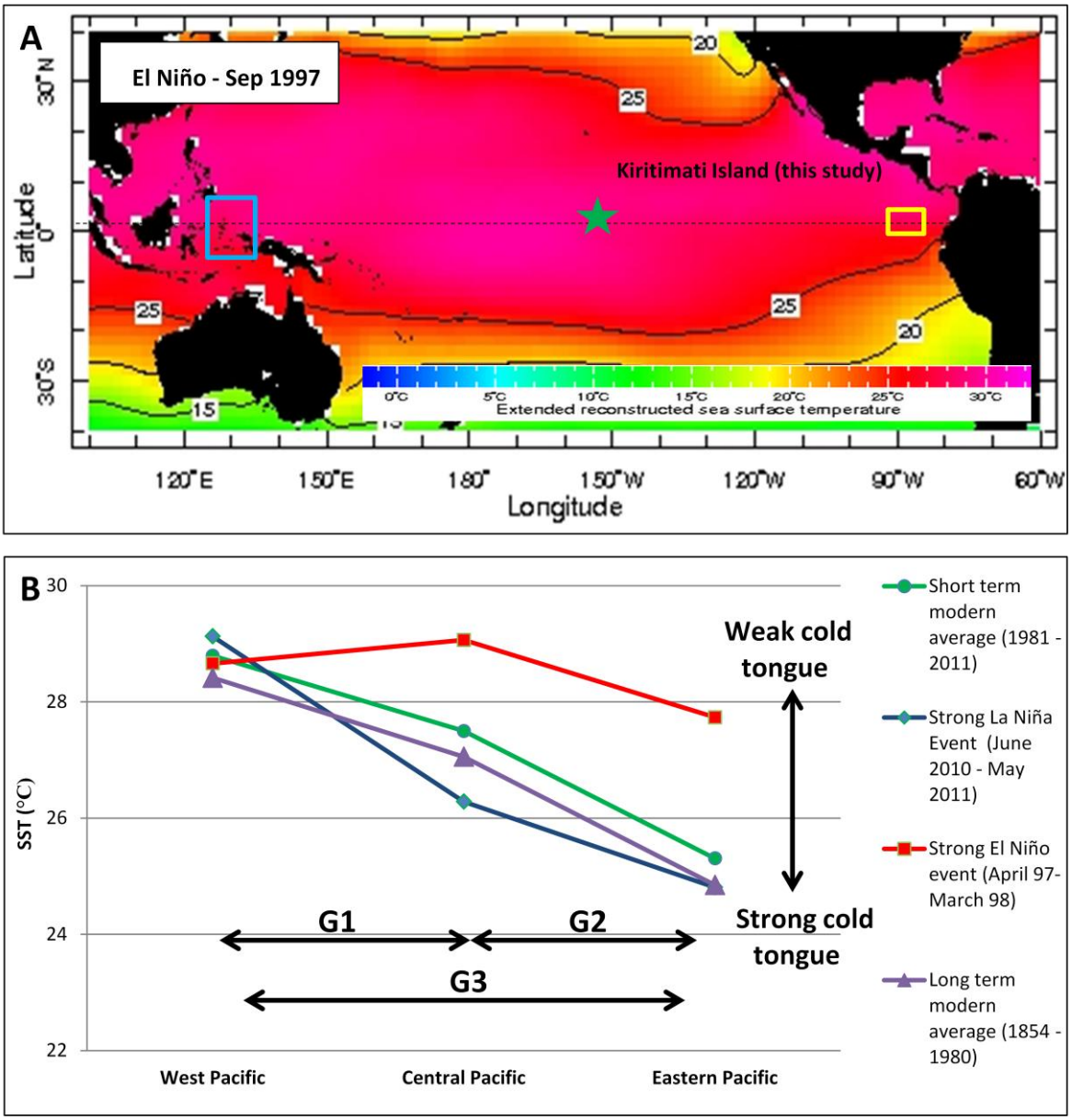

Figure 33. **A)** (2003) Smith *et al.* (2008) (details as in Figure 32). **B)** Three point modern Pacific SST gradients during a strong El Niño (red line with square), a La Niña event (blue line with diamonds). SSTs for each location during both ENSO events are yearlong averages. Two modern averages are also calculated. Short-term average is from 1981 to 2011 (green line with circle) and a long-term average 1854 – 1980 (purple line with triangle). SST data is from monthly mean SSTs from the 2° by 2° ERSST dataset (Xue et al. 2003; Smith et al. 2008).

The dual gradients from the two modern plots and the two ENSO phases show distinct slopes (Figure 33B) Both modern averages have very similar dual gradient patterns, but, the short term average (1980 – 2011) is ~0.5°C warmer than the long term average (1854-1980) in all three regions. This offset may reflect global warming-related heating of the surface ocean.

The dual gradient calculated from average annual SSTs that overlap with the recent La Niña events show unique characteristics, such as G1 having a steeper slope than G2. This result occurs because the increased trade winds during the La Niña event push colder waters over Kiritimati Island (CP), where SSTs cool significantly and in turn, reduce the gradient between the CP and the EP. Cooler SSTs in the CP result in a stronger gradient between the CP and WP regions. Therefore, it can be suggested that when G1 is greater than G2, the Walker circulation may be enhanced, driving stronger easterly trade winds that push cool SSTs from the EP to the CP.

The dual gradient calculated from annual SSTs that overlap with the 1997/98 El Niño event is the most distinctive as it varies substantially from the other dual gradients. Warming in the CP during this particular event resulted in SSTs that surpassed WP SSTs and consequently, a positive G1 gradient was calculated. Mean SSTs in the EP were considerably higher during this event than the other three gradients, which suggests that the cold tongue was significantly weaker. A weak cold tongue is a result of a reduced Walker circulation, weaker trade winds and reduced upwelling in the EP. Therefore, if this dual gradients observed in the Holocene gradients, it would indicate a weakening of the SST gradient and a reduced Walker circulation.

The dual gradients observed in Figure 33 present an advantage over the traditional two point gradients in determining the zonal configuration of SSTs across the equatorial Pacific basin because they show very distinct slopes for modern SSTs and for extreme ENSO events. By assessing the range of modern gradients, a more insightful explanation can be provided for this study's reconstructed Holocene SST gradients, and hypotheses regarding past mean states can be determined.

5.6.2 Mid to late-Holocene mean-gradient

As the SSTs in the WP were all warmer than SSTs in the EP, the Holocene dual gradients were also all similar to the two modern averaged dual gradients (Figure 34). This overall pattern of warming towards the west is in line with previous results regarding east-west gradient reconstructions (Koutavas *et al.* 2002; Koutavas *et al.* 2006; Marchitto *et al.* 2010), and the spatial pattern of SSTs fits with the modern mechanisms that drive tropical climates (Cane 2005). There does, however, appear to be centennial-millennial scale

changes in the relative configuration of SSTs between the east, west and central equatorial Pacific that differ from today.

Both the 3-3.5 kyr BP () and the 5.5-6 kyr BP () time periods show an unusually shallow G1 followed by a very steep G2, which is caused by warmer than average SST at Kiritimati Island. The SST calculated for the 5.5-6 kyr BP period was only based on one coral, and there is a large error range associated with this estimate. During these periods, G1shares some similarities to a modern El Niño state, although the G2 gradient does not. The change in SSTs from CP to EP is very high (large G2) because SSTs in the eastern part of the basin remained cool as warming occurred in the central and western regions of the basin. The mean cool SST in the EP could indicate continual upwelling driven by easterly winds, similar to modern average dynamics. However, it could be possible that the easterly winds dissipated at a more rapid rate in comparison to the average modern gradient allowing the CP SSTs to warm anomalously. Reduced easterly winds could allow the IPWP to expand, which would have a warming effect in the CP. This occurrence is similar to the recently-recognised ENSO-Modoki pattern (Ashok *et al*. 2007), where anomalous SSTs are observed in the CP during the El Niño-Modoki, but SSTs do not change significantly in the EP. This explanation is consistent with preliminary modelling results presented in Section 5.4.

The 1-1.5 kyr BP (), 4-4.5 kyr BP () time periods reveal distinct gradients where G1 is greater than G2 (Table 8). These periods have similarities to a modern dual gradient during a La Niña event, where cool SSTs stretch from the EP to the CP. The dual SST gradient plots for the 1-1.5 kyr BP and the 4-4.5 kyr BP time periods suggest that a mean prominent cold-tongue was a major feature in the equatorial Pacific. The strength of the cold-tongue for the 1.5-2 kyr BP is comparable to the dual gradient for the strong La Niña event (Figure 29). This feature was even more pronounced during the 4-4.5 kyr BP period as its G2 gradient was substantially lower. This 500 year period is, therefore, characterised by the strongest equatorial cold-tongue. Dual gradients from these two periods provide evidence to suggest that a prominent cold-tongue, which is driven by an enhanced Walker circulation, was a major feature of the Pacific mean state. Furthermore, the dual gradients over the 6 kyr period suggest that the equatorial Pacific mean SST configurations have undergone marked changes more than once.

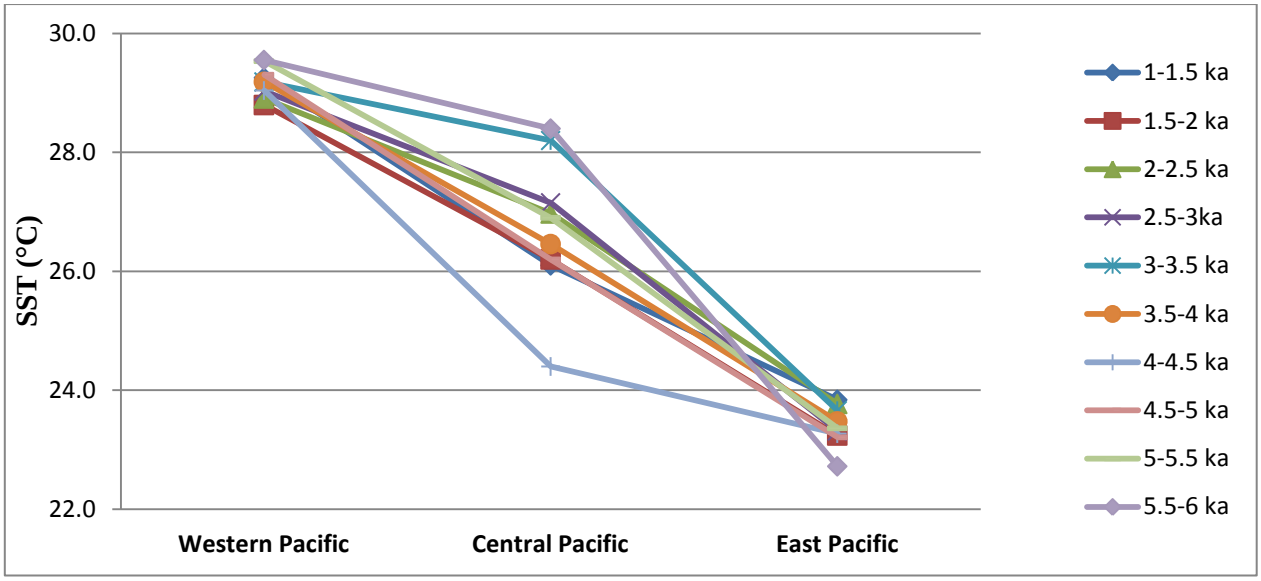

Figure 34. 500 year average dual gradients (WP to CP and CP to EP) plotted from 6-1 kyr BP. SSTs for each region represent thick black lines from Figure 30. Plot shows the distinctive mean dual gradients have occurred since the mid-Holocene, which implies that major shifts in zonal SSTs have taken place.

Table 8. 500 year mean G1, G2 and G3 measurements for the mid to late-Holocene and four modern G1, G2 and G3 measurements.

Period	Gradient 1 (CP-WP) °C	Gradient 2 (EP-CP) °C	Gradient 3 (EP – WP) °C
Short term modern average (1981 - 2011)	-1.29	-2.19	-3.49
Long term modern average (1854 - 1980)	-1.36	-2.21	-3.56
Strong La Niña Event (June 2010 - May 2011)	-2.84	-1.47	-4.32
Strong El Niño event (April 97-March 98)	0.41	-1.33	-0.93
1-1.5 kyr	-3.15	-2.26	-5.42
1.5-2 kyr	-2.60	-2.96	-5.56
2-2.5 kyr	-1.93	-3.20	-5.14
2.5-3 kyr	-1.88	-3.84	-5.72
3-3.5 kyr	-0.98	-4.54	-5.53
3.5-4 kyr	-2.73	-2.98	-5.71
4-4.5 kyr	-4.64	-1.13	-5.77
4.5-5 kyr	-3.11	-2.99	-6.10
5-5.5 kyr	-2.63	-3.54	-6.17
5.5-6 kyr	-1.15	-5.68	-6.83

Past studies have documented the mean state of east-west SST gradient throughout the Holocene and are in general agreement about its evolution (Koutavas *et al.* 2006; Marchitto *et al.* 2010). These large-scale changes in the gradient can be broken down into two major periods—the early to mid-Holocene (~10-4 kyr BP) and the late-Holocene (~4-0 kyr BP). Reconstructed gradients from the early to mid-Holocene are consistent with numerous studies that suggest the equatorial Pacific SST gradient was enhanced during this period (Koutavas *et al.* 2002; Koutavas *et al.* 2006; Donders *et al.* 2008; Marchitto *et al.* 2010). The increase in the east-west gradient during the mid-Holocene was on average 20% (1°C) higher than modern values and potentially peaked at 6 kyr at 30% (1.5°C) higher than modern (Koutavas et al. 2006). The reconstructed mean SST gradients from this period (8–5 kyr BP) have often led to the conditions being termed La Niña-like (Koutavas *et al.* 2002; Koutavas *et al.* 2006). Results from the CP indicate a steadily increasing G2 from 6-4 kyr BP and this increase implies that the mean gradient was strengthening over this period and that two distinctly different zonal SST states existed. For example, at 6 kyr BP SST configuration would have been characterised by an expanded IPWP, whereas at 4-4.5 kyr BP, the Pacific cold-tongue would have been the prominent feature. This result is not consistent with past findings that suggest that the east-west was relatively stable but overall decreasing (Koutavas *et al.* 2006). This result is a potentially significant finding because the CP SSTs make it possible to calculate G2, which is more accurate in recreating the strength of the Pacific cold tongue than the traditional G3. The CP SSTs suggests that the mean state of the Pacific has been much more variable during the mid-Holocene than previously thought.

The late-Holocene period has also been discussed in terms of mean gradient evolution. It is suggested that at ~4.5 kyr BP (±0.5 kyr BP) there was a shift in the mean SST gradient, which consisted of a gradual weakening. The transition was from a stronger mid-Holocene SST gradient to a weakener late-Holocene modern-like SST gradient (Koutavas *et al.* 2006). The proposed change of dynamics during this transition was a reduction in the easterly trade winds, cooling in the WP and warming in the EP. This hypothesis is similar to this study's results in that at ~4-4.5 kyr BP, G2 was very low (i.e. prominent cold-tongue), and over the next 1.5 kyr, a marked transition occurred. During this transition, the strengthened cold-tongue dissipated (increased G2) as SSTs increased over the next 1.5 kyr in the CP. The CP data correlates well with the timing of the transition at ~4.5 kyr (±0.5 kyr). However, it was suggested that the mean state of the Pacific returned to

modern-like or present day conditions for the duration of the late-Holocene. The CP data contradicts this suggestion as it shows that there was a decrease in G2 (strengthened cold-tongue) at ~1-2 kyr. The low G2 value suggests that mean conditions during this period were substantially different from modern conditions and more similar to the mid-Holocene, in which there was consistent strengthening of the cold tongue.

The evolution of the dual equatorial Pacific gradients can be compared with other studies that have measured SST gradients sporadically over the late-Holocene. In the last 1000 years, zonal SST gradient reconstructions from the little ice age (LIA) (~0.35 to 0.15 kyr) and the medieval warming period (MWP) (~1.05 to 0.75 kyr) have indicated significant variability in the Pacific SST gradient (Cobb *et al.* 2003). Results showed that during the LIA, the SST gradient was reduced and during the MWP, it was increased. The suggestion of an increased SST gradient ~1.05 to 0.75 kyr BP is consistent with the results from this study for 1-1.5 kyr BP period, where it was suggested that there was an enhanced cold-tongue. A continuous evolution of the SST gradient from 1.2 kyr to modern shows a large range of gradient strengths (3.7 to 5.5°C) and calculates a mean gradient of ~4.6°C (gradients are measured from west-east giving positive values) (Conroy 2010). Although the majority of this reconstruction does not overlap with the data from this study, it does show similar centennial to centennial-millennial variations in the gradient. Another mean SST gradient has been measured at ~1.7 kyr BP (Glasbergen 2010). This result overlaps with the estimate for the 2-1.5 kyr BP period calculated in this study and both results indicate that there was an increased gradient at this time.

Findings from this study show promising correlations with previously documented Holocene SST gradient shifts and agree with previous reconstructed gradients from the 1-2 kyr period. The results add new information on how mean zonal SST configuration has evolved since the mid-Holocene, suggesting that mean zonal SSTs have been more variable than previously thought. The dual gradient method presents a clear advantage in reconstructing zonal SSTs than the traditional east-west SST gradient. Additional SST data from the CP and the EP will help to build on the solid foundation regarding mean state evolution presented here. Furthermore, the results provide data that climate models can use to test their capabilities of reproducing the Holocene mean state and further their ability to predict future climate change.

5.7 Comparison against ENSO

To increase understanding of Holocene mean state – ENSO interactions, the EP-CP (G2) and the EP-WP (G3) mean gradient strengths are plotted against two lake records in the EP (Moy *et al.* 2002; Conroy *et al.* 2008). The lake records represent increased precipitation associated with El Niño events (Figure 35). Mean changes in G3 reveal a weakening trend for the duration of the reconstruction. G2 also shows an overall weakening trend, particularly from ~3.5 kyr BP to ~1 kyr BP. The weakening trends of both gradients could be attributed to warming in the EP (Figure 30). Another notable feature in G2 evolution occurs during 4.5-4 kyr BP where G2 is significantly reduced. This period is the only time where significant cooling occurred in the CP. Therefore, it is likely that the reduced gradient during this period was caused by the cooling in the CP, which may have occurred as a result of an intensified Walker circulation and a strengthened cold-tongue. During the mid to late-Holocene, both lake records indicate an increase in precipitation as a result of warmer SST in the EP due to an increase in El Niño frequency. For the most part, ENSO activity is reduced from 6-2.5 kyr BP and enhanced from 2-1 kyr BP.

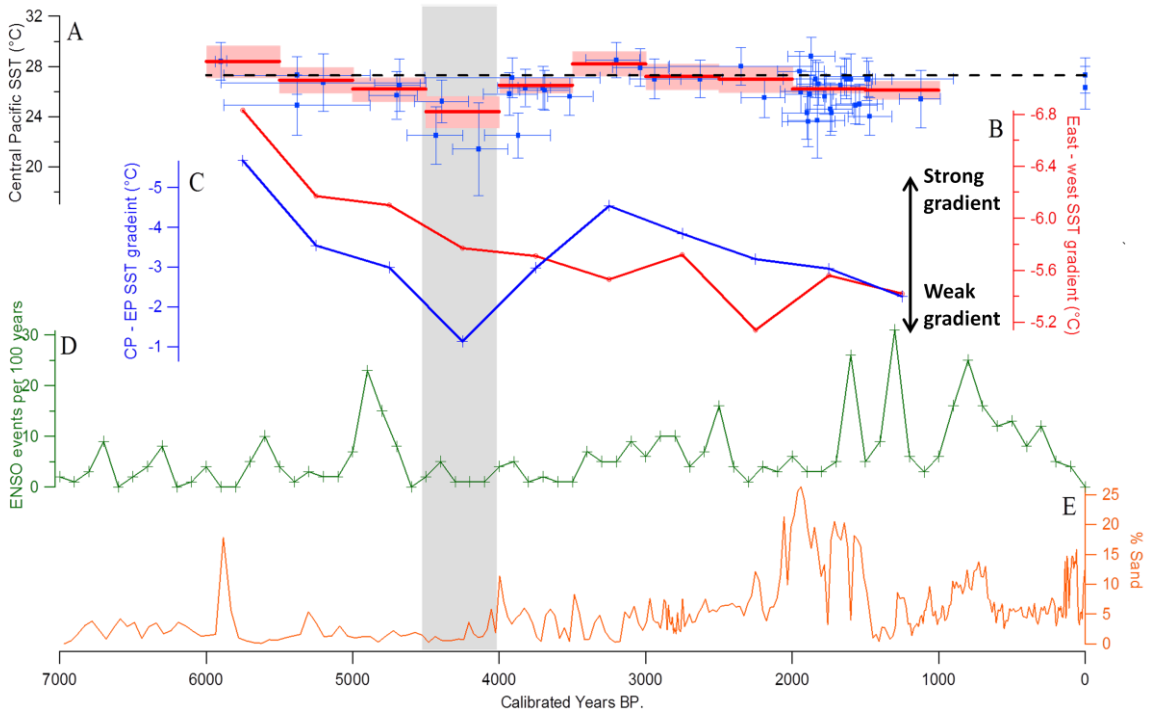

Figure 35. Comparison of mean SST gradient change and ENSO variability. **A)** (details as in Figure 26). **B)** Red line represents changes in mean G3 from 6-1 kyr BP. **C)** Blue line represents changes in G2 from 6-1 kyr BP. Markers in both G2 and G3 are positioned in the middle of every 500 year period they represent. **D)** ENSO frequency

over the last 7 kyr, from sedimentation in Laguna Pallcacocha, (southern Ecuador) using red colour intensity (Moy et al. 2002). **E)** Percentage of sand deposited in El Junco Crater Lake (Galápagos Islands) using laser-diffraction particle size analyser. Grey shading represents 4.5-4 kyr BP period where a decrease in G2 correlates with significant cooling in the CP and minimal ENSO activity.

Over the mid to late-Holocene, the observed reduction in G2 and in G3 strengths corresponds with an increase in ENSO frequency (Figure 35). The ENSO proxies used in Figure 35 are consistent with other records that indicate reduced mid-Holocene ENSO behaviour and increased late-Holocene (Tudhope *et al.* 2001; Moy *et al.* 2002; Woodroffe *et al.* 2003; Gagan *et al.* 2004; McGregor & Gagan 2004; Conroy *et al.* 2008; Makou *et al.* 2010), and thus, they give a good indication of broad changes in ENSO frequency. During the 4.5-4 kyr BP period, there is a marked decrease in the strength of G2. Previously reconstructed dual gradients suggested that the zonal SST for this period was typical of a mean La Niña-like or La Niña Modoki-like state (see section5.6.2). During this period, the ENSO proxies indicate little or no ENSO activity. This correlation and the link between decreasing G3 and G2 (due to increasing EP SST) with an increase in ENSO frequency indicates that mean zonal SSTs over centennial to millennial time scales influence ENSO. Specifically, significantly cooler mean SSTs in the CP correlate with a decrease in ENSO behaviour, and mean warming of SSTs in the EP correlate with an increase in ENSO behaviour.

A notable correlation is observed during 2-1.5 kyr BP when mean cooling in the EP, CP and WP (Figure 30) occurs as ENSO reaches is greatest intensity (Tudhope *et al.* 2001; Moy *et al.* 2002; Woodroffe *et al.* 2003; Gagan *et al.* 2004; McGregor & Gagan 2004; Conroy *et al.* 2008; Makou *et al.* 2010). Although this finding is somewhat inconsistent with the previously observed average trends over the 5 kyr BP period, it was calculated using limited and inconsistent data, which varied by ~4°C (Figure 30). Thus, further SST records would be useful from the EP during this period to clarify this discrepancy.

The overall trends observed regarding ENSO and mean SST gradient evolution in Figure 35 suggest that a reduction in mean SSTs driven by warming in the EP results in an increase in El Niño events. This finding is consistent with both model and data-based studies for the last 1 kyr that suggest that ENSO varies more with warmer SST than cooler SST in the EP (Cane 2005). If the dynamics of the tropical Pacific respond to EP warming

and a reduced gradient under future warming, the results presented here suggest that an increase in El Niño events are likely to occur.

Because observational records show that El Niño events have increased in frequency since the late 1970s (Trenberth & Hoar 1997) and that the mean SST gradient has strengthened during the last 130 years (Karnauskas *et al.* 2009), it is possible that the interaction between the mean SST gradient strength and ENSO in the Holocene may have changed in recent decades. This finding implies that other mean state components may be having a considerable influence on ENSO behaviour. The mean thermocline is another mean state component that plays a major role in influencing ENSO behaviour, and it is suggested that it relates El Niño frequency and amplitude (Fedorov & Philander 2001). The thermocline is also responsible for the oscillation of ENSO because its response to changes in SST and SLP are delayed (Cane 2005). Despite the significance of the influence that mean thermocline has on ENSO (Cane 2005; Collins *et al.* 2010), little is known regrading how it might change in the future. Climate models' ability to consistently forecast mean thermocline gradients is generally poor as predictions vary substantially (Guilyardi 2006; Guilyardi *et al.* 2009).

Although predicting future ENSO under a warming climate is currently beyond climate model capabilities (Collins *et al.* 2010), the perspectives on mean state evolution provided in this thesis offer a solid foundation that can be build on to further test and improve models. Additionally, more paleo data regarding the mean state and ENSO will help to improve the understanding of how the mean state influenced marked changes in ENSO behaviour in the late-Holocene.

6. Conclusion

This study screened over 100 corals from Kiritimati Island in the CP for diagenesis. The Sr/Ca ratio from 45 well-preserved samples were used to reconstruct Holocene SSTs. Based on this analysis, the following conclusions can be made:

- Centennial-millennial scale mean SST evolution reveals that there was a significant shift in mean SSTs during 4.5-4 kyr BP. At this time average SSTs were ~2.9°C ± 1.1°C cooler than modern temperatures.
- Weighted mean SSTs from 5.5-4.3 kyr BP provided evidence to suggest that the mean state of the Pacific was a La Niña-like or La Niña Modoki-like mean state.

This finding has ruled out the previous scenario in which an El Niño Modoki-like mean state or meridional changes occurred during the mid-Holocene.

- By compiling all available climate records from the equatorial Pacific, this study provided an extensive data set to observe basin-wide mean SST evolution. This comparison of WP, CP and EP mean SSTs indicated that mean SSTs in CP and the WP underwent similar long-term variations, whereas the EP revealed a more consistent warming trend since the mid-Holocene.
- To quantify changes in mean SSTs across the equatorial basin since the mid-Holocene, dual gradients were calculated. The results correlated well with previously documented late-Holocene SST gradients and the mid to late-Holocene SST gradient shift. The results suggest that an enhanced Pacific cold-tongue was a prominent feature from 4.5-4 kyr BP and that zonal SSTs have fluctuated more than previously thought.
- Weakening in the G2 and G3 gradient due to warming EP SSTs, correlated with increasing El Niño frequency. Furthermore, the period with the strongest equatorial cold-tongue (4.5-4 kyr BP) correlated to a period with minimal to no ENSO activity by two commonly agreed ENSO proxies. Therefore, the results indicate that centennial to millennial trends in mean SSTs have influenced ENSO behaviour since the mid-Holocene.

The new perspectives on mean state evolution provided in this thesis have helped to establish a solid foundation upon which further studies can build. More low and high resolution SST data from the CP would help to confirm the extent of the mid-Holocene cooling event observed in the results. Furthermore, the data from this study, particularly from the 2-1.5 kyr BP period, provides a good opportunity for comparison with climate models that may help to increase models' accuracy. Subsequently, climate models' perspectives on the mean state may provide a more thorough understanding of the mean state dynamics since the mid-Holocene.

7. References

Abram, N. J., McGregor, H. V., Gagan, M. K., Hantoro, W. S. and Suwargadi, B. W., 2009, "Oscillations in the southern extent of the Indo-Pacific Warm Pool during the mid-Holocene." *Quaternary Science Reviews*, **28**,(25-26), 2794-2803.

Al-Horani, F., A., Al-Moghrabi, S. M. and de Beer, D., 2003, "The mechanism of calcification and its relation to photosynthesis and respiration in the scleractinian coral Galaxea fascicularis." *Marine Biology*, **142**, 419-426.

Alibert, C. and McCulloch, M. T., 1997, "Strontium/Calcium Ratios in Modern Porites Corals From the Great Barrier Reef as a Proxy for Sea Surface Temperature: Calibration of the Thermometer and Monitoring of ENSO." *Paleoceanography*, **12**,(3), 345-363.

Allemand, D., Ferrier-Pagès, C., Furla, P., Houlbrèque, F., Puverel, S., Reynaud, S., Tambutté, É., Tambutté, S. and Zoccola, D., 2004, "Biomineralisation in reef-building corals: from molecular mechanisms to environmental control." *Comptes Rendus Palevol*, **3**,(6-7), 453-467.

Allison, N. and Finch, A. A., 2004, "High-resolution Sr/Ca records in modern Porites lobata corals: Effects of skeletal extension rate and architecture." *Geochem. Geophys. Geosyst.*, **5**,(5), 1-10.

Allison, N., Finch, A. A., Webster, J. M. and Clague, D. A., 2007, "Palaeoenvironmental records from fossil corals: The effects of submarine diagenesis on temperature and climate estimates." *Geochimica et Cosmochimica Acta*, **71**,(19), 4693-4703.

Andreasen, D. J. and Ravelo, A. C., 1997, "Tropical Pacific Ocean thermocline depth reconstructions for the Last Glacial Maximum." *Paleoceanography*, **12**,(3), 395-413.

Ashok, K., Behera, S. K., Rao, S. A., Weng, H. and Yamagata, T., 2007, "El Niño Modoki and its possible teleconnection." *J. Geophys. Res.*, **112**,(C11), 1-81.

Bathurst, R. G. C. (1975). *Developments in Sedimentology 12, Carbonate Sediments and Their Diagenesis,* 2nd ed, 658pp,. Amsterdam., Elsevier,.

Beck, J. W., Edwards, R. L., Ito, E., Taylor, F. W., Recy, J., Rougerie, F., Joannot, P. and Henin, C., 1992, "Sea-Surface Temperature from Coral Skeletal Strontium/Calcium Ratios." *Science*, **257**,(5070), 644-647.

Bjerknes, J., 1969, "Atmosphere Teleconnections from the Equatorial Pacific." *Monthly Weather Review*, **97**,(3), 163-172.

Brown, J., Tudhope, A. W., Collins, M. and McGregor, H. V., 2008, "Mid-Holocene ENSO: Issues in quantitative model-proxy data comparisons." *Paleoceanography*, **23**,(3), PA3202.

Bureau of Meteorology. (2011). "S.O.I. (Southern Oscillation Index) Archives." Retrieved 20/09/2011, from http://www.bom.gov.au/climate/current/soihtm1.shtml.

Bureau of Meteorology a. (2011). "About ENSO monitoring graphs." 12/08/2011, from http://www.bom.gov.au/climate/enso/indices/about.shtml.

Cane, M. A., 2005, "The evolution of El Niño, past and future." *Earth and Planetary Science Letters*, **230**,(3-4), 227-240.

Clarke, A. J. and Shu, L., 2000, "Quasi biennial winds in the far western equatorial Pacific phase Locking El Niño to the seasonal cycle." *Geophysical Research Letters*, **27**,(6), 771-774.

Clement, A., Seager, R., Cane, M., A. and Zebiak, S., E., 1996, "An Ocean Dynamical Thermostat." *Climate*, **9**, 2190-2196.

Clement, A. C., Seager, R. and Cane, M. A., 2000, "Suppression of El Niño during the Mid-Holocene by Changes in the Earths Orbit." *Paleoceanography*, **15**,(6), 731-737.

Cobb, K. M., Charles, C. D., Cheng, H. and Edwards, R. L., 2003, "El Nino/Southern Oscillation and tropical Pacific climate during the last millennium." *Nature*, **424**,(6946), 271-276.

Cohen, A. and McConnaughey, T., 2003, "Geochemical perspectives on coral mineralization." *Reviews in mineralogy and geochemistry*, **54**,(1), 151-187.

Cohen, A. L. and Hart, S. R., 2004, "Deglacial sea surface temperatures of the western tropical Pacific: A new look at old coral." *Paleoceanography*, **19**,(4), PA4031.

Collins, M., An, S.-I., Cai, W., Ganachaud, A., Guilyardi, E., Jin, F.-F., Jochum, M., Lengaigne, M., Power, S., Timmermann, A., Vecchi, G. and Wittenberg, A., 2010, "The impact of global warming on the tropical Pacific Ocean and El Nino." *Nature Geoscience*, **3**,(6), 391-397.

Conroy, J. L., Overpeck, J. T., Cole, J. E., Shanahan, T. M. and Steinitz-Kannan, M., 2008, "Holocene changes in eastern tropical Pacific climate inferred from a Galápagos lake sediment record." *Quaternary Science Reviews*, **27**,(11-12), 1166-1180.

Conroy, J. L., Overpeck, J T, Cole, J E. , 2010, "El Niño/Southern Oscillation and changes in the zonal gradient of tropical Pacific sea surface temperature over the last 1.2 ka." *PAGES news*, **18**,(1), 32-34.

Conroy, J. L., Restrepo, A., Overpeck, J. T., Steinitz-Kannan, M., Cole, J. E., Bush, M. B. and Colinvaux, P. A., 2009, "Unprecedented recent warming of surface temperatures in the eastern tropical Pacific Ocean." *Nature Geoscience*, **2**,(1), 46-50.

Corrège, T., 2006, "Sea surface temperature and salinity reconstruction from coral geochemical tracers." *Palaeogeography, Palaeoclimatology, Palaeoecology*, **232**,(2-4), 408-428.

Corrège, T., Gagan, M. K., Beck, J. W., Burr, G. S., Cabioch, G. and Le Cornec, F., 2004, "Interdecadal variation in the extent of South Pacific tropical waters during the Younger Dryas event." *Nature*, **428**,(6986), 927-929.

Cuif, J.-P., Dauphin, Y., Berthet, P. and Jegoudez, J., 2004, "Associated water and organic compounds in coral skeletons: Quantitative thermogravimetry coupled to infrared absorption spectrometry." *Geochem. Geophys. Geosyst.*, **5**,(11), Q11011.

de Villiers, S., Nelson, B. K. and Chivas, A. R., 1995, "Biological Controls on Coral Sr/Ca and Î´18O Reconstructions of Sea Surface Temperatures." *Science*, **269**,(5228), 1247-1249.

DiNezio, P., Clement, A. and Vecchi, G., 2010, "Reconciling Differing Views of Tropical Pacific Climate Change." *Eos Trans. AGU*, **91**,(16).

Donders, T. H., Wagner-Cremer, F. and Visscher, H., 2008, "Integration of proxy data and model scenarios for the mid-Holocene onset of modern ENSO variability." *Quaternary Science Reviews*, **27**,(5-6), 571-579.

Evans, M. N., Fairbanks, R. G. and Rubenstone, J. L., 1998, "A proxy index of ENSO teleconnections." *Nature*, **394**,(6695), 732-733.

Evans, M. N., Fairbanks, R. G. and Rubenstone, J. L., 1999, "The thermal oceanographic signal of El Niño reconstructed from a Kiritimati Island coral." *J. Geophys. Res.*, **104**,(C6), 13409-13421.

Fedorov, A. V. and Philander, S. G. H., 2001, "A stability analysis of tropical ocean–atmosphere interactions (bridging measurements of, and theory for El Nino)." *Climate*, **14**, 3086–3101.

Felis, T. and Pätzold, J., 2003, "Climate records from corals." *Marine Science Frontiers for Europe*, (ed L. F. Wefer G, Mantoura F),11-27. Springer-Verlag Berlin Heidelberg.

Ferrier-Pagès, C., Boisson, F., Allemand, D. and Tambutte´, E., 2002, "Kinetics of strontium uptake in the scleractinian coral Stylophora pistillata." *Marine Ecology Progress Series*, **245**, 93–100.

Gagan, M. K., Ayliffe, L. K., Hopley, D., Cali, J. A., Mortimer, G. E., Chappell, J., McCulloch, M. T. and Head, M. J., 1998, "Temperature and Surface-Ocean Water Balance of the Mid-Holocene Tropical Western Pacific." *Science*, **279**,(5353), 1014-1018.

Gagan, M. K., Hendy, E. J., Haberle, S. G. and Hantoro, W. S., 2004, "Post-glacial evolution of the Indo-Pacific Warm Pool and El Niño-Southern oscillation." *Quaternary International*, **118-119**, 127-143.

Galbraith, R. F., Roberts, R. F. and Yoshida, H., 2005, "Error Variation on OSL Palaeodose Estimates From Single Aliquots of Quartz: a factoial Experiment." *Radiation Measurements* **39**, 289-307.

Glasbergen, L., 2010, "Coral Sr/Ca records from Kiritimati and Rambutso Island: An eastside-westside story of late-Holocene sea surface temperatures." School of Earth and Environmental Sciences, Univeristy of Wollongong.

Glasbergen, L., 2010, "Coral Sr/Ca records from Kiritimati and Rambutso Island: An eastside-westside story of late-Holocene sea surface temperatures. School of Earth and Environmental Sciences, Univeristy of Wollongong.

Global Change Master Directory. (2011). "Monthly and Weekly Nino 3.4 Region SST Index: East Central Tropical Pacific." Retrieved 25/08/2011, from http://gcmd.nasa.gov/KeywordSearch/Metadata.do?Portal=GCMD&KeywordPath=|%5BFreetext%3D%27el+nino%27%5D&NumericId=19738&MetadataView=Data&MetadataType=0&lbnode=mdlb1.

Goodkin, N. F., Hughen, K. A. and Cohen, A. L., 2007, "A multicoral calibration method to approximate a universal equation relating Sr/Ca and growth rate to sea surface temperature." *Paleoceanography*, **22**,(1), PA1214.

Guilyardi, E., 2006, "El Niño–mean state–seasonal cycle interactions in a multi-model ensemble." *Climate Dynamics*, **26**,(4), 329-348.

Guilyardi, e., Andrew Wittenberg, Alexey Fedorov, Mat Collins, Chunzai Wang, Antoni etta Capotondi, Geert Jan van Oldenborgh, and Tim Stockdale, 2008, "Understanding El Niño in ocean–atmosphere general circulation models:

Progress and Challenges." *American Meteorological Society*, **90**, 325-340.

Guilyardi, E., Wittenberg, A., Fedorov, A., Collins, M., Wang, C., Capotondi, A., van Oldenborgh, J. and Stockdale, T., 2009, "Understanding El Niño in ocean–atmosphere general circulation models: Progress and Challenges." *American Meteorological Society*, **90**, 325-340.

Held, I. M. and Soden, B. J., 2006, "Robust responses of the hydrological cycle to global warming." *Climate*, **19**, 5686–5699.

Hendy, E. J., Gagan, M. K., Alibert, C. A., McCulloch, M. T., Lough, J. M. and Isdale, P. J., 2002, "Abrupt Decrease in Tropical Pacific Sea Surface Salinity at End of Little Ice Age." *Science*, **295**,(5559), 1511-1514.

Hendy, E. J., Gagan, M. K., Lough, J. M., McCulloch, M. and deMenocal, P. B., 2007, "Impact of skeletal dissolution and secondary aragonite on trace element and isotopic climate proxies in Porites corals." *Paleoceanography*, **22**,(4), 4101.

Karnauskas, K. B., Seager, R., Kaplan, A., Kushnir, Y. and Cane, M. A., 2009, "Observed Strengthening of the Zonal Sea Surface Temperature

Gradient across the Equatorial Pacific Ocean." *Journal of Climate*, **22**,(16), 4316-4321.

Karspeck, A. R. and Cane, M. A., 2002, "Tropical Pacific 1976–77 Climate Shift in a Linear, Wind-Driven Model." *Journal of Physical Oceanography*, **32**,(8), 2350-2360.

Kienast, S. S., Kienast, M., Jaccard, S., Calvert, S. E. and François, R., 2006, "Testing the silica leakage hypothesis with sedimentary opal records from the eastern equatorial Pacific over the last 150 kyrs." *Geophysical Research Letters*, **33**,(15), 15607.

Koutavas, A., deMenocal, P. B., Olive, G. C. and Lynch-Stieglitz, J., 2006, "Mid-Holocene El Niño–Southern Oscillation (ENSO) attenuation revealed by individual foraminifera in eastern tropical Pacific sediments." *Geology*, **34**,(12), 993-996.

Koutavas, A., Lynch-Stieglitz, J., Marchitto, T. M. and Sachs, J. P., 2002, "El Niño-Like Pattern in Ice Age Tropical Pacific Sea Surface Temperature." *Science*, **297**,(5579), 226-230.

Koutavas, A. and Sachs, J. P., 2008, "Northern timing of deglaciation in the eastern equatorial Pacific from alkenone paleothermometry." *Paleoceanography*, **23**,(4), PA4205.

Lea, D. W., Pak, D. K., Belanger, C. L., Spero, H. J., Hall, M. A. and Shackleton, N. J., 2006, "Paleoclimate history of Galápagos surface waters over the last 135,000 yr." *Quaternary Science Reviews*, **25**,(11-12), 1152-1167.

Leduc, G., Vidal, L., Tachikawa, K., Rostek, F., Sonzogni, C., Beaufort, L. and Bard, E., 2007, "Moisture transport across Central America as a positive feedback on abrupt climatic changes." *Nature*, **445**,(7130), 908-911.

Liu, Z., Kutzbach, J. and Wu, L., 2000, "Modeling climate shift of El Nino variability in the Holocene." *Geophys. Res. Lett.*, **27**,(15), 2265-2268.

Longman, M. W., 1980, "Carbonate diagenetic textures from nearsurface diagenetic environments." *Journal Name: Am. Assoc. Pet. Geol. Bull.; (United States); Journal Volume: 64:4*, Medium: X; Size: Pages: 461-487.

Makou, M. C., Eglinton, T. I., Oppo, D. W. and Hughen, K. A., 2010, "Postglacial changes in El Niño and La Niña behavior." *Geology*, **38**,(1), 43-46.

Marchitto, T. M., Muscheler, R., Ortiz, J. D., Carriquiry, J. D. and van Geen, A., 2010, "Dynamical Response of the Tropical Pacific Ocean to Solar Forcing During the Early Holocene." *Science*, **330**,(6009), 1378-1381.

McGregor, H. V. and Abram, N. J., 2008, "Images of diagenetic textures in Porites corals from Papua New Guinea and Indonesia." *Geochem. Geophys. Geosyst.*, **9**,(10), Q10013.

McGregor, H. V., Fischer, M. J., Gagan, M. K., Fink, D. and Woodroffe, C. D., 2011b, "Environmental control of the oxygen isotope composition of Porites coral microatolls." *Geochimica et Cosmochimica Acta*, **75**,(14), 3930-3944.

McGregor, H. V. and Gagan, M. K., 2003, "Diagenesis and geochemistry of porites corals from Papua New Guinea: Implications for paleoclimate reconstruction." *Geochimica et Cosmochimica Acta*, **67**,(12), 2147-2156.

McGregor, H. V. and Gagan, M. K., 2004, "Western Pacific coral D18O records of anomalous Holocene variability in the El Niño-Southern Oscillation." *Geophysical Research Letters*, **31**,(11), L11204.

McGregor, H. V., Hellstrom, J., Fink, D., Hua, Q. and Woodroffe, C. D., 2011a, "Rapid U-series dating of young fossil corals by laser ablation MC-ICPMS." *Quaternary Geochronology*, **6**,(2), 195-206.

McPhaden, M. J., Zebiak, S. E. and Glantz, M. H., 2006, "ENSO as an Integrating Concept in Earth Science." *Science*, **314**,(5806), 1740-1745.

Moy, C. M., Seltzer, G. O., Rodbell, D. T. and Anderson, D. M., 2002, "Variability of El Nino/Southern Oscillation activity at millennial timescales during the Holocene epoch." *Nature*, **420**,(6912), 162-165.

Müller, A., Gagan, M. K. and McCulloch, M. T., 2001, "Early marine diagenesis in corals and geochemical consequences for paleoceanographic reconstructions." *Geophysical Research Letters*, **28**,(23), 4471-4474.

Nothdurft, L. and Webb, G., 2007, "Microstructure of common reef-building coral genera Acropora, Pocillopora, Goniastrea and Porites: constraints on spatial resolution in geochemical sampling." *Facies*, **53**,(1), 1-26.

Nothdurft, L. and Webb, G., 2009, "Earliest diagenesis in scleractinian coral skeletons: implications for palaeoclimate-sensitive geochemical archives." *Facies*, **55**,(2), 161-201.

Nurhati, I. S., Cobb, K. M., Charles, C. D. and Dunbar, R. B., 2009, "Late 20th century warming and freshening in the central tropical Pacific." *Geophysical Research Letters*, **36**,(21), L21606.

Ogilvie, M., M., 1896, "Systematic study of Madreporan corals.", Phil Trans Roy Soc London, **187, 1**83-345.

Otto-Bliesner, B., Schneider, R., Brady, E., Kucera, M., Abe-Ouchi, A., Bard, E., Braconnot, P., Crucifix, M., Hewitt, C., Kageyama, M., Marti, O., Paul, A., Rosell-Melé, A., Waelbroeck, C., Weber, S., Weinelt, M. and Yu, Y., 2009, "A comparison of PMIP2 model simulations and the MARGO proxy reconstruction for tropical sea surface temperatures at last glacial maximum." *Climate Dynamics*, **32**,(6), 799-815.

Otto and Bliesner, B. L., 1999, "El Niño/La Niña and Sahel precipitation during the Middle Holocene." *Geophys. Res. Lett.*, **26**,(1), 87-90.

Reynaud, S., Ferrier-Pages, C., Boisson, F., Allemand, D. and Fairbanks, R., G., 2004, "Effect of light and temperature on calcification and strontium uptake in the scleractinian coral Acropora verweyi " *Marine Ecology Progress Series*, **279**, 105-112.

Reynolds, R. W., Rayner, N. A. and Smith, T. M., 2002, "An improved in situ and satellite SST analysis for climate." *Journal of Climate*, **15**, 1609-1625.

Rodbell, D. T., Seltzer, G. O., Anderson, D. M., Abbott, M. B., Enfield, D. B. and Newman, J. H., 1999, "An ~15,000-Year Record of El Niño-Driven Alluviation in Southwestern Ecuador." *Science*, **283**,(5401), 516-520.

Sandweiss, D. H., Richardson, J. B., Reitz, E. J., Rollins, H. B. and Maasch, K. A., 1996, "Geoarchaeological Evidence from Peru for a 5000 Years B.P. Onset of El Niño." *Science*, **273**,(5281), 1531-1533.

Sayani, H. R., Cobb, K. M., Cohen, A. L., Elliott, W. C., Nurhati, I. S., Dunbar, R. B., Rose, K. A. and Zaunbrecher, L. K., 2011, "Effects of diagenesis on paleoclimate reconstructions from modern and young fossil corals." *Geochimica et Cosmochimica Acta*, **75**,(21), 6361-6373.

Sinclair, D. J. and Risk, M. J., 2006, "A numerical model of trace-element coprecipitation in a physicochemical calcification system: Application to coral biomineralization and trace-element [`]vital effects'." *Geochimica et Cosmochimica Acta*, **70**,(15), 3855-3868.

Smith, T. M., Reynolds, R. W., Peterson, T. C. and Lawrimore, J., 2008, "Improvements to NOAA's Historical Merged Land-Ocean Surface Temperature Analysis (1880-2006)." *Journal of Climate*, **21**, 2283-2296.

Solomon, S., D., Qin, D., Manning, M., Chen, Z., Marquis, M., Averyt, K., B., M, T. and Miller, H. L. (2007). Contribution of Working Group I to the Fourth Assessment Report of the Intergovernmental Panel on Climate Change. Cambridge, United Kingdom and New York, NY, USA., Cambridge University Press.

Stoll, H. M., Schrag, D. P. and Clemens, S. C., 1999, "Are seawater Sr/Ca variations preserved in quaternary foraminifera?" *Geochimica et Cosmochimica Acta*, **63**,(21), 3535-3547.

Stott, L., Cannariato, K., Thunell, R., Haug, G. H., Koutavas, A. and Lund, S., 2004, "Decline of surface temperature and salinity in the western tropical Pacific Ocean in the Holocene epoch." *Nature*, **431**,(7004), 56-59.

Stott, L., Poulsen, C., Lund, S. and Thunell, R., 2002, "Super ENSO and Global Climate Oscillations at Millennial Time Scales." *Science*, **297**,(5579), 222-226.

Stott, L., Timmermann, A. and Thunell, R., 2007, "Southern Hemisphere and Deep-Sea Warming Led Deglacial Atmospheric CO2 Rise and Tropical Warming." *Science*, **318**,(5849), 435-438.

Sun, D.-Z. and Liu, Z., 1996, "Dynamic Ocean-Atmosphere Coupling: A Thermostat for the Tropics." *Science*, **272**,(5265), 1148-1150.

Timmermann, A., Oberhuber, J., Bacher, A., Esch, M., Latif, M. and Roeckner, E., 1999, "Increased El Nino frequency in a climate model forced by future greenhouse warming." *Nature*, **398**,(6729), 694-697.

Trenberth, K. E., 1997, "The definition of El Nino." *Bulletin of the American Meteorological Society*, **78**, 2771-2777.

Trenberth, K. E. and Hoar, T. J., 1996, "The 1990-1995 El Niño-Southern Oscillation Event: Longest on Record." *Geophysical Research Letters*, **23**,(1), 57-60.

Trenberth, K. E. and Hoar, T. J., 1997, "El Niño and climate change." *Geophysical Research Letters*, **24**,(23), 3057-3060.

Tudhope, A. W., Chilcott, C. P., McCulloch, M. T., Cook, E. R., Chappell, J., Ellam, R. M., Lea, D. W., Lough, J. M. and Shimmield, G. B., 2001, "Variability in the El Niño-Southern Oscillation Through a Glacial-Interglacial Cycle." *Science*, **291**,(5508), 1511-1517.

Vecchi, G. A. and Soden, B. J., 2007, "Global warming and the weakening of the tropical circulation." *Climate*, **20**, 4316–4340.

Vecchi, G. A., Soden, B. J., Wittenberg, A. T., Held, I. M., Leetmaa, A. and Harrison, M. J., 2006, "Weakening of tropical Pacific atmospheric circulation due to anthropogenic forcing." *Nature*, **441**,(7089), 73-76.

Walker, G. T., 1923, "Correlation in seasonal variations of weather VIII: A preliminary study of world weather,." *Mem. Indian Meteor. Dept.*,, **24**,(75–131).

Wang and An, 2002, "A mechanism for decadal changes of ENSO behavior: roles of background wind changes." *Climate Dynamics*, **18**,(6), 475-486.

Wang, C. a. P., Joel, 2004, "Understanding ENSO Physics—A Review." *Earth's Climate: The Ocean-Atmosphere Interaction, Geophysical Monograph Series*, **147**.

Wei, G., Sun, M., Li, X. and Nie, B., 2000, "Mg/Ca, Sr/Ca and U/Ca ratios of a porites coral from Sanya Bay, Hainan Island, South China Sea and their relationships to sea surface temperature." *Palaeogeography, Palaeoclimatology, Palaeoecology*, **162**,(1-2), 59-74.

Wittenberg, A. T., 2009, "Are historical records sufficient to constrain ENSO simulations?" *Geophysical Research Letters*, **36**,(12), L12702.

Woodroffe, C. D., Beech, M. R. and Gagan, M. K., 2003, "Mid-late Holocene El Nino variability in the equatorial Pacific from coral microatolls." *Geophysical Research Letters*, **30**,(7).

Woodroffe, C. D. and McLean, R. F., 1998, "Pleistocene morphology and Holocene emergence of Christmas (Kiritimati) Island, Pacific Ocean." *Coral Reefs*, **17**,(3), 235-248.

Xue, Y., Smith, T. M. and Reynolds, R. W., 2003, "Interdecadal changes of 30-yr SST normals during 1871-2000." *Journal of Climate*, **16**, 1601-1612.

Yan, X.-H., Ho, C.-R., Zheng, Q. and Klemas, V., 1992, "Temperature and Size Variabilities of the Western Pacific Warm Pool." *Science*, **258**,(5088), 1643-1645.

Zeko, D., 2009, "Ocean Temperatures from the Sr/Ca Ratio of Coral Microatolls: a Tool to Investigate Past El Niño Events. ." School of Earth and Environmental Sciences, Univeristy of Wollongong.

Zheng, W., Braconnot, P., Guilyardi, E., Merkel, U. and Yu, Y., 2008, "ENSO at 6ka and 21ka from ocean–atmosphere coupled model simulations." *Climate Dynamics*, **30**,(7), 745-762.

8. Appendix: (Data CD)

Appendix 1: XRD results

Appendix 2: Thin section images and ratings

Appendix 3: X-rays and coral mill paths

Appendix 4: Sr/Ca results